Anita Maria HAIDER

Theoretical approach to determine the mechanical properties of biopolymer networks

DIPLOMA THESIS

written to obtain the academic degree of Diplom-Ingenieurin

Diploma Programme Technical Mathematics

Graz University of Technology

Supervisor:
Univ.-Prof. Dipl.-Ing. Dr.techn. Gerhard A. HOLZAPFEL

Co-Advisor:
Dipl.-Ing. Michael J. UNTERBERGER

Institute of Biomechanics

Graz, February 2012

STATUTORY DECLARATION

I declare that I have authored this thesis independently, that I have not used other than the declared sources/resources, and that I have explicitly marked all material which has been quoted either literally or by content from the used sources.

.....	.....
date	(signature)

Abstract

Fathoming the functions of the human body and especially the progression of disease is the subject of current research. Many researchers from different disciplines work together to attain a better understanding behind these features. Biomechanics is a part of this research field which deals with the development, extension and application of mechanics to biological systems. The relation between diseases and abnormal mechanically behavior of cells have been detected by many researchers. Here, we focus on the investigation of mechanical properties of individual filaments and networks of filaments, which occur on subcellular level. Recently, a new mathematical description of the worm-like chain model was developed from purely mechanical considerations. Based on the micro-sphere model a new continuum mechanical formulation for describing the mechanical properties of filament networks was established. It acts as a multiscale approach, which incorporates the single filament model. In the present thesis we perform a closer analysis on this recently developed network model. The neglected part of the micro-sphere model is discussed and a specific parameter is examined more precisely. To confirm the appropriate application of these two models, we fit these models to experimental data of fibrin, a protein which plays a key role in hemostasis.

Kurzfassung

Die Erforschung der Funktionen des menschlichen Körpers und insbesondere der Verlauf einer Erkrankung ist Gegenstand aktueller wissenschaftlicher Tätigkeit. Viele Forschungsgruppen aus unterschiedlichen Bereichen arbeiten zusammen, um ein besseres Verständnis für all diese Mechanismen zu erlangen. Zu diesen Forschungsbereichen gehört auch die Biomechanik, die sich im Allgemeinen mit der Entwicklung, Erweiterung und Anwendung der Mechanik auf biologische Systeme befasst. Der Zusammenhang von Krankheiten und abnormalem mechanischen Verhalten von Zellen wurde bereits von einigen Forschern publiziert. Unser Hauptaugenmerk liegt dabei auf der Erforschung der mechanischen Eigenschaften von einzelnen Filamenten und Netwerken von Filamenten, die auf subzellulärer Ebene vorkommen. Erst kürzlich wurde eine neue mathematische Formulierung des worm-like chain Modells entwickelt, die auf rein mechanischer Erklärung basiert. Ebenfalls erst kürzlich wurde eine neue kontinuumsmechanische Formulierung zur Beschreibung von Filament-Netzwerken, basierend auf dem micro-sphere Modell, aufgestellt. Dieses Netzwerkmodell agiert auf mehreren Größenskalen, in welchem das Modell des einzelnen Filaments integriert ist. In der vorliegenden Diplomarbeit führen wir eine genauere Analyse des kürzlich entwickelten Netzwerkmodells durch. Dabei diskutieren wir den vernachlässigten Teil des micro-sphere Modells und nehmen einen bestimmten Netzwerkparameter genauer unter die Lupe. Um die geeignete Anwendung dieser beiden erst kürzlich entwickelten Modelle zu bestätigen, fitten wir diese Modelle an experimentelle Daten von Fibrin, ein Protein dem in der Hämostase eine wichtige Rolle zukommt.

Acknowledgment

I am heartily thankful to my supervisor Professor Gerhard A. Holzapfel for allowing me to join his team, for his expertise, and for his encouragement. I consider it an honor to work with Michael J. Unterberger. His brilliant advice, his right timely hints, his skills and his ongoing support were invaluable for me. I am indebted to all members of the Institute of Biomechanics for providing a warm research atmosphere, sharing knowledge, and encouragements. I would also like to thank my family, loved ones and friends for their incessant support, infinite empathy and heartwarming advice through my entire life. Lastly, I offer my regards and blessings to all of those who supported me in any respect during the completion of this thesis.

Contents

1 Introduction

The uniqueness of the human body in its structures and functions fascinates the modern science of different disciplines. This complex biological system still includes many open questions which wait to be resolved today. This is especially important if pathological processes cause human diseases. 'War on Cancer' was an initiative by former U.S. president Richard Nixon in the year 1971, with the aim to find the cure for the disease of cancer within the next 25 years. We lost this war, unfortunately. The World Health Organization (WHO)[1] reports that cardiovascular diseases and cancer are the number one cause of death in percent to total number of death worldwide. In the last few decades many researchers revealed the connection between the abnormal mechanical properties of cells to diseases such as arthritis (Trickey et al. 2000), asthma (An et al. 2006), atherosclerosis (Ohashi and Sato 2005), cancer (Suresh 2007), glaucoma (Zeng et al. 2010) or malaria (Nash et al. 1989).

Materials in biological systems such as fibers (biopolymers) exhibit extraordinary mechanical behavior. They are not comparable with engineering materials such as rubber, steel or ceramic. A new theory has to be developed to close this gap. This is the mission of biomechanics. Biomechanics is the development, extension and application of mechanics to biological systems. This science provides an important knowledge to better understand the mechanism behind disease progression (Lee and Lim 2007). Through the investigations of mechanical properties on the molecular, cellular, tissue, organ, and organism levels, the biomechanics contributes significantly in the research of diseases. The insights of biomechanics assist the improvements in the detection, diagnosis and treatment of diseases (Lee and Lim 2007).

The focus in this thesis lies on the determination of mechanical properties of biological materials on cellular and subcellular levels, such as fibers and networks of fibers. The term biopolymer, as we define it, is introduced in Section 1.1. By single filament models we have the opportunity to determine mechanical properties of single fibers. One of the well-known models is the worm-like chain model by Kratky and Porod (1949). A new approach was developed recently by Holzapfel and Ogden (2011) to describe mechanical behavior of biopolymers. In the human body, single fibers interact together and thereby form a network. Network models such as the eight chain model by Arruda and Boyce (1993) describe the mechanical behaviors of this kind of biological materials. Currently a new network model by Unterberger et al. (submitted) is in the development phase. The underlying idea of this model is based on the micro-sphere model for rubber elasticity which goes back to Miehe

[1] `http://www.who.int/gho/mortality_burden_disease/causes_death_2008` accessed on February 2, 2012

et al. (2004) and which includes the eight chain model as a special case.

The fundamental framework for the development of these models is provided by the classical continuum mechanics, which we introduce briefly in Chapter 2. The highlights of this work are the investigations of the models which act on single filaments and networks, which we address in Chapter 3. In particular, we focus on the recently developed models of Holzapfel and Ogden (2011) and Unterberger et al. (submitted). In Chapters 4 and 5, we take a closer look on the Unterberger model. Experiments on biopolymers are useful either to confirm or to re-evaluate the theory. Therefore, in Chapter 6 we fit these models to experimental data of the biopolymer fibrin, which are taken from Hudson et al. (2010) and Kang et al. (2009).

1.1 Characterization of biopolymers

Biopolymers are a class of polymers, which are formed in living organisms. A polymer is a large macromolecule made up of repetitive subunits called monomers, which are linked together by covalent bonds. Biopolymers exist outside (collagen in extracellular matrix, fibrin in blood clots) and inside of cells (actin filaments, intermediate filaments, and microtubules create the cytoskeleton). The coarse structure of an eukaryotic cell consists of cell membrane, nucleus and cytoplasm which includes organelles, cytoskeleton and cytosol. Organelles accomplish a special function within the cell. The main ingredients of the cytoplasm are water and proteins. From the biomechanical point of view, the cytoskeleton, the interior skeleton of a cell, plays the main role. On the left side in Figure 1.1 we illustrate these components and on the right we show a microscopic view of a blood clot.

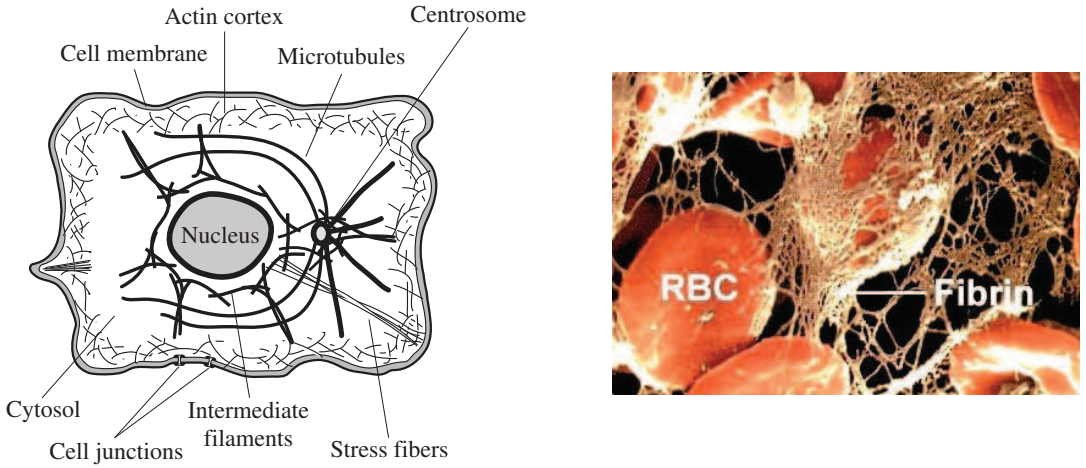

Figure 1.1: Schematic view of a typical eukaryotic cell with mechanically important components (left). View of a blood clot (right) with red blood cells (RCB) embedded by fibrin, `www.ch.ic.ac.uk/local/projects/bhonoah/bloodcoagulation.html` accessed on February 6, 2012.

Roughly biopolymers can be classified according to three different main categories. Namely in nucleic acids, proteins and polysaccharides but it should be mentioned that this classification is not strict. Amino acids are the monomers in proteins, in polysaccharides or carbohydrates the monomers are monosaccharides and nucleic acids are polymers of nucleotides. The biological function of nucleic acids, such as DNA and RNA, is to store and transmit genetic information, whereas the main function of polysaccharides is to store energy. The proteins play an important role in many different functions of cells and tissues. For instance, they serve as enzymatic catalysts, they are responsible for the transport of molecules, they are the communicators between cells and they determine the structure of cells and tissues. This represents only a very brief introduction to the biological functions of biopolymers. For a detailed discussion on this topic the reader is referred to van der Maarel (2008) and Voet et al. (2010). Lipids are macromolecules but not polymers because of their structure, see Voet et al. (2010). They are not made up of repeating chains of monomers. Water takes 70 percent of a total cell weight, proteins, nucleic acids, and polysaccharides around 26 percent (Alberts et al. 2008). For more information of its structures and functions of each component, the reader is referred to Alberts et al. (2008).

In polymer physics two measurements are essential, the contour length L and the persistence length L_p. The contour length is the total unfolded length of a polymer or in other words the arc length along the polymer backbone. The persistence length is a measure of the bending stiffness of polymers and it describes the flexibility of a polymer chain. This is characterized by its flexural rigidity B with units of $\mathrm{Pa\,m^4}$. In the beam theory, which is a field within the linear theory of elasticity, the flexural rigidity can be written as a product of the Young's modulus E and the second moment of inertia I, i.e. $B = EI$. The filament's shape fluctuates at finite temperature T and thus it yields thermal energy, which we write as a product of the Boltzmann constant k_B and the temperature. The persistence length is a characteristic length scale which is direct proportional to the flexural rigidity and inversely proportional to thermal energy, such that

$$L_\mathrm{p} = \frac{EI}{k_\mathrm{B}T}. \tag{1.1}$$

Through a variety of experimental methods the persistence length can be measured.

Biopolymers exhibit different behaviors in terms of their flexibility. Thus, we classify each type of biopolymer in one of the three categories, flexible, semiflexible or rigid. If $L_\mathrm{p} \gg L$, we say that the polymer is rigid and it means that the thermal energy is not sufficient to bend its contour. This kind of polymers exhibits virtually no entropic elasticity. Conversely, if the persistence length is much smaller than the contour length, i.e. $L_\mathrm{p} \ll L$, the filament is called flexible and its thermal fluctuations dominate. The entropy is of crucial impact to straightening this kind of polymers. The last type of polymers is called semiflexible. This category includes those polymers whose persistence and contour lengths are of the same order. Most of the biologically relevant polymers belong to this category. This kind of polymers exhibits a balance between the thermal fluctuation and the stiffness of the filament.

1.2 F-actin

Actin filaments are one of the major components within the cytoskeleton. They belong to the structural proteins which make significant contributions to determine the shape of the cell surface. Further, they play a key role in the mechanical response of the cell and cell motility. The subunit of actin filament is globular actin (G-actin) which polymerizes to long filamentous F-actin. The structure of F-actin is composed of two chains of polymerized G-actin, which are arranged helically, see Figure 1.2. More detailed information on

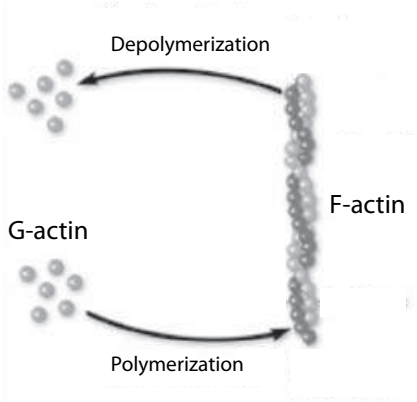

Figure 1.2: Actin filament, adopted from Kamm and Mofrad (2006)

the biology of actin filament can be found in Alberts et al. (2008). The mechanical properties of F-actin are well known. It measures a diameter of about $8\,\mathrm{nm}$ (Ott et al. 1993), Le Goff et al. (2002) determined the persistence length of about $16\,\mu\mathrm{m}$ and its specific contour length which depends on the experiments, measures *in vitro* $10 - 20\,\mu\mathrm{m}$ (Liu and Pollack 2002) and *in vivo* $\sim 1\,\mu\mathrm{m}$ (Fernández et al. 2006). F-actin belongs to the class of semiflexible polymers.

1.3 Fibrin

Fibrin is an essential component of hemostasis. Together with platelets they stop bleeding by forming blood clots in the injuries of blood vessels. Fibrin gives the major structural framework of blood clots (Weisel 2004) and as a result wound healing takes place. The blood clot has to be strong enough to be resistant to the shearing force of the blood stream. The process of blood clotting starts when the precursor protein fibrinogen is converted to fibrin by the enzyme thrombin. A schematic diagram of the formation of fibrin is illustrated in Figure 1.3 which we adopted from Mosesson (2005). In more detail, fibrinogen is synthesized by the liver and it is an elongated protein with $45\,\mathrm{nm}$ in length, see Weisel (2004). By cleaving fibrinopeptides from the central domain of fibrinogen through thrombin, the exposed knobs can interact with the ends of another molecule. It results in a half

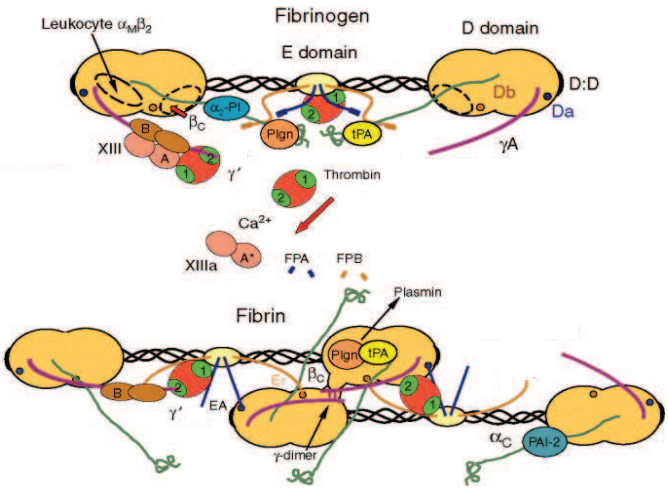

Figure 1.3: Schematic diagram of the structure of fibrinogen and the formation of fibrin, adopted from Mosesson (2005)

staggered structure, which is called protofibril and which has a periodicity of $22.5\,\mathrm{nm}$. The aggregation of protofibrils forms a fibrin fiber. The average concentration of fibrinogen in the blood is about $2.5\,\mathrm{g/l}$ (Weisel 2004). The transglutaminase factor XIIIa or the fibrin stabilizing factor, respectively, is an enzyme that ligates fibrin to form an insoluble clot or fibrin polymer. These ligations increase the stiffness of the clot substantially. Fibrin exhibits viscoelastic properties which are analyzed in detail in Weisel (2004).

2 Continuum mechanics

Continuum mechanics describes the motion and deformation of continuous media under the influence of forces. The matter is composed of molecules which are formed by atomic and subatomic particles. In the continuum theory the molecular structure of the material is neglected and only the behavior of the material as a whole is deemed important. For this reason it is assumed that the material is continuously distributed throughout its volume and it completely fills the space it occupies. In this way the macroscopic behavior is explained. The subject of continuum mechanics is commonly divided into three main parts, see, e.g., Holzapfel (2000). The first part is the kinematics, the study of motion and deformation. The concept of stress, that means the study of stress in a continuum, is the second part. And the third part treats the constitutive equations, which establish the relations between stresses and deformations. These three parts must comply with the balance principles, the mathematical description of the fundamental laws of physics governing the motion of a continuum. These need to be fulfilled in all points and times. More detailed information on continuum mechanics is also given by Ogden (1997).

2.1 Kinematics

The kinematics describes the changes of a continuum body over time, without considering the forces that cause these changes. The (solid) body is formed by a coherent set of material points or particles and is subjected to different types of configuration during the motion, which we specify next.

2.1.1 Configuration and motion

We denote a continuum body by $\mathcal{B}$ and represent a particle of it by $P \in \mathcal{B}$. A configuration of $\mathcal{B}$ is defined by a one-to-one mapping $\boldsymbol{\kappa}\colon \mathcal{B} \to \mathbb{E}^3$, which takes the particles of $\mathcal{B}$ to a region in the Euclidean space $\mathbb{E}^3$, as depicted in Figure 2.1. The region, indicated by Ω, is the image set of the configuration $\boldsymbol{\kappa}$ and a subset of $\mathbb{E}^3$. We define Ω as a set of places occupied by the particles of $\mathcal{B}$ through

$$\Omega := \boldsymbol{\kappa}(\mathcal{B}) = \{\boldsymbol{\kappa}(P), P \in \mathcal{B}\} \subset \mathbb{E}^3. \tag{2.1}$$

At a freely chosen but fixed reference time t, we identify the image of $\boldsymbol{\kappa}$ as reference (or undeformed) configuration. It is common but not necessary to choose the reference time at $t = 0$. This is why we label the reference configuration and region by the subscript 0, i.e.

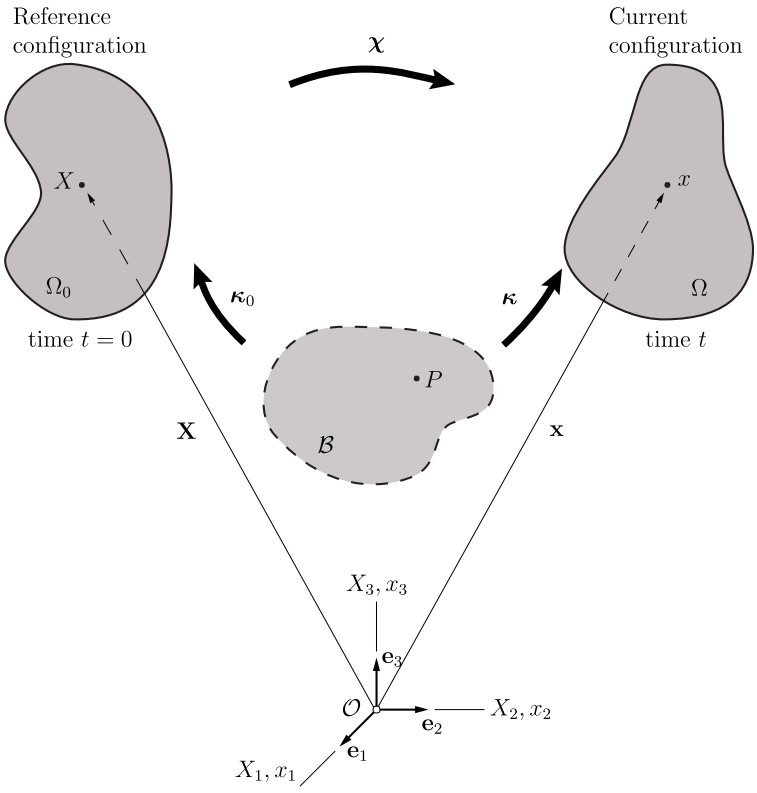

Figure 2.1: Configuration and motion

by $\boldsymbol{\kappa}_0$ and Ω_0, respectively, as we see in Figure 2.1. The body $\mathcal{B}$ deforms subsequently and moves over a period of time $t \in \mathbb{R}^+$ and this configuration of $\mathcal{B}$ at t is known as current (or deformed) configuration. The place (or position vector) $\mathbf{x}$ occupied by the particle $P \in \mathcal{B}$ in the configuration $\boldsymbol{\kappa}$ is constituted by

$$\mathbf{x} = \boldsymbol{\kappa}(P), \quad P = \boldsymbol{\kappa}^{-1}(\mathbf{x}), \tag{2.2}$$

see Figure 2.1. Moreover, it is common to distinguish between material (or referential) coordinates, which is often referred to as the Lagrangian description, and the spatial (or current) coordinates, which is referred to as the Eulerian description. In the Lagrangian description, we observe the changes of a particular particle throughout the deformation process, however in the Eulerian description, we observe what happens at a spatially fixed observation point as time changes. For further notations, we label uppercase letters for the reference configuration and lowercase letters for the current configuration. In the reference configuration we define the position vector $\mathbf{X}$ by its components $X_A, A = 1, 2, 3,$ relative to some coordinate system with orthonormal basis $\{\mathbf{E}_A\}$ centered at some convenient origin $\mathcal{O}$, $\mathbf{X} = X_A \mathbf{E}_A$. The position vector $\mathbf{x}$ in the current configuration is represented by its components $x_a, a = 1, 2, 3,$ which are relative to a coordinate system with orthonormal

basis $\{\mathbf{e}_a\}$ centered at o, $\mathbf{x} = x_a\mathbf{e}_a$. In the following we assume the origins $\mathcal{O}, o$ and the basis vectors of reference and spatial coordinates to coincide, i.e. the set of $\{\mathbf{E}_A\}$ is identical to $\{\mathbf{e}_a\}$.

The motion of the body $\mathcal{B}$ can be described by a one-parameter family of configurations $\boldsymbol{\kappa}_t\colon \mathcal{B} \to \mathbb{E}^3$, where t identifies the parameter. We write for the position vector of the particle $P \in \mathcal{B}$ at time t

$$\mathbf{x} = \boldsymbol{\kappa}_t(P) = \boldsymbol{\kappa}(P, t) \tag{2.3}$$

and at the given instant of time $t = 0$

$$\mathbf{X} = \boldsymbol{\kappa}_0(P), \tag{2.4}$$

respectively. If we use the inverse of the reference configuration $P = \boldsymbol{\kappa}_0^{-1}(\mathbf{X})$ in $(2.3)_2$, we obtain a definition of the motion $\boldsymbol{\chi}$ of the continuum body $\mathcal{B}$

$$\mathbf{x} = \boldsymbol{\kappa}\left(\boldsymbol{\kappa}_0^{-1}(\mathbf{X}, t)\right) =: \boldsymbol{\chi}(\mathbf{X}, t). \tag{2.5}$$

The motion is a mapping function $\boldsymbol{\chi}\colon \mathbb{E}^3 \to \mathbb{E}^3$ of the reference configuration into the current configuration in the Lagrangian description. Furthermore, we assume that $\boldsymbol{\chi}$ is continuously differentiable in finite regions so that $\boldsymbol{\chi}$ is invertible and its inverse, written in Eulerian form, is given by

$$\mathbf{X} = \boldsymbol{\chi}^{-1}(\mathbf{x}, t), \tag{2.6}$$

i.e. it identifies the particles which pass through $\mathbf{x}$ during the motion, as mentioned above.

2.1.2 Deformation gradient

The fundamental quantity in continuum mechanics is the deformation gradient which describes the deformation of a continuum body occurring when the body moves from the reference region Ω_0 to current region Ω. If the body is in motion, it is able to change its position (translation), orientation (rotation) and shape (deformation). The motion is called rigid body motion if it includes translation and rotation. It is time-dependent and means that the distance between an arbitrary pair of particles of the body remains constant. However, the deformation of a body can be characterized by the change in distance between two adjacent points. For further consideration, let the material be elastic, where deformations are history (or time) independent. The deformation gradient of Ω relative to the reference configuration Ω_0 gives the relationship of a material line $\mathrm{d}\mathbf{X}$ before deformation to the line $\mathrm{d}\mathbf{x}$ after deformation. It should be pointed out that $\mathrm{d}\mathbf{x}$ consists of the same material as $\mathrm{d}\mathbf{X}$.

Before we define $\mathrm{d}\mathbf{X}$ and $\mathrm{d}\mathbf{x}$, we consider a material (or undeformed) curve $\mathbf{X} = \boldsymbol{\Gamma}(\xi)$ in the reference configuration and the spatial (or deformed) curve $\mathbf{x} = \boldsymbol{\gamma}(\xi, t)$ at time t in the current configuration, where ξ denotes the parametrization indicated in Figure 2.2. By using equation $(2.5)_2$, we define the parametric equation for the spatial curve at a fixed time t

$$\mathbf{x} = \boldsymbol{\gamma}(\xi, t) = \boldsymbol{\chi}(\boldsymbol{\Gamma}(\xi), t). \tag{2.7}$$

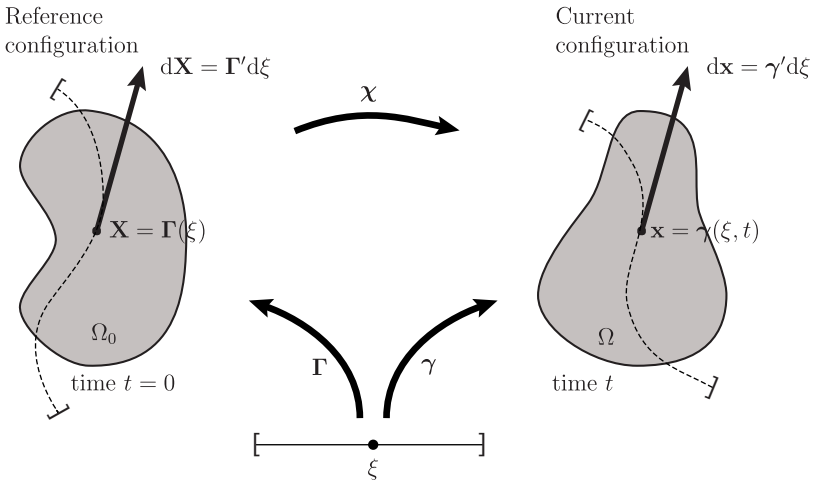

Figure 2.2: Deformation of a material curve $\boldsymbol{\Gamma} \subset \Omega_0$ into a spatial curve $\boldsymbol{\gamma} \subset \Omega$

Now we define the material tangent vector $\mathrm{d}\mathbf{X}$ and the spatial tangent vector $\mathrm{d}\mathbf{x}$

$$\mathrm{d}\mathbf{X} = \boldsymbol{\Gamma}'(\xi)\mathrm{d}\xi, \qquad \mathrm{d}\mathbf{x} = \boldsymbol{\gamma}'(\xi, t)\mathrm{d}\xi, \tag{2.8}$$

where the prime denotes differentiation with respect to ξ. By using $(2.7)_2$, $(2.8)_1$ and the chain rule we get

$$\frac{\mathrm{d}\mathbf{x}}{\mathrm{d}\xi} = \boldsymbol{\gamma}'(\xi, t) = \frac{\partial \boldsymbol{\chi}(\mathbf{X}, t)}{\partial \mathbf{X}} \boldsymbol{\Gamma}'(\xi) = \frac{\partial \boldsymbol{\chi}(\mathbf{X}, t)}{\partial \mathbf{X}} \frac{\mathrm{d}\mathbf{X}}{\mathrm{d}\xi}, \tag{2.9}$$

and by definition of the deformation gradient through

$$\mathbf{F}(\mathbf{X}, t) := \frac{\partial \boldsymbol{\chi}(\mathbf{X}, t)}{\partial \mathbf{X}}, \tag{2.10}$$

we receive the fundamental relation

$$\mathrm{d}\mathbf{x} = \mathbf{F}(\mathbf{X}, t)\mathrm{d}\mathbf{X}. \tag{2.11}$$

The deformation gradient $\mathbf{F}$ is a second order tensor and it contains the information about the local behavior of motion in the neighborhood of a point. More specifically, the deformation gradient describes the change in length and orientation of an arbitrary line element $\mathrm{d}\mathbf{X}$ at $\mathbf{X}$ in the reference configuration to the line element $\mathrm{d}\mathbf{x}$ at $\mathbf{x}$ in the current configuration. In the physical sense, we demand that $\mathbf{F}\mathrm{d}\mathbf{X} \neq \mathbf{0}$ holds for all $\mathrm{d}\mathbf{X} \neq \mathbf{0}$, i.e. the deformation gradient $\mathbf{F}$ is a non-singular tensor. This requires the condition

$$J(\mathbf{X}, t) := \det \mathbf{F}(\mathbf{X}, t) \neq 0, \tag{2.12}$$

where we defined J as the Jacobian determinant. Since $J \neq 0$, there exists the inverse of the deformation gradient $\mathbf{F}^{-1}$,

$$\mathbf{F}^{-1}(\mathbf{x}, t) = \frac{\partial \boldsymbol{\chi}^{-1}(\mathbf{x}, t)}{\partial \mathbf{x}}. \tag{2.13}$$

Next, we consider the transformation of surface and volume elements. First, we investigate the change of an infinitesimal volume element between the reference $\mathrm{d}V$ and current $\mathrm{d}v$ configurations. The volume of the infinitesimal parallelepiped whose edges are $\mathrm{d}\mathbf{X}^{(1)}, \mathrm{d}\mathbf{X}^{(2)}, \mathrm{d}\mathbf{X}^{(3)}$ is given by

$$\mathrm{d}V = \left(\mathrm{d}\mathbf{X}^{(1)} \times \mathrm{d}\mathbf{X}^{(2)}\right) \cdot \mathrm{d}\mathbf{X}^{(3)} = \det\left(\mathrm{d}\mathbf{X}^{(1)}, \mathrm{d}\mathbf{X}^{(2)}, \mathrm{d}\mathbf{X}^{(3)}\right). \tag{2.14}$$

In the current configuration we obtain

$$\begin{aligned} \mathrm{d}v &= \left(\mathrm{d}\mathbf{x}^{(1)} \times \mathrm{d}\mathbf{x}^{(2)}\right) \cdot \mathrm{d}\mathbf{x}^{(3)} \\ &= \left(F_{1i}\mathrm{d}X_i^{(1)} \times F_{2i}\mathrm{d}X_i^{(2)}\right) \cdot F_{3i}\mathrm{d}X_i^{(3)} \\ &= \det\mathbf{F}\left(\mathrm{d}\mathbf{X}^{(1)} \times \mathrm{d}\mathbf{X}^{(2)}\right) \cdot \mathrm{d}\mathbf{X}^{(3)} \\ &= \det\mathbf{F}\mathrm{d}V = J\mathrm{d}V, \end{aligned} \tag{2.15}$$

where we can infer that the Jacobian determinant J is a measure for volume change. If $J = 1$ we say that the material is incompressible and its deformation is called isochoric or volume-preserving. This implies that the volume does not change during deformation. In the physical sense, we require that the volume of a material element should be positive, so that we can conclude from (2.15) that

$$J(\mathbf{X}, t) = \det\mathbf{F}(\mathbf{X}, t) > 0. \tag{2.16}$$

Finally, we consider the neighborhood of the point $\mathbf{X} \in \mathcal{B}_0$, which we label as an infinitesimal vector element of material surface $\mathrm{d}\mathbf{S}$. Let $\mathbf{N}$ be a unit vector normal to a infinitesimal surface element $\mathrm{d}S$, then $\mathrm{d}\mathbf{S} = \mathbf{N}\mathrm{d}S$. In the current configuration $\mathbf{n}$ is a unit vector normal to the surface $\mathrm{d}s$, such that $\mathrm{d}\mathbf{s} = \mathbf{n}\mathrm{d}s$. The infinitesimal volume element $\mathrm{d}v$ is now expressed by a dot product $\mathrm{d}v = \mathrm{d}\mathbf{s} \cdot \mathrm{d}\mathbf{x}$. Equation (2.15) yields

$$\mathrm{d}v = \mathrm{d}\mathbf{s} \cdot \mathrm{d}\mathbf{x} = J\mathrm{d}V = J\mathrm{d}\mathbf{S} \cdot \mathrm{d}\mathbf{X} \tag{2.17}$$

and with (2.11) and the rule $\mathbf{u} \cdot \mathbf{A}\mathbf{v} = \mathbf{A}^\top\mathbf{u} \cdot \mathbf{v}$ we obtain

$$\left(\mathbf{F}^\top\mathrm{d}\mathbf{s} - J\mathrm{d}\mathbf{S}\right) \cdot \mathrm{d}\mathbf{X} = 0. \tag{2.18}$$

The latter equation holds for arbitrary material line elements $\mathrm{d}\mathbf{X}$, hence it follows

$$\left(\mathbf{F}^\top\mathrm{d}\mathbf{s} - J\mathrm{d}\mathbf{S}\right) = \mathbf{0}. \tag{2.19}$$

Consequently, we obtain the relation between the vector elements of the infinitesimally small areas $\mathrm{d}\mathbf{s}$ and $\mathrm{d}\mathbf{S}$

$$\mathrm{d}\mathbf{s} = J\mathbf{F}^{-\top}\mathrm{d}\mathbf{S}, \tag{2.20}$$

which is known as Nanson's formula.

2.1.3 Decomposition of deformations

In the section above, the deformation gradient supplies the transfer of the material line from $\mathrm{d}\mathbf{x}$ to $\mathrm{d}\mathbf{X}$ and it includes both information about the change in length and orientation. We want to use a strain measure instead of $\mathbf{F}$, which either refers to the reference or current configuration and where the rigid body motion has no effect. In this section we will extract the information of interest out of the deformation gradient. The polar decomposition theorem, a fundamental theorem in continuum mechanics, yields the possibility to do that. Ogden (1997, p. 92) mentioned it as follows

Theorem 2.1.1. (Polar decomposition) *For any non-singular second order tensor* $\mathbf{F}$ *there exist unique positive definite symmetric second-order tensors* $\mathbf{U}$ *and* $\mathbf{v}$ *(i.e.* $\mathbf{U} = \mathbf{U}^\top, \mathbf{v} = \mathbf{v}^\top$*) and an orthogonal second-order tensor* $\mathbf{R}$ *(i.e.* $\mathbf{R}^{-1} = \mathbf{R}^\top$*) such that*

$$\mathbf{F} = \mathbf{R}\mathbf{U} = \mathbf{v}\mathbf{R} \tag{2.21}$$

Proof. see Ogden (1997, p. 92) □

The right (or material) stretch tensor $\mathbf{U}$ and the left (or spatial) stretch tensor $\mathbf{v}$ measure the local stretch or contraction. The right stretch tensor $\mathbf{U}$ acts on the reference configuration while the left stretch tensor $\mathbf{v}$ acts on the current configuration. Whereas, the rotation tensor $\mathbf{R}$ measures the local rotation and maps between the reference and current configurations. By using equation (2.11) and $(2.21)_1$, we obtain

$$\mathrm{d}\mathbf{x} = \mathbf{R}(\mathbf{U}\mathrm{d}\mathbf{X}). \tag{2.22}$$

This equation can be interpreted as follows, first the material line $\mathrm{d}\mathbf{X}$ is stretched by $\mathbf{U}$ and then rotated into the spatial line $\mathrm{d}\mathbf{x}$ by $\mathbf{R}$. Hence, the tensor $\mathbf{R}$ maps from the reference configuration to current configuration, like $\mathbf{F}$. If $\mathbf{R} = \mathbf{I}$, the deformation is called pure stretch and if $\mathbf{U} = \mathbf{v} = \mathbf{I}$, it is referred to as rigid body motion. Another important strain measure in material coordinates is the right Cauchy-Green tensor $\mathbf{C}$, which is introduced through

$$\mathbf{C} = \mathbf{F}^\top\mathbf{F}. \tag{2.23}$$

On use of $(2.21)_1$, we get the relation between right Cauchy-Green and right stretch tensor

$$\mathbf{C} = \mathbf{U}^\top\mathbf{R}^\top\mathbf{R}\mathbf{U} = \mathbf{U}^2. \tag{2.24}$$

Since $\mathbf{U}$ is symmetric we are able to conclude that $\mathbf{C}$ is symmetric as well. As we can see, the rigid rotation is eliminated in equation (2.24). For the sake of completeness, we

introduce the left Cauchy-Green tensor $\mathbf{b}$, which is a strain measure with respect to spatial coordinates and is defined by

$$\mathbf{b} = \mathbf{F}\mathbf{F}^{\top}. \tag{2.25}$$

Using equation $(2.21)_2$, we obtain the relation of the left Cauchy-Green to the left stretch tensor, by

$$\mathbf{b} = \mathbf{v}\mathbf{R}\mathbf{R}^{\top}\mathbf{v}^{\top} = \mathbf{v}^2, \tag{2.26}$$

and by using equation $(2.21)_1$ and (2.24), we achieve the relation between the left and the right Cauchy-Green tensor, through

$$\mathbf{b} = \mathbf{R}\mathbf{U}\mathbf{U}^{\top}\mathbf{R}^{\top} = \mathbf{R}\mathbf{C}\mathbf{R}^{\top}. \tag{2.27}$$

A brief physical interpretation of $\mathbf{U}$ is now mentioned. We consider the distance between two points $\mathbf{X} \in \Omega_0$ and $\mathbf{Y} \in \Omega_0$, where $\mathbf{Y}$ is very close to $\mathbf{X}$, as shown in Figure 2.3. We

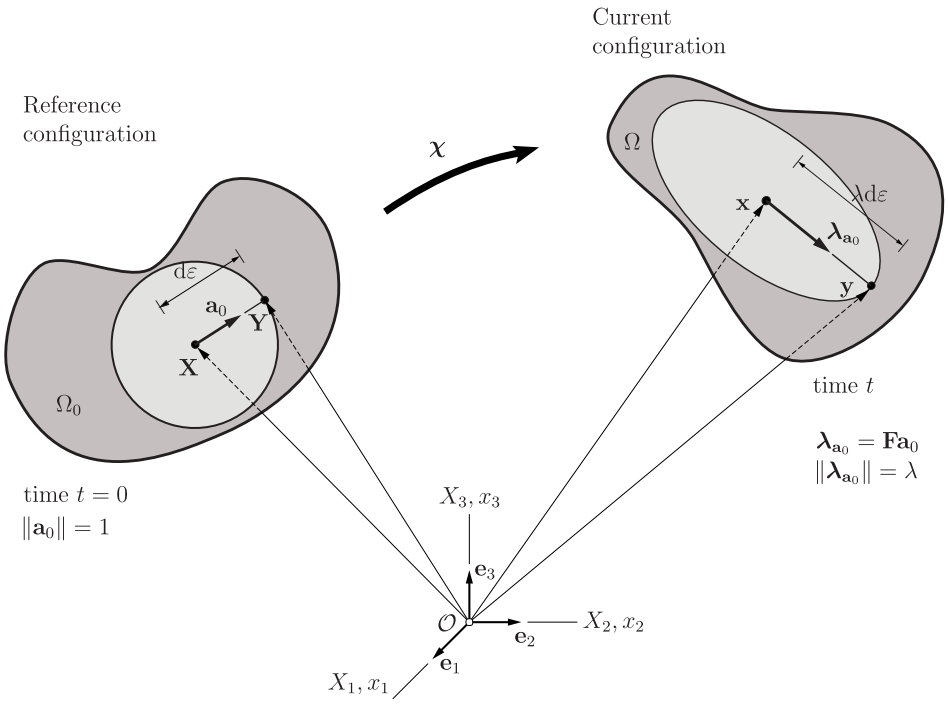

Figure 2.3: Deformation of a material line element into a spatial line element

denote $\mathrm{d}\varepsilon = \|\mathbf{Y}-\mathbf{X}\|$ as the length of the material line $\mathrm{d}\mathbf{X} = \mathbf{Y}-\mathbf{X}$ in the Euclidean norm. From the geometric view $\mathrm{d}\varepsilon$ denotes the radius of a sphere with center $\mathbf{X}$. The direction of $\mathrm{d}\mathbf{X}$ is described by the unit vector $\mathbf{a}_0$, i.e. $\|\mathbf{a}_0\| = 1$. In the current configuration, by applying the deformation gradient to $\mathbf{a}_0$, we obtain the stretch vector $\boldsymbol{\lambda}_{\mathbf{a}_0}$ through

$$\boldsymbol{\lambda}_{\mathbf{a}_0} = \mathbf{F}\mathbf{a}_0. \tag{2.28}$$

Now, consider the two neighboring points $\mathbf{x}$ and $\mathbf{y}$ in the current configuration. The difference of this two points can be linearly approximated by using Taylor's expansion, such that

$$\mathbf{y} - \mathbf{x} \approx \|\mathbf{Y} - \mathbf{X}\|\mathbf{F}\mathbf{a}_0 = \mathrm{d}\varepsilon\boldsymbol{\lambda}_{\mathbf{a}_0}, \tag{2.29}$$

see Holzapfel (2000, Sec. 2.5). The stretch λ in the direction $\mathbf{a}_0$ at $\mathbf{X}$ is defined by the ratio of current to reference lengths, i.e.

$$\lambda = \frac{\|\mathbf{y} - \mathbf{x}\|}{\|\mathbf{Y} - \mathbf{X}\|} = \|\boldsymbol{\lambda}_{\mathbf{a}_0}\| \tag{2.30}$$

the stretch ratio is given by the length of $\boldsymbol{\lambda}_{\mathbf{a}_0}$ and therefore always positive. The change in length referring to the current configuration is therefore determined by

$$\|\mathbf{y} - \mathbf{x}\| = \|\boldsymbol{\lambda}_{\mathbf{a}_0}\|\mathrm{d}\varepsilon = \lambda\mathrm{d}\varepsilon. \tag{2.31}$$

If $\lambda > 1, \lambda = 1$ or $\lambda < 1$ we say that there is an expansion, no stretch or compression, respectively, in the current configuration. Now, we consider the square of λ,

$$\begin{aligned} \lambda^2 = \|\boldsymbol{\lambda}_{\mathbf{a}_0}\|^2 &= \boldsymbol{\lambda}_{\mathbf{a}_0} \cdot \boldsymbol{\lambda}_{\mathbf{a}_0} = \mathbf{F}\mathbf{a}_0 \cdot \mathbf{F}\mathbf{a}_0 \\ &= \mathbf{a}_0 \cdot \mathbf{F}^\top\mathbf{F}\mathbf{a}_0 = \mathbf{a}_0 \cdot \mathbf{C}\mathbf{a}_0 > 0 \quad \text{for } \mathbf{a}_0 \neq \mathbf{0}. \end{aligned} \tag{2.32}$$

In addition to the already known symmetry of $\mathbf{C}$, equation (2.24), we can deduce now from equation (2.32) that $\mathbf{C}$ is positive definite at each $\mathbf{X} \in \Omega_0$. Due to the positive definiteness of $\mathbf{C}$, we can infer that the equation (2.32) defines an ellipsoid centered on $\mathbf{x}$. With respect to a geometrical interpretation, we are able to say that the stretch tensor $\mathbf{U}$ or Cauchy-Green tensor $\mathbf{C}$, respectively, transforms the material within a sphere in the reference configuration into an ellipsoid in the current configuration, see Figure 2.3.

2.1.4 Examples of deformations

We complete the section kinematics with two examples of deformations, which we will use in the course of this work. The first assumption we make is that the deformation of the body is homogeneous, i.e. independent of the position vector $\mathbf{X}$. A further assumption is that the material is incompressible, meaning that the volume of the body remains constant. In this case, the deformation is referred to as isochoric and $\det \mathbf{F} = 1$ holds.

At first we discuss the equibiaxial deformation. Since the basis vectors in reference and current configurations coincide, the deformation of the body in the current configuration can be specified generally in the form

$$x_1 = \lambda_1 X_1, \quad x_2 = \lambda_2 X_2, \quad x_3 = \lambda_3 X_3, \tag{2.33}$$

where λ_1, λ_2 and λ_3 denotes the stretch ratio in x_1-, x_2- and x_3-directions. The deformation gradient, which we defined in (2.10), with respect to the chosen reference and current basis

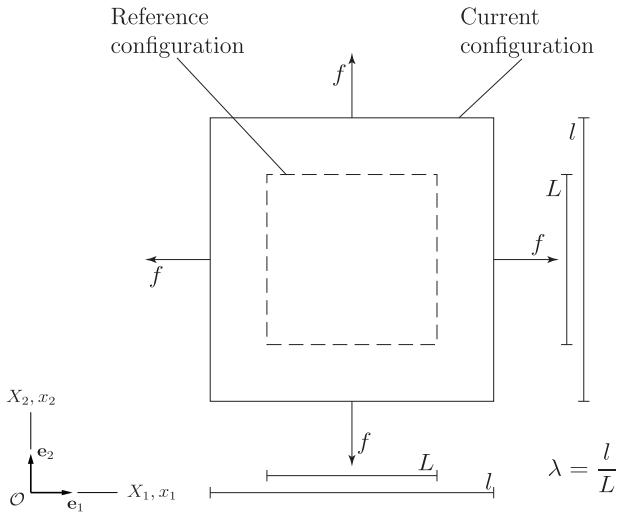

Figure 2.4: Equibiaxial deformation in which the force f causes an uniform extension λ in x_1- and x_2-direction. The dashed line represents the body with length L in x_1- and x_2-direction in reference configuration and the solid line illustrates the body with equal length of l in both axes direction in current configuration.

vectors has the following matrix representation

$$[\mathbf{F}] = \begin{bmatrix} \lambda_1 & 0 & 0 \\ 0 & \lambda_2 & 0 \\ 0 & 0 & \lambda_3 \end{bmatrix}. \tag{2.34}$$

Now, consider a body in x_1x_2-plane, which we stretch by λ uniformly in x_1- and x_2-direction, as pictured in Figure 2.4. In this sense, $\lambda_1 = \lambda_2 = \lambda$ and by the condition of isochoric deformation, i.e. $\det \mathbf{F} = \lambda_1\lambda_2\lambda_3 = 1$, we obtain $\lambda_3 = \lambda^{-2}$. Finally, the equibiaxial deformation has the matrix representation

$$[\mathbf{F}] = \begin{bmatrix} \lambda & 0 & 0 \\ 0 & \lambda & 0 \\ 0 & 0 & \lambda^{-2} \end{bmatrix}. \tag{2.35}$$

The second type of deformation, which we mention here, is the simple shear deformation, which is illustrated by Figure 2.5. Based on this illustration we can specify the deformation of the body in current configuration in the following way

$$\begin{aligned} x_1 &= X_1 + (\tan\varphi)\, X_2, \\ x_2 &= X_2, \\ x_3 &= X_3. \end{aligned} \tag{2.36}$$

The simple shear deformation is defined as an isochoric plane deformation, which means

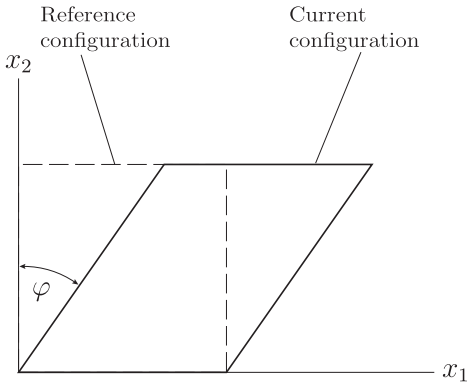

Figure 2.5: Simple shear deformation with shear angle φ and deformation $\gamma = \tan\varphi$. No change in length and orientation occurs in x_1-direction. The dashed line represents the body in the reference configuration and the solid line in the current configuration.

that the deformation is restricted to two axes, e.g. on x_1- and x_2-direction. Beyond that, no shear deformations may occur in x_3-direction. From this consideration, the body does not change its length and direction by the deformation in x_1-direction. By defining the amount of shear through $\gamma = \tan\varphi$, the deformation gradient in matrix form is deducible from equations (2.36) and with equation (2.10), such that

$$[\mathbf{F}] = \begin{bmatrix} 1 & \gamma & 0 \\ 0 & 1 & 0 \\ 0 & 0 & 1 \end{bmatrix} . \tag{2.37}$$

2.2 Concept of stress

The previous section dealt with the motion and especially the deformation of a continuum body. This is caused by external forces acting on the body and give rise to interactions between neighboring material points in the interior part of the body. In order to study these, we introduce the concept of stress.

Let us consider a deformable body during a finite motion. At time t the body $\mathcal{B}$ occupies an arbitrary region Ω with boundary surface $\partial\Omega$, as shown in Figure 2.6. We distinguish between external forces, which act on parts or the whole of the boundary surface, and the internal forces, which act on an imaginary surface within the interior of the body. Let the body be separated into two parts by a plane surface. As illustrated in Figure 2.6, we denote $\mathbf{n}$ as an outward normal vector relative to an infinitesimal spatial surface element $\mathrm{d}s$ at the point $\mathbf{x}$. The plane surface passes through the material point $\mathbf{x}$. The Cauchy (or true) traction vector $\mathbf{t}$ is a measure of force per unit area. Analogously, the quantities $\mathbf{X}, \mathrm{d}S, \mathbf{N}$ and $\mathbf{T}$ are defined in the reference configuration. The vector $\mathbf{t}$ depends linearly on the surface normal. This leads us to another important axiom in continuum mechanics.

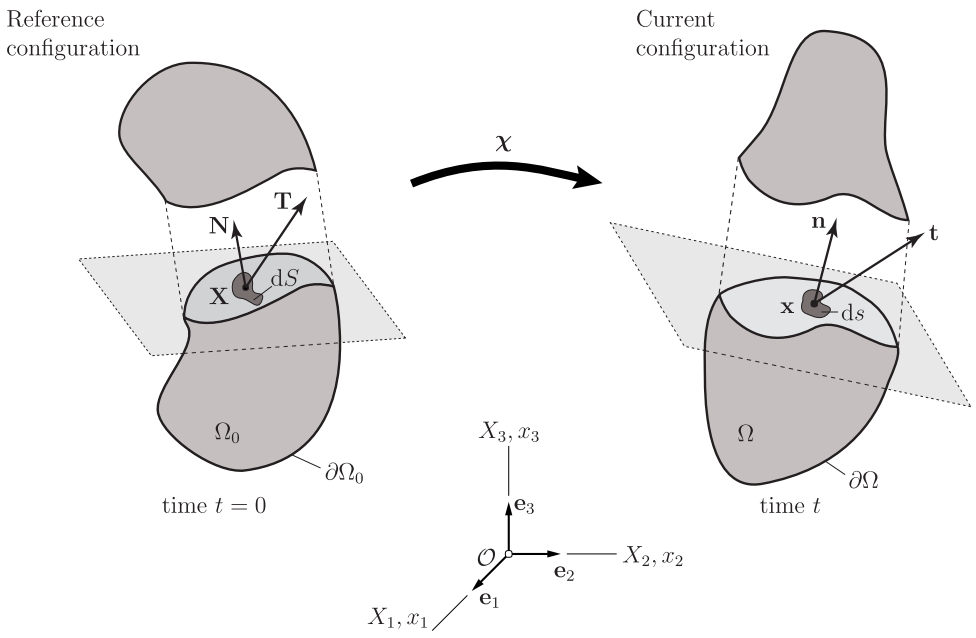

Figure 2.6: The concept of stress

Theorem 2.2.1. (Cauchy's theorem) *The stress vector* $\mathbf{t}(\mathbf{x}, \mathbf{n}, t)$ *in a point* $\mathbf{x}$ *of a body depends linearly on the normal* $\mathbf{n}$ *of a surface element, i.e. there exists a second-order tensor field* $\boldsymbol{\sigma}$ *independent of* $\mathbf{n}$ *such that*

$$\mathbf{t}(\mathbf{x}, \mathbf{n}, t) = \boldsymbol{\sigma}(\mathbf{x}, t)\mathbf{n}. \tag{2.38}$$

Proof. see Ogden (1997, Sec. 3.3) □

The second-order tensor $\boldsymbol{\sigma}$ is a spatial tensor and known as Cauchy (or true) stress tensor. In order to satisfy the conservation of angular momentum in the static equilibrium, we need the necessary and sufficient condition that the Cauchy stress tensor is symmetric, i.e. $\boldsymbol{\sigma} = \boldsymbol{\sigma}^\top$. Using equation (2.38) and Nanson's formula (2.20) the traction on an area element $\mathrm{d}s$ in the current configuration can be represented

$$\mathbf{t}\mathrm{d}s = \boldsymbol{\sigma}\mathbf{n}\mathrm{d}s = J\boldsymbol{\sigma}\mathbf{F}^{-\top}\mathbf{N}\mathrm{d}S. \tag{2.39}$$

Thus we are able to define the first Piola-Kirchhoff stress tensor $\mathbf{P}$ by

$$\mathbf{P} := J\boldsymbol{\sigma}\mathbf{F}^{-\top}. \tag{2.40}$$

The nominal stress tensor or engineering stress $\mathbf{P}^\top$ is often used to represent experimental data. Now, we are able to formulate for the traction vector $\mathbf{T}$ a similar relation, as was

postulated in the Cauchy's theorem for $\mathbf{t}$

$$\mathbf{T}(\mathbf{X}, \mathbf{N}, t) = \mathbf{P}(\mathbf{X}, t)\mathbf{N}. \tag{2.41}$$

Derivation of the relation between $\boldsymbol{\sigma}$ and $\mathbf{P}$ can be done by

$$\begin{aligned} \mathbf{t}\mathrm{d}s &= \mathbf{T}\mathrm{d}S \\ \boldsymbol{\sigma}\mathbf{n}\mathrm{d}s &= \mathbf{P}\mathbf{N}\mathrm{d}S \\ \boldsymbol{\sigma}\mathrm{d}\mathbf{s} &= \mathbf{P}\mathrm{d}\mathbf{S}. \end{aligned} \tag{2.42}$$

Completing this section, we introduce further stress tensors, which are commonly used in practical nonlinear mechanics. A very useful stress tensor in computational mechanics is the second Piola-Kirchhoff stress tensor $\mathbf{S}$, which describes the state of stress in the reference configuration and is defined by

$$\mathbf{S} = J\mathbf{F}^{-1}\boldsymbol{\sigma}\mathbf{F}^{-\top} = \mathbf{F}^{-1}\mathbf{P}. \tag{2.43}$$

By restatement latter equation we get the following expression for the Cauchy stress tensor

$$\boldsymbol{\sigma} = J^{-1}\mathbf{F}\mathbf{S}\mathbf{F}^{\top} = J^{-1}\mathbf{P}\mathbf{F}^{\top}. \tag{2.44}$$

If we consider

$$\mathbf{S}^{\top} = J\mathbf{F}^{-1}\boldsymbol{\sigma}^{\top}\mathbf{F}^{-\top}, \tag{2.45}$$

we can infer that $\mathbf{S}$ is symmetric because $\boldsymbol{\sigma}$ is symmetric. However, the first Piola-Kirchhoff stress tensor $\mathbf{P}$ is in general not symmetric but it satisfies the connection

$$\mathbf{F}\mathbf{P} = \mathbf{S}^{\top}\mathbf{F}^{\top}. \tag{2.46}$$

Another useful measure of stress is the Kirchhoff stress $\boldsymbol{\tau}$, which also has no obvious physical interpretation. This is defined by

$$\boldsymbol{\tau} = J\boldsymbol{\sigma}. \tag{2.47}$$

and compared with $(2.44)_1$ yields

$$\boldsymbol{\tau} = \mathbf{F}\mathbf{S}\mathbf{F}^{\top}. \tag{2.48}$$

Note, for incompressible materials ($J = 1$) $\boldsymbol{\tau} = \boldsymbol{\sigma}$ holds.

2.3 Balance laws and constitutive equations

The basic equations consist of the classical balance principles and the constitutive (or material) equations. Thereby the balance equations describe the universal principle which are axiomatically required for all points of the material body $\mathcal{B}$ and must be satisfied for all times t. The constitutive equations provide the link between the quantities of the kine-

matics and kinetics, which we introduced in Section 2.1 and 2.2, for example the relation between stress and deformation. Furthermore, the material equations represent the individual characteristic of any particular material.

In the literature usually the following three fundamental balance equations are specified, these are the conservation of mass, momentum and energy. Consider the current mass density ρ, the particle velocity $\mathbf{v}(\mathbf{x},t)$, which is defined by $\mathbf{v}(\mathbf{x},t) = \partial\mathbf{x}/\partial t$, the body force $\mathbf{b}(\mathbf{x},t)$, and the Cauchy stress $\boldsymbol{\sigma}(\mathbf{x},t)$, the following balance laws are postulated in Ogden (1997, Chap. 3).

Conservation of mass

$$\frac{\partial\rho}{\partial t} + \rho\mathrm{div}\mathbf{v} = 0 \tag{2.49}$$

Conservation of linear momentum

$$\mathrm{div}\boldsymbol{\sigma} + \rho\mathbf{b} = \rho\frac{\partial\mathbf{v}}{\partial t} \tag{2.50}$$

Conservation of angular momentum

$$\boldsymbol{\sigma} = \boldsymbol{\sigma}^{\top} \tag{2.51}$$

Equations (2.49) and (2.50) provide 4 equations for 10 unknowns (ρ, 3 components of $\mathbf{v}$ and with equation (2.51), 6 components of $\boldsymbol{\sigma}$). These balance equations provide a set of equations to describe a continuum mechanical system, but more unknown variables are involved than equations are available. The material specific behavior yields the additional equations to determine the continuum system.

The aims of constitutive laws are to develop mathematical models for representing the real behavior of matter and to determine the material response. In other words they describe an ideal material and the predictions should provide a very close approximation to the observed behavior of the real material. This can be achieved by fitting mathematical equations to experimental data. In the literature many principles are postulated which conduce to support the formulation of constitutive equations. Here we make no attempt to review the large number of constitutive theories available in continuum mechanics. We will provide the basic concept of constitutive equations. More precisely, the purpose of constitutive laws is to specify the material behavior as a function of strain and stress state in appropriate form. The crucial variable is the Helmholtz free energy function Ψ, which is referred to as the strain-energy function or stored energy function. In the hyperelasticity theory such an energy function is assumed to exist. For convenience we focus on homogeneous materials, which means the distribution of the internal structure is such, that every material point has the same mechanical behavior. The (purely mechanical) constitutive equation for hyperelastic materials is expressed by

$$\mathbf{P} = \mathfrak{G}(\mathbf{F}) = \frac{\partial\Psi(\mathbf{F})}{\partial\mathbf{F}}, \tag{2.52}$$

where $\mathfrak{G}$ is referred to as response function and $(2.52)_1$ as general constitutive law, see Holzapfel (2000, Sec. 6.1). It follows for the symmetric Cauchy stress tensor using equation $(2.44)_2$,

$$\boldsymbol{\sigma} = \mathfrak{g}(\mathbf{F}) = J^{-1}\frac{\partial \Psi(\mathbf{F})}{\partial \mathbf{F}}\mathbf{F}^{\top} = J^{-1}\mathbf{F}\left(\frac{\partial \Psi(\mathbf{F})}{\partial \mathbf{F}}\right)^{\top}. \tag{2.53}$$

The strain-energy function is a scalar-valued function of one tensorial variable. In the reference configuration where $\mathbf{F} = \mathbf{I}$ we assume that the strain-energy function vanishes. From physical view we conclude that Ψ increases with deformation. Therefore we require

$$\Psi(\mathbf{I}) = 0 \qquad \text{and} \qquad \Psi(\mathbf{F}) \geq 0. \tag{2.54}$$

At thermodynamic equilibrium the strain-energy function attains its global minimum for $\mathbf{F} = \mathbf{I}$. To guarantee the existence of (unique) solutions for a given constitutive model further conditions on the strain-energy function are necessary, for example the polyconvexity of the strain-energy function.

At the end of this section, we want to obtain a constitutive equation for an incompressible hyperelastic material, i.e. $J = \det \mathbf{F} = 1$, which we use later in Section 3.2.2. For this reason we include a side condition to the strain-energy function, which we define by a Lagrange multiplier ζ, so that

$$\Psi = \Psi(\mathbf{F}) - \zeta(J - 1) \tag{2.55}$$

holds, see Holzapfel (2000, Sec. 6.3). The Lagrange multiplier can be interpreted as a hydrostatic pressure. With (2.52) and

$$\frac{\partial J}{\partial \mathbf{F}} = J\mathbf{F}^{-\top}, \tag{2.56}$$

we obtain for the first Piola-Kirchhoff stress tensor

$$\mathbf{P} = \frac{\partial \Psi(\mathbf{F})}{\partial \mathbf{F}} - \zeta\mathbf{F}^{-\top}. \tag{2.57}$$

The second Piola-Kirchhoff stress tensor is recovered by multiplying equation (2.57) by $\mathbf{F}^{-1}$ from the lefthand

$$\mathbf{S} = \mathbf{F}^{-1}\frac{\partial \Psi(\mathbf{F})}{\partial \mathbf{F}} - \zeta\mathbf{F}^{-1}\mathbf{F}^{-\top} = \mathbf{F}^{-1}\frac{\partial \Psi(\mathbf{F})}{\partial \mathbf{F}} - \zeta\mathbf{C}^{-1}. \tag{2.58}$$

By multiplying equation (2.57) by $\mathbf{F}^{\top}$ from the righthand, the Cauchy stress tensor is a consequence of equation $(2.44)_2$

$$\boldsymbol{\sigma} = \frac{\partial \Psi(\mathbf{F})}{\partial \mathbf{F}}\mathbf{F}^{\top} - \zeta\mathbf{I}. \tag{2.59}$$

In Holzapfel (2000, Sec. 6.1) the following rule was deduced

$$\left(\frac{\partial \Psi(\mathbf{F})}{\partial \mathbf{F}}\right)^{\top} = 2\frac{\partial \Psi(\mathbf{C})}{\partial \mathbf{C}}\mathbf{F}^{\top}, \tag{2.60}$$

so that it follows

$$\boldsymbol{\sigma} = 2\mathbf{F}\frac{\partial \Psi(\mathbf{C})}{\partial \mathbf{C}}\mathbf{F}^{\top} - \zeta\mathbf{I}. \tag{2.61}$$

3 Models for biopolymers

In Section 1.1 we discussed about two different levels of organisation of biopolymers. In this chapter we want to specify the modeling on both of these organisation levels. To describe the mechanical behavior of individual polymers we use an appropriate single filament model. We are introducing different types of single filament models with reference to Kuhn (1934), Kratky and Porod (1949), and Holzapfel and Ogden (2011). These models are describing some kinds of filaments very well but differ in their approaches of basic equations. Single filament models act usually on the scale around $10\,\mathrm{nm}$. In contrast, a network model, describes the mechanical behavior of networks of polymers, incorporates the information from the single filament and acts on different length scale, from $10\,\mathrm{nm}$ up to $1\,\mu\mathrm{m}$. In addition, we will discuss in this chapter a network model, which was recently devised by Unterberger et al. (submitted). The authors formulated a multi-scale approach to modeling cross-linked actin networks. We will also specify the basic concept of this network model which is made available by Miehe et al. (2004).

3.1 Single filament model

We are interested in the behavior of elastic filaments or more specifically, in the response to an applied force acting on a filament. Currently there are two types of single filament models to study the characteristics of biopolymers which have proved to be successful. The freely-jointed chain (FJC) model which goes back to Kuhn (1934) is a rather simple model, but it provides the basic elements of single filament modeling. The second type is one of the most commonly used model, the worm-like chain (WLC) model. Its basic concept was supplied by Kratky and Porod (1949). A few decades later, several researchers provided a mathematical description of the worm-like chain model to achieve a force-extension expression. With the concept of statistical mechanics Marko and Siggia (1995), Bustamante et al. (1994) and MacKintosh et al. (1995) achieved an applicable formulation. From the view of mechanical equilibrium, Holzapfel and Ogden (2011) developed recently another approach to the worm-like chain model. The FJC model describes flexible polymers very well, whereas the WLC model is usually used for semiflexible biopolymers. Both types of models are introduced in the following section and in particular we demonstrate the mechanical approach by Holzapfel and Ogden (2011).

3.1.1 Freely-jointed chain model

The freely-jointed chain (FJC) model, introduced by Kuhn (1934), belongs to the family of discrete models. The polymer is characterized by ideal chains. This implies that we neglect the interactions among non-neighbouring monomers and describe the path traced by a polymer by random walk. Every polymer is a sequence of monomers, which are considered as a chain with N segments. These segments are linked with frictionless hinges. Each segment is regarded as a rigid rod of equal length l_k, the so-called Kuhn length, so that the contour length or total unfolded length, respectively, is $L = Nl_\mathrm{k}$, see Figure 3.1. Let $\mathbf{r}_1, \ldots, \mathbf{r}_N$ be the vectors corresponding to the individual monomers. The end-to-end

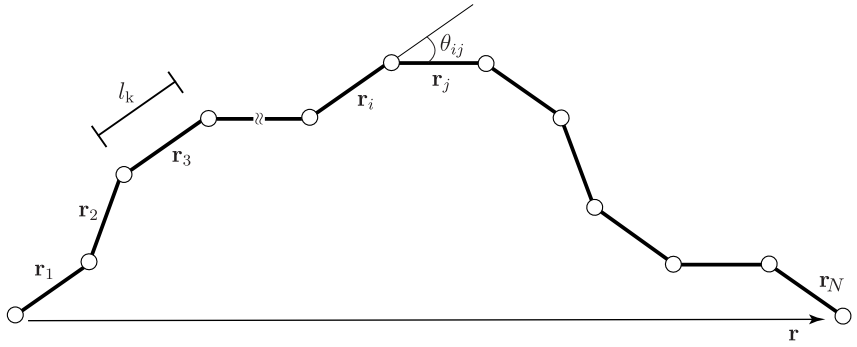

Figure 3.1: Illustration of freely-jointed chain model with N segments of length l_k, linked with hinges. The corresponding vectors to the individual monomers are $\mathbf{r}_1, \ldots, \mathbf{r}_N$ and the end-to-end vector is $\mathbf{r}$. The angle between the vectors $\mathbf{r}_i$ and $\mathbf{r}_j$ is denoted by θ_{ij}.

vector $\mathbf{r}$, the vector between the starting point of the first monomer and the endpoint of the last monomer, as shown in the Figure 3.1, is given by

$$\mathbf{r} = \sum_{i=1}^{N} \mathbf{r}_i. \tag{3.1}$$

This results in an end-to-end distance of $r = \|\mathbf{r}\|$. The inner product denoted by a dot of two vectors is

$$\begin{aligned} \mathbf{r}_i \cdot \mathbf{r}_i &= l_\mathrm{k}^2, \\ \mathbf{r}_i \cdot \mathbf{r}_j &= l_\mathrm{k}^2 \cos\theta_{ij}. \end{aligned} \tag{3.2}$$

The average over all possible chain configurations can be revealed by the mean square end-to-end distance, which are expressed as

$$\begin{aligned}\langle \mathbf{r}^2 \rangle = \langle \mathbf{r} \cdot \mathbf{r} \rangle &= \left\langle \sum_{i=1}^{N} \mathbf{r}_i \cdot \sum_{j=1}^{N} \mathbf{r}_j \right\rangle \\ &= \sum_{i=1}^{N} \langle \mathbf{r}_i \cdot \mathbf{r}_i \rangle + 2 \sum_{i=1}^{N-1} \sum_{j=i+1}^{N} \langle \mathbf{r}_i \cdot \mathbf{r}_j \rangle \\ &= N l_\mathrm{k}^2 + 2 l_\mathrm{k}^2 \sum_{i=1}^{N-1} \sum_{j=i+1}^{N} \langle \cos \theta_{ij} \rangle,\end{aligned} \tag{3.3}$$

where angle brackets denote the mean. Since the monomers are uncorrelated, meaning that $\langle \mathbf{r}_i \cdot \mathbf{r}_j \rangle = 0$ and therefore $\langle \cos \theta_{ij} \rangle = 0$, the mean square end-to-end distance for an ideal chain is accordingly

$$\langle \mathbf{r}^2 \rangle = N l_\mathrm{k}^2 = L l_\mathrm{k}. \tag{3.4}$$

By applying a force f at the ends of the chain we change the configuration of the chain and hence also its end-to-end distance r. Now we want to find a relation between these two quantities. In this way of looking, the elasticity is purely based on the entropy. In other words, we have to apply energy to lower the number of possible configurations of a chain, and this in turn means that we decrease the entropy. The entropic elasticity theory of chain molecules is explained in the context of statistical mechanics. Boltzmann's equation contributes significantly to that theory and describes the relation between the entropy η of a system and the probability distribution P. It reads as

$$\eta = k_\mathrm{B} \ln P \tag{3.5}$$

and defines the strain-energy function by

$$\psi = -\eta T, \tag{3.6}$$

where the force can be deduced by

$$f = \frac{\mathrm{d}\psi}{\mathrm{d}r}. \tag{3.7}$$

To perform latter equation for the FJC model, we have to make a quick side trip into the statistical mechanics. The FJC model can be based either on Gaussian or on non-Gaussian (inverse Langevin) statistics in order to specify the change of entropy. The Gaussian statistics, which refers to Kuhn (1934) and Kuhn (1936), does not consider the finite extensibility of the chain and the force depends linearly on the relative stretch r/L. Alternatively, the inverse Langevin statistic as introduced by Kuhn and Grün (1942), provides a nonlinear theory, which takes into account the limiting case, in which the end-to-end distance can reach only the contour length. The probability density, introduced by Kuhn and Grün

(1942), has the form

$$P = P_0 \exp\left(-N\frac{r}{L}\mathscr{L}^{-1}\left(\frac{r}{L}\right) - N\ln\left(\frac{\mathscr{L}^{-1}\left(\frac{r}{L}\right)}{\sinh\left(\mathscr{L}^{-1}\left(\frac{r}{L}\right)\right)}\right)\right), \tag{3.8}$$

where P_0 denotes a normalization constant and $\mathscr{L}$ the Langevin function, which is defined by

$$\mathscr{L}\left(\frac{r}{L}\right) = \coth\left(\frac{r}{L}\right) - \frac{L}{r}. \tag{3.9}$$

Therefore, the strain-energy function of the freely-jointed chain model can be expressed as

$$\psi_{\mathrm{FJC}} = \psi_0 + k_{\mathrm{B}}TN\left(\frac{r}{L}\mathscr{L}^{-1}\left(\frac{r}{L}\right) - \ln\left(\frac{\mathscr{L}^{-1}\left(\frac{r}{L}\right)}{\sinh\left(\mathscr{L}^{-1}\left(\frac{r}{L}\right)\right)}\right)\right), \tag{3.10}$$

where ψ_0 denotes an energy stored in the reference chain. By the derivative of the strain-energy function with respect to r, we obtain a force-extension relation for the freely-jointed chain, see Treloar (1975, Sec. 6.3), with inverse Langevin statistics through

$$f = \frac{k_{\mathrm{B}}T}{l_{\mathrm{k}}}\mathscr{L}^{-1}\left(\frac{r}{L}\right). \tag{3.11}$$

The inverse Langevin function can be approximated by Padé approximation

$$\mathscr{L}^{-1}\left(\frac{r}{L}\right) \approx \frac{r}{L}\frac{\left(3 - \left(\frac{r}{L}\right)^2\right)}{\left(1 - \left(\frac{r}{L}\right)^2\right)}, \tag{3.12}$$

as shown in Cohen (1991). In this way it can be proved that for small stretches the force of the inverse Langevin chain coincides with the force of the Gaussian chain.

At the end of this section, we consider the limiting case of the FJC model, which occurs if $r/L \to 1$, see equation (3.11) and (3.12). In this context, the force which we apply to stretch the filament, goes to infinity. This is obvious considering the assumption that the segments of the chain are inextensible. The maximum of the end-to-end distance may only reach the contour length and not beyond that. Consequently, equation (3.11) presents the inextensible FJC model. But usually, biopolymers are able to expand beyond their contour length. Extensible models have the ability to allow r/L becoming greater than one. In this case we need energy to store the elasticity in the system. This can be visualized by pulling on a spring. An extensible FJC model was introduced by Smith et al. (1996), but we do not treat this in detail.

3.1.2 Worm-like chain model

Now we discuss a continuous model, the worm-like chain (WLC) model, which is based on thermal fluctuations. This property is reflected by an additional parameter, the persistence length L_p. The first idea of this model was proposed by Kratky and Porod (1949). As opposed to Kuhn's conception, Kratky and Porod said that a chain consists of N rods of length l, which are joined together that each rod will influence the direction of a rod from the previous in a certain way. Kratky and Porod (1949) coined the term of persistence length of a chain, by declaring that the average of the cosine of the angle of deviation together with the length of a rod l are a quantity of it, which is defined as

$$L_\mathrm{p} = -\frac{l}{\ln(\cos\theta)} \approx -\frac{l}{\cos\theta - 1}, \tag{3.13}$$

where the latter approximation is obtained by applying Taylor series. Assumed that all bending angles are equally likely and independent of each other, then the correlation between two bond vectors $\mathbf{r}_i$ and $\mathbf{r}_j$ results in

$$\langle \mathbf{r}_i \cdot \mathbf{r}_j \rangle = l^2 (\cos\theta)^{|j-i|}. \tag{3.14}$$

Furthermore, Kratky and Porod (1949) considered the rod as continuously flexible by executing the limiting case by letting the number of segments to go to infinity ($N \to \infty$) and by letting the length of the rod to go to zero ($l \to 0$), with the restriction that the contour length remains constant ($L \to NL$). For this limiting process, which we denote by $\lim_{worm}$, we perform the following steps

$$\begin{aligned}
\lim_{worm} (\cos\theta)^N &= \lim_{worm} \exp\left(N \ln(\cos\theta)\right) \\
&\overset{\text{Taylor expansion}}{=} \lim_{worm} \exp\left(N\left(\cos\theta - 1 - \frac{(\cos\theta - 1)^2}{2} + \dots\right)\right) \\
&= \lim_{worm} \exp\left(Nl\left(\frac{\cos\theta - 1}{l} - \frac{(\cos\theta - 1)^2}{2l} + \dots\right)\right) \\
&= \exp\left(-\frac{L}{L_\mathrm{p}}\right).
\end{aligned} \tag{3.15}$$

Again, we are interested in the mean square end-to-end distance. The end-to-end vector, with tangent unit vector $\mathbf{t}(s) = \frac{\partial \mathbf{r}(s)}{\partial s}$ at a distance s from the starting point along the contour, can be written as

$$\mathbf{r} = \int_0^L \mathbf{t}(s)\mathrm{d}s. \tag{3.16}$$

The orientation correlation function for a worm-like chain decays exponentially, so that the

mean square end-to-end distance can be calculated through

$$\begin{aligned}\langle \mathbf{r}^2 \rangle &= \int_0^L \int_0^L \langle \mathbf{t}(s) \cdot \mathbf{t}(s') \rangle \mathrm{d}s' \mathrm{d}s \\ &= \int_0^L \int_0^L \langle \cos\theta(s-s') \rangle \mathrm{d}s' \mathrm{d}s \\ &= \int_0^L \int_0^L \exp\left(-\frac{|s-s'|}{L_\mathrm{p}}\right) \mathrm{d}s' \mathrm{d}s.\end{aligned} \tag{3.17}$$

We split the integrand into the region $s < s'$ and $s > s'$

$$\begin{aligned}\langle \mathbf{r}^2 \rangle &= \int_0^L \left(\int_0^s \exp\left(-\frac{(s-s')}{L_\mathrm{p}}\right) \mathrm{d}s' + \int_s^L \exp\left(-\frac{(s'-s)}{L_\mathrm{p}}\right) \mathrm{d}s' \right) \mathrm{d}s \\ &= \int_0^L \left(L_\mathrm{p} \exp\left(\frac{(s'-s)}{L_\mathrm{p}}\right)\Big|_0^s + L_\mathrm{p}\left(-\exp\left(\frac{(s-s')}{L_\mathrm{p}}\right)\right)\Big|_s^L \right) \mathrm{d}s \\ &= \int_0^L L_\mathrm{p}\left(1 - \exp\left(-\frac{s}{L_\mathrm{p}}\right) - \exp\left(\frac{(s-L)}{L_\mathrm{p}}\right) + 1\right) \mathrm{d}s \\ &= L_\mathrm{p} \int_0^L \left(2 - \exp\left(-\frac{s}{L_\mathrm{p}}\right) - \exp\left(\frac{(s-L)}{L_\mathrm{p}}\right)\right) \mathrm{d}s \\ &= L_\mathrm{p}\left(2s + L_\mathrm{p}\exp\left(-\frac{s}{L_\mathrm{p}}\right) - L_\mathrm{p}\exp\left(\frac{(s-L)}{L_\mathrm{p}}\right)\right)\Big|_0^L \\ &= L_\mathrm{p}\left(2L + L_\mathrm{p}\left(\exp\left(-\frac{L}{L_\mathrm{p}}\right) - 1 - 1 + \exp\left(-\frac{L}{L_\mathrm{p}}\right)\right)\right) \\ &= 2L_\mathrm{p}L - 2L_\mathrm{p}^2\left(1 - \exp\left(-\frac{L}{L_\mathrm{p}}\right)\right)\end{aligned} \tag{3.18}$$

and therefore we attain the formulation of the mean square end-to-end distance

$$\langle \mathbf{r}^2 \rangle = 2L_\mathrm{p}L\left(1 - \frac{L_\mathrm{p}}{L}\left(1 - \exp\left(-\frac{L}{L_\mathrm{p}}\right)\right)\right). \tag{3.19}$$

This result was carried out by Rubinstein and Colby (2003). Consider now limiting cases of latter equation. If $L \gg L_\mathrm{p}$

$$\langle \mathbf{r}^2 \rangle = 2L_\mathrm{p}L, \tag{3.20}$$

follows. This limit provides us the relationship between the Kuhn length and the persistence length. By comparison with equation (3.4), we obtain

$$l_\mathrm{k} = 2L_\mathrm{p}. \tag{3.21}$$

Another limiting case occurs when $L \ll L_\mathrm{p}$, for this purpose we use the following series

expansion for the approximation

$$\exp\left(-\frac{L}{L_\mathrm{p}}\right) \approx 1 - \frac{L}{L_\mathrm{p}} + \frac{1}{2}\left(\frac{L}{L_\mathrm{p}}\right)^2 - \frac{1}{6}\left(\frac{L}{L_\mathrm{p}}\right)^3 + \dots \tag{3.22}$$

in equation (3.19) and receive thereby

$$\begin{aligned}\langle \mathbf{r}^2 \rangle &\approx 2L_\mathrm{p}L\left(1 - \frac{L_\mathrm{p}}{L}\left(1 - 1 + \frac{L}{L_\mathrm{p}} - \frac{1}{2}\left(\frac{L}{L_\mathrm{p}}\right)^2 + \frac{1}{6}\left(\frac{L}{L_\mathrm{p}}\right)^3 - \dots\right)\right) \\ &= 2L_\mathrm{p}L\left(1 - 1 + \frac{1}{2}\left(\frac{L}{L_\mathrm{p}}\right) - \frac{1}{6}\left(\frac{L}{L_\mathrm{p}}\right)^2 + \dots\right) \\ &= L^2 - \frac{1}{3}\frac{L^3}{L_\mathrm{p}} + \dots \approx L^2.\end{aligned} \tag{3.23}$$

This limiting case reflects the nature of a stiff biopolymers.

The numerical treatment of the WLC was first done by Fixman and Kovac (1973) and some analytical details were furnished by Kovac and Crabb (1982). This was then complemented by Bustamante et al. (1994) and Marko and Siggia (1995) to get a force-extension relation, as we mentioned above. To obtain this relation, we consider a single filament, whose end points lie on the x_1-axis, as illustrated in Figure 3.2. Suppose that one end is

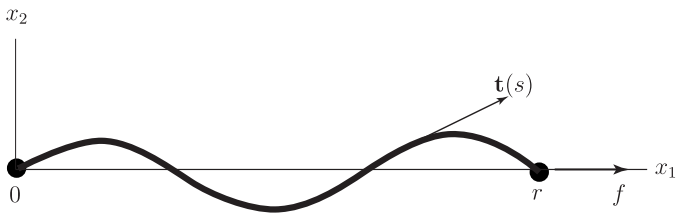

Figure 3.2: Single filament with a fixed end at $x_1 = 0$. The force f acting in x_1-direction overcomes the second end to $x_1 = r$. The unit tangent $\mathbf{t}(s)$ defined by parameterization of arc length $s \in [0, L]$.

fixed at $x_1 = 0$. Let r_0 be the second end point on the x_1-axis, which is referred to as the end-to-end distance when no force is applied. We describe the path of a filament through the parametrization of the arc length $s \in [0, L]$. Let $\mathbf{t}(s)$ be a unit tangent vector at s and $\mathbf{r}(s)$ the position vector along the chain, so that

$$\mathbf{t}(s) = \frac{\partial \mathbf{r}(s)}{\partial s}. \tag{3.24}$$

The curvature κ is defined by

$$\kappa = \left|\frac{\partial^2 \mathbf{r}(s)}{\partial^2 s}\right| \tag{3.25}$$

and the bending energy per unit length of the filament mounts to $\frac{1}{2}k_{\mathrm{B}}TL_{\mathrm{p}}\kappa^2$, where k_{B} is the Boltzmann constant with value $1.38 \times 10^{-23}\mathrm{Nm/K}$ and T is the absolute temperature. If we now apply a force f in the x_1-direction the end $x_1 = r_0$ changes to $x_1 = r$, see Figure 3.2, and thus work was done, which acts against the effect of thermal fluctuations. This can be described by the term $\int_{r_0}^{r} f\mathrm{d}x$. The effective energy of a stretched filament, which mentioned by Marko and Siggia (1995) is written as

$$E_{\mathrm{WLC}} = \frac{1}{2}k_{\mathrm{B}}TL_{\mathrm{p}}\int_0^L \kappa^2 \mathrm{d}s - \int_{r_0}^{r} f\mathrm{d}x. \tag{3.26}$$

To achieve a useful relation between f and r/L, Marko and Siggia used the Boltzmann distribution $\exp\left(-\frac{E_{\mathrm{WLC}}}{k_{\mathrm{B}}T}\right)$ and obtained the following interpolation formula

$$f = \frac{k_{\mathrm{B}}T}{4L_{\mathrm{p}}}\left(\frac{4r}{L} + \frac{1}{\left(1-\frac{r}{L}\right)^2} - 1\right), \tag{3.27}$$

which is a very useful approximation for semiflexible, inextensible filaments.

3.1.3 Holzapfel-Ogden model

Another approach to obtain a force-extension relation for the worm-like chain model was carried out by Holzapfel and Ogden (2011). This concept is based on a pure mechanical analysis and the extensible case of a filament is incorporated from the beginning. Let us now discuss the basic concept of this model.

We start with the analysis of the **kinematics**, before we examine the equilibrium equations and complete the analysis by material laws. The filament is described by a plane curve, which we illustrated in Figure 3.3(left) in the reference and in Figure 3.3(right) in current configurations. The arc length s, the tangent vector $\mathbf{t}$ and the curvature κ are defined in the previous section. Let θ be the angle between the unit tangent vector $\mathbf{t}$ and the x_1-axis and let u be the transverse deviation from the x_1-axis. In the reference configuration we denote S as the distance along the chain from the origin $\mathcal{O}$. The change in arc length, which we define as the local stretch of deformed to undeformed length, is given through

$$\frac{\mathrm{d}s}{\mathrm{d}S} = s'(S) =: \lambda(S), \tag{3.28}$$

where the prime denotes the derivative with respect to S. The local stretch is defined in $\lambda \in (0, \infty)$ and the relation between s and S is one-to-one. Let $\mathbf{x}(s)$ be the position vector at position s in the current configuration. The derivative of $\mathbf{x}(s)$ with respect to s defined the unit tangent vector through

$$\mathbf{x}'(s) = \frac{\mathrm{d}\mathbf{x}}{\mathrm{d}s} = \mathbf{t}(s). \tag{3.29}$$

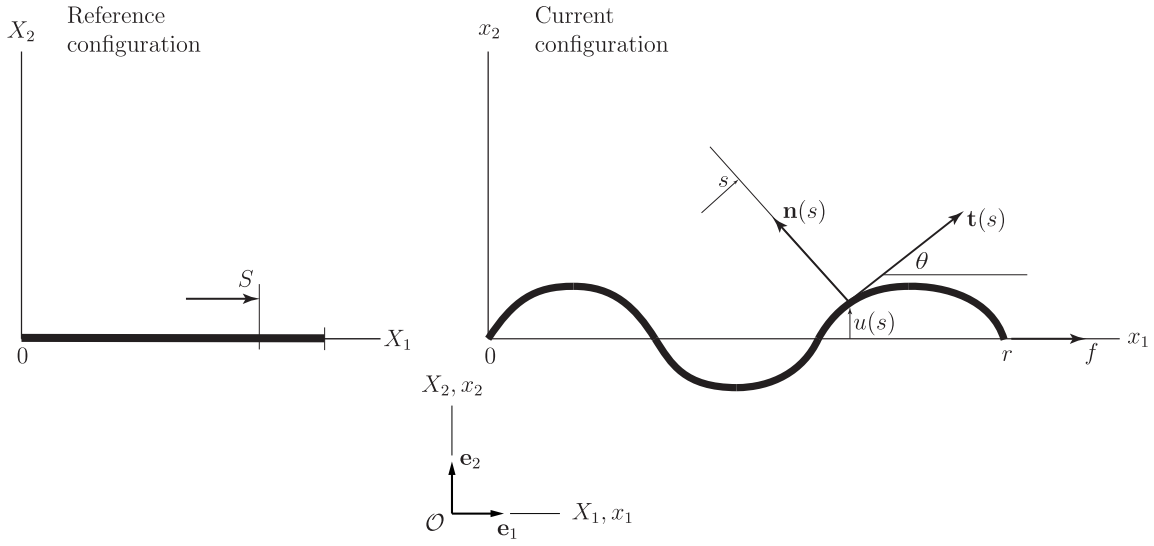

Figure 3.3: An elastic biopolymer in a straight unstretched reference configuration (left) lying along the X_1-axis with the arc length parameter S. In the deformed or current configuration (right), both ends of the filament lying on the x_1-axis and a force f is applied on the right-hand end of the filament along x_1-direction. The related arc length parameter is s and r is the end-to-end distance. The unit tangent and the unit normal vectors are $\mathbf{t}$ and $\mathbf{n}$, respectively. The tangent makes an angle θ with the x_1-axis and u denotes the lateral displacement from the x_1-axis.

According to Figure 3.3, we write the unit tangent vector $\mathbf{t}$ and unit normal vector $\mathbf{n}$ with respect to the current configuration with basis vectors $\mathbf{e}_1$ and $\mathbf{e}_2$, respectively, in the following form

$$\mathbf{t}(s) = \cos\theta(s)\mathbf{e}_1 + \sin\theta(s)\mathbf{e}_2, \quad \mathbf{n}(s) = -\sin\theta(s)\mathbf{e}_1 + \cos\theta(s)\mathbf{e}_2. \tag{3.30}$$

The infinitesimal lateral displacement $\mathrm{d}u$ from x_1-axis, can be expressed geometrically by

$$\frac{\mathrm{d}u}{\mathrm{d}s} = \sin\theta. \tag{3.31}$$

For a plane curve the curvature is defined as the derivative of the angle with respect to the arc length

$$\kappa(s) = \frac{\mathrm{d}\theta(s)}{\mathrm{d}s} = \theta'(s). \tag{3.32}$$

Considering the derivative of the tangent vector with respect to s, by using equation $(3.30)_2$ and $(3.32)_1$ we obtain

$$\frac{\mathrm{d}\mathbf{t}}{\mathrm{d}s} = \frac{\mathrm{d}\mathbf{t}}{\mathrm{d}\theta}\frac{\mathrm{d}\theta}{\mathrm{d}s} = (-\sin\theta\mathbf{e}_1 + \cos\theta\mathbf{e}_2)\frac{\mathrm{d}\theta}{\mathrm{d}s} = \kappa(s)\mathbf{n}(s). \tag{3.33}$$

When we consider the quantities in the reference configuration with respect to the parameter S we put henceforth a bar over these quantities. By the notation $\bar{\theta}(S) = \theta(s)$ and by equation $(3.28)_2$ and $(3.32)_1$, the modified curvature is defined by

$$\bar{\kappa}(S) = \frac{\mathrm{d}\bar{\theta}(S)}{\mathrm{d}S} = \frac{\mathrm{d}\theta(s)}{\mathrm{d}s}\frac{\mathrm{d}s}{\mathrm{d}S} = \lambda(S)\kappa(s) = \bar{\theta}'(S) \tag{3.34}$$

Finally, we consider the derivative of $\bar{u}$ with respect to S. The notation $\bar{u}(S) = u(s)$ and equation (3.31) and (3.28) yields

$$\bar{u}'(S) = \frac{\mathrm{d}\bar{u}}{\mathrm{d}S} = \frac{\mathrm{d}u}{\mathrm{d}s}\frac{\mathrm{d}s}{\mathrm{d}S} = \lambda(S)\sin\bar{\theta}(S). \tag{3.35}$$

In the next step we establish the **equilibrium equations** in consideration of an unshearable biopolymer. For this purpose we use the theory of a planar steady-state problems for elastic rods as support, which is discussed in detail in Antman (2005, Chap. 4). Consider the cross section of an 'unshearable' biopolymer at location s, the resultant force $\mathbf{p}$ consists of a tangential and a normal component and is written as

$$\mathbf{p} = t\mathbf{t} + n\mathbf{n} = (t\cos\theta - n\sin\theta)\,\mathbf{e}_1 + (t\sin\theta + n\cos\theta)\,\mathbf{e}_2, \tag{3.36}$$

where t describes the tension in the tangential direction and n acts as a Lagrange multiplier required to prevent shearing in the cross section of the biopolymer. The moment belonging to this resultant force about the origin $\mathcal{O}$ is $\mathbf{x} \times \mathbf{p}$. At this location s there acts also a resultant contact couple $\mathbf{m}$ with a bending moment m in the biopolymer, such that

$$\mathbf{m} = m\mathbf{t} \times \mathbf{n}. \tag{3.37}$$

We consider a material segment $[c, s]$ of the filament, which is in equilibrium when the sum of resultant forces and moments acting on this segment are each zero. Assuming additionally that a body force $\mathbf{b}$ is acting along this segment and there are no body couples per unit length in the deformed configuration. In this way we obtain

$$\begin{aligned} \mathbf{p}(s) - \mathbf{p}(c) + \int_c^s \mathbf{b}(\xi)\mathrm{d}\xi &= \mathbf{0}, \\ \mathbf{m}(s) - \mathbf{m}(c) + \mathbf{x}(s)\times\mathbf{p}(s) - \mathbf{x}(c)\times\mathbf{p}(c) + \int_c^s \mathbf{x}(\xi)\times\mathbf{b}(\xi)\mathrm{d}\xi &= \mathbf{0}, \end{aligned} \tag{3.38}$$

see Antman (2005, Chap. 4). Let c be a constant. Taking the derivative with respect to s the equations in (3.38) result in

$$\begin{aligned} \mathbf{p}'(s) + \mathbf{b}(s) &= \mathbf{0}, \\ \mathbf{m}'(s) + \mathbf{x}'(s)\times\mathbf{p}(s) + \mathbf{x}(s)\times\mathbf{p}'(s) + \mathbf{x}(s)\times\mathbf{b}(s) &= \mathbf{0}. \end{aligned} \tag{3.39}$$

By rearranging the equation $(3.39)_2$ and using $(3.39)_1$, we get

$$\begin{aligned} \mathbf{m}'(s) + \mathbf{x}'(s) \times \mathbf{p}(s) + \mathbf{x}(s) \times (\mathbf{p}'(s) + \mathbf{b}(s)) &= \mathbf{0} \\ \mathbf{m}'(s) + \mathbf{x}'(s) \times \mathbf{p}(s) &= \mathbf{0}. \end{aligned} \tag{3.40}$$

For convenience we introduce a vector $\widetilde{\mathbf{c}}(s)$ such that $\widetilde{\mathbf{c}}'(s) = \mathbf{b}$ holds. Then we can deduce from equation $(3.39)_1$ that $\mathbf{p} + \widetilde{\mathbf{c}}$ is a constant. In the two-dimensional case, where f is acting only in x_1 direction and g is a normal reaction in x_2 direction, we can thus write

$$\mathbf{p} + \widetilde{\mathbf{c}} = f\mathbf{e}_1 + g\mathbf{e}_2. \tag{3.41}$$

Without loss of generality we assume that $\widetilde{\mathbf{c}}$ has only a transverse component, i.e. $\widetilde{\mathbf{c}}(s) = \widetilde{c}(s)\mathbf{e}_2$. This assumption converts equation (3.41) into

$$\mathbf{p} = f\mathbf{e}_1 - c\mathbf{e}_2, \tag{3.42}$$

where c is defined by $c := \widetilde{c} - g$. Comparing the latter equation with equation (3.36), we achieve

$$t\cos\theta - n\sin\theta = f, \quad t\sin\theta + n\cos\theta = -c. \tag{3.43}$$

By multiplication of $(3.43)_1$ with $\cos\theta$ and $(3.43)_2$ with $\sin\theta$, followed by summation these preliminary results, we obtain one of the two translation balance equations. The second one is achieved by multiplication of $(3.43)_1$ with $\sin\theta$ and $(3.43)_2$ with $\cos\theta$ and subsequent subtraction. By doing this, we get the following two translational balance equations

$$t = f\cos\theta - c\sin\theta \quad \text{and} \quad n = -f\sin\theta + c\cos\theta, \tag{3.44}$$

respectively. The rotational balance equation is deduced by substituting equation $(3.36)_1$ in $(3.40)_2$ and by using equation (3.29) and (3.37) we obtain

$$\frac{\mathrm{d}m}{\mathrm{d}s}\underbrace{\mathbf{t}\times\mathbf{n}}_{\mathbf{e}_3} + t\underbrace{(\mathbf{t}\times\mathbf{t})}_{\mathbf{0}} + n\underbrace{(\mathbf{t}\times\mathbf{n})}_{\mathbf{e}_3} = \mathbf{0}, \tag{3.45}$$

so that it follows

$$m' + n = 0. \tag{3.46}$$

The final step is to establish the **constitutive laws**. We consider an elastic energy U, which is stored in a biopolymer, per unit length in the reference configuration. Generally, this energy depends on the stretch λ and the curvature $\bar{\kappa}$, i.e. $U = U(\lambda, \bar{\kappa})$. The connection between the tensile force t and bending moment m, respectively, and the stored energy were discussed by Steigmann and Ogden and are given by

$$t = \frac{\partial U}{\partial \lambda}, \quad m = \frac{\partial U}{\partial \bar{\kappa}}. \tag{3.47}$$

If the biopolymer exhibits no stretch, i.e. $\lambda = 1$ and no bending, i.e. $\bar{\kappa} = 0$, then the tensile force and bending moment have to vanish. Thus we demand

$$U(1,0) = 0, \quad U_\lambda(1,0) = 0, \quad U_{\bar{\kappa}}(1,0) = 0, \tag{3.48}$$

where the subscripts denote the partial derivatives. We do not distinguish between bending up and bending down, this means that the bending moment m has the same sign as $\bar{\kappa}$ and further we consider only local extension and not a contraction of the biopolymer, which means that for $\lambda > 1$ it follows that

$$U_\lambda(\lambda, \bar{\kappa}) > 0 \quad \text{for any } \bar{\kappa}. \tag{3.49}$$

Additionally, in an energy minimizing configuration U should be a locally convex function of λ and $\bar{\kappa}$, i.e.

$$U_{\lambda\lambda} \geq 0, \quad U_{\bar{\kappa}\bar{\kappa}} \geq 0, \quad U_{\lambda\lambda} U_{\bar{\kappa}\bar{\kappa}} - U_{\lambda\bar{\kappa}}^2 \geq 0, \tag{3.50}$$

which is according to Steigmann and Ogden. For a small $\bar{\kappa}$ and with the constant stretch modulus $\mu_0 > 0$ and a constant bending stiffness B_0, we may assume a simple decoupled model in the form

$$U(\lambda, \bar{\kappa}) = \frac{1}{2}\mu_0 \left(\lambda - 1\right)^2 + \frac{1}{2} B_0 \bar{\kappa}^2. \tag{3.51}$$

This model yields

$$t = U_\lambda = \mu_0 \left(\lambda - 1\right), \quad m = U_{\bar{\kappa}} = B_0 \bar{\kappa} \tag{3.52}$$

and further

$$U_{\lambda\lambda} = \mu_0, \quad U_{\bar{\kappa}\bar{\kappa}} = B_0, \quad U_{\lambda\bar{\kappa}} = 0. \tag{3.53}$$

The specified model (3.51) fulfills all conditions of U, as indicated in (3.48), (3.49) and (3.50). Now we are able to deduce the equilibrium equation for a single biopolymer with using the model (3.51). To this end we consider the functions with respect to S, i.e. we replace t, n, c, m and θ in equation (3.44) and (3.46) by $\bar{t}, \bar{n}, \bar{c}, \bar{m}$ and $\bar{\theta}$. Furthermore, we assume that $\bar{\theta}$ is very small, so that $\cos\bar{\theta} \approx 1$ and $\sin\bar{\theta} \approx \bar{\theta}$ can be approximated and furthermore $\bar{c}$ is a linear function in $\bar{\theta}$. By using equation $(3.44)_1$, neglecting the second order terms in $\bar{\theta}$ and with $(3.52)_2$, we obtain

$$t \approx f = \mu_0 \left(\lambda - 1\right) \quad \Rightarrow \quad \lambda = 1 + \frac{f}{\mu_0}. \tag{3.54}$$

In this way it follows that λ is constant, independent of position S. The rotational equilibrium equation (3.46) as a function of the arc length S takes the form

$$\frac{\mathrm{d}\bar{m}}{\mathrm{d}S}\frac{\mathrm{d}S}{\mathrm{d}s} + \bar{n} = \lambda^{-1}\bar{m}' + \bar{n} = 0. \tag{3.55}$$

By substituting equation (3.44) in the latter equation and with equation $(3.52)_4$, it follows

that $m' = B_0\bar{\kappa}' = B_0\bar{\theta}''$ and we get the approximation

$$\lambda^{-1}B_0\bar{\theta}'' - f\bar{\theta} = \bar{c}. \tag{3.56}$$

Since $\bar{c}' = \bar{b}$ and by differentiation of (3.56) we receive

$$\lambda^{-1}B_0\bar{\theta}''' - f\bar{\theta}' = \bar{b}. \tag{3.57}$$

The differentiation of $\bar{u}' = \lambda \sin\bar{\theta}$ results in $\bar{u}'' = \lambda\cos\bar{\theta}\bar{\theta}'$ and by using the approximation $\cos\bar{\theta} \approx 1$ we get $\bar{u}'' \approx \lambda\bar{\theta}'$. In this way, equation (3.57) leads to

$$\lambda^{-2}B_0\bar{u}'''' - \lambda^{-1}f\bar{u}'' = \bar{b}. \tag{3.58}$$

If $\lambda = 1$, we say that the filament is inextensible, meaning that $s = S$ and therefore we can drop the bars henceforth. The equilibrium equation (3.58) for the inextensible case takes the form

$$B_0u'''' - fu'' = b, \tag{3.59}$$

which recovers the classical Euler beam equation if there is no body force.

The body force term is necessary for finding non-trivial solutions of the mechanical boundary-value problem. To obtain a force-extension relation of the governing equations (3.58) and (3.59), the Fourier series were used in Holzapfel and Ogden (2011). The result of the force versus end-to-end distance for the extensible case, which depends on the end-to-end distance with zero force r_0, has the form

$$\frac{r}{L} = 1 + \frac{f}{\mu_0} - \frac{\left(1 + 2\dfrac{f}{\mu_0}\right)\left(1 + \dfrac{f}{\mu_0}\right)^2}{\left(1 + \dfrac{fL^2}{\pi^2B_0} + \dfrac{f^2L^2}{\pi^2B_0\mu_0}\right)^2}\left(1 - \frac{r_0}{L}\right), \tag{3.60}$$

This formula includes bending and stretching properties. With the transformation of force f to a dimensionless measure

$$f^\star = \frac{L^2}{\pi^2B_0}f \tag{3.61}$$

and by using the dimensionless parameter

$$\alpha = \frac{\pi^2B_0}{\mu_0L^2}, \tag{3.62}$$

the extensible Holzapfel-Ogden model (3.60) becomes

$$\frac{r}{L} = 1 + \alpha f^\star - \frac{(1 + 2\alpha f^\star)(1 + \alpha f^\star)^2}{(1 + f^\star + \alpha f^{\star 2})^2}\left(1 - \frac{r_0}{L}\right). \tag{3.63}$$

The inextensible case is included in the extensible formulation, when $\mu_0 \to \infty$ and therefore $\alpha \to 0$. Thus the inextensible Holzapfel-Ogden model is given by

$$\frac{r}{L} = 1 - \frac{1}{(1+f^\star)^2}\left(1 - \frac{r_0}{L}\right). \tag{3.64}$$

The achieved models can be adopted for both flexible and semiflexible filaments.

3.2 Network model

In human body filaments do not appear in single form but rather together with other filaments of the same type or even other types. A network model should describe the elasticity response of these interactions of filaments. In the literature there are a variety of these types of models, such as the affine three chain model by Wang and Guth (1952), the non-affine four chain model by Treloar (1954), which describes a full network, and the non-affine eight chain model by Arruda and Boyce (1993), which is the most prominent network model today. Another formulation of a full network model is provided by Miehe et al. (2004) and is called the micro-sphere model. Unterberger et al. (submitted) made use of this concept recently, and formulated a new approach to model a cross-linked actin network. Before we discuss Unterberger's model in detail, we introduce the basic concept of the micro-sphere model.

3.2.1 Micro-sphere model

The non-affine micro-sphere model proposed by Miehe et al. (2004) is a microscopically motivated model for rubberlike materials. The authors worked out a new formulation of a micro-macro approach to describe the elasticity response of a material. This is constructed by a new constitutive setting of the micro-mechanical response of a single polymer chain considered in a constrained environment and by a new non-affine micro-to-macro transition. The implementation of the first point is carried out by two micro-kinematic variables, the stretch λ of the chain and the contraction ν of the cross section of a micro-tube that contains the chain. The second point provides the bridge between the microscopic kinematic variables and the macroscopic continuum deformation measures. This is achieved by a homogenization procedure of micro-state variables defined on the micro-sphere of space orientations and this defines the three-dimensional overall response of the polymer network. The constitutive model was obtained through the following three steps. The first step describes the link between the micro and macro line and area stretches through a fluctuation field on a micro-sphere. The fluctuation field is determined by a minimization of the macroscopic free energy, which we obtained by the single filament model, which we have carried out for the Holzapfel-Ogden model in Section 3.1.3. The second step considers a tube constraint, which describes the restriction of the movement of a single chain. This part for example illustrates the cross-links in a polymer network. The last step addresses

a numerical approximation of an integral over a sphere, the so-called 21-point integration scheme by Bažant and Oh (1986) is used.

To begin with the **kinematics**, we focus on the definition of micro-kinematic variables of the chain. For that purpose, we consider a single chain, which is constrained by a straight tube to draft the interactions of chains in a network and introduce the two micro-kinematic variables, the stretch λ and the tube contraction ν. Depending on the specific model to describe the single chain determines the remaining parameters of the single filament model. Miehe et al. (2004) made use of the freely-jointed chain model, which we introduced in Section 3.1.1. By using the usual notation, the end-to-end distance r and the end-to-end distance at zero force r_0, the dimensionless stretch λ is defined as

$$\lambda := \frac{r}{r_0}. \tag{3.65}$$

Consider an inextensible filament, $\lambda \in (0, L/r_0)$. In view of the second micro-kinematic variable, it is assumed that the polymer chain is confined in a tube of constant diameter d and that both ends are fixed at the center of the end cross section. The dimensionless tube area contraction with $\nu \in (0, \infty)$, which describes the network constraint to the single chain, can be described by

$$\nu := \left(\frac{d_0}{d}\right)^2, \tag{3.66}$$

where d_0 is the initial diameter of the tube. The variable ν describes the number of allowed conformations of the chain inside of the tube and the initial diameter can be interpreted as material parameter of the undeformed network.

Now we investigate the formulation of the micro-to-macro transition, which links the two micro-kinematic variables λ and ν to the line-stretch $\bar{\lambda}$ and to the area-stretch $\bar{\nu}$, respectively of the macro-continuum. First of all, we consider some stretch assumption. Let $\mathbf{\Pi}$ be a unit orientation vector with the Euclidean norm $\|\mathbf{\Pi}\| = 1$, which describes the direction between the end points of the polymer in the reference configuration. The isochoric stretch vector $\boldsymbol{\pi}$ is defined by the transformation through the macroscopic isochoric deformation gradient $\mathbf{F}$ and is given by

$$\boldsymbol{\pi} = \mathbf{F}\mathbf{\Pi}, \tag{3.67}$$

see Figure 3.4.

The macro-stretch of a material line element is then defined by

$$\bar{\lambda} = \frac{\|\boldsymbol{\pi}\|}{\|\mathbf{\Pi}\|} = \|\boldsymbol{\pi}\| = \sqrt{\boldsymbol{\pi} \cdot \boldsymbol{\pi}}. \tag{3.68}$$

By recalling the definition of Cauchy-Green tensor $\mathbf{C} = \mathbf{F}^\top \mathbf{F}$ and by using (3.67), the macro-stretch can be written as

$$\bar{\lambda} = \sqrt{\mathbf{F}\mathbf{\Pi} \cdot \mathbf{F}\mathbf{\Pi}} = \sqrt{\mathbf{\Pi} \cdot \mathbf{F}^\top \mathbf{F}\mathbf{\Pi}} = \sqrt{\mathbf{\Pi} \cdot \mathbf{C}\mathbf{\Pi}}. \tag{3.69}$$

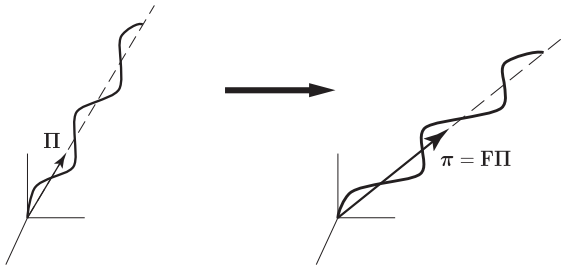

Figure 3.4: The unit vector $\mathbf{\Pi}$ in the reference configuration (left) is deformed by deformation gradient $\mathbf{F}$ into the vector $\mathbf{\Pi}$ in the current configuration (right) in the three dimensional space.

A further assumption of Miehe's conception is that the micro-stretches λ fluctuate around the macro-stretches $\bar{\lambda}$ and the relation can be expressed with the stretch-fluctuation field $\widetilde{f}$

$$\lambda = \bar{\lambda}\widetilde{f}. \tag{3.70}$$

The fluctuation field on the unit sphere Ω is determined by a principle of minimum averaged free energy, which is in line with the concept of homogenization principles and is explained by the p-root averaging operator

$$\lambda = \langle\bar{\lambda}\rangle_p := \left(\frac{1}{|\Omega|}\int_\Omega \bar{\lambda}^p \mathrm{d}A\right)^{1/p}, \tag{3.71}$$

where $\mathrm{d}A$ is the infinitesimal area element of Ω with total area $|\Omega| = 4\pi$ and p an additional material parameter of the polymer network.

Next, consider an area element with unit normal $\mathbf{\Pi}$ in the reference configuration. The area vector $\mathbf{a}$ can be described by

$$\mathbf{a} = \mathbf{F}^{-\top}\mathbf{\Pi}, \tag{3.72}$$

compare with Nanson's formula (2.20). Subsequently the macro-area stretch of a material element is

$$\bar{\nu} = \frac{\|\mathbf{a}\|}{\|\mathbf{\Pi}\|} = \|\mathbf{a}\| = \sqrt{\mathbf{a}\cdot\mathbf{a}}. \tag{3.73}$$

If we regard the inverse of Cauchy-Green tensor and equation (3.72), the macro-area stretch becomes

$$\bar{\nu} = \sqrt{\mathbf{F}^{-\top}\mathbf{\Pi}\cdot\mathbf{F}^{-\top}\mathbf{\Pi}} = \sqrt{\mathbf{\Pi}\cdot\mathbf{F}^{-1}\mathbf{F}^{-\top}\mathbf{\Pi}} = \sqrt{\mathbf{\Pi}\cdot\mathbf{C}^{-1}\mathbf{\Pi}}. \tag{3.74}$$

The relation between the micro-tube contraction and the macro-area stretch is proposed by Miehe et al. (2004) through

$$\nu = (\bar{\nu})^q. \tag{3.75}$$

The non-linearity between the microscopic tube contraction and the macroscopic area results from an additional material parameter q. A geometrical interpretation of conceptual

linking of micro-kinematic variables to macro-kinematic variables is shown in Miehe et al. (2004).

The contributions from the line stretch and area stretch result in an additive decomposition of the free energy function ψ into the contribution of the free energy ψ_{f} of the free motion of the chain and the contribution of the free energy ψ_{c} of the tube constraint, such that

$$\psi(\lambda, \nu) = \psi_{\mathrm{f}}(\lambda) + \psi_{\mathrm{c}}(\nu). \tag{3.76}$$

This decomposition is translated to the macroscopic scale with the result

$$\Psi(\mathbf{F}) = \Psi_{\mathrm{f}}(\mathbf{F}) + \Psi_{\mathrm{c}}(\mathbf{F}), \tag{3.77}$$

and subsequently

$$\boldsymbol{\tau} = \boldsymbol{\tau}_f + \boldsymbol{\tau}_c - \zeta \mathbf{I}. \tag{3.78}$$

It should be assumed, that the undeformed network is homogeneous and isotropic. Further, the network consists of n chains per unit reference volume, where it represents the number of filaments of the network and is also called filament density. These filaments are randomly distributed in a three-dimensional unit sphere. The elastic free energy of a network is equal to the sum of the elastic free energies ψ_{f}^i of the individual chains, i.e

$$\Psi_{\mathrm{f}} = \sum_{i=1}^{n} \psi_{\mathrm{f}}^i(\bar{\lambda}^i). \tag{3.79}$$

The macroscopic free energy of the non-affine network model for unconstrained chains is denoted by Miehe et al. (2004) as

$$\Psi_{\mathrm{f}}(\mathbf{F}) = n\psi_{\mathrm{f}}(\langle \bar{\lambda} \rangle_p). \tag{3.80}$$

For the tube constraint the macroscopic free energy is written as

$$\Psi_{\mathrm{c}}(\mathbf{F}) = \langle n\psi_{\mathrm{c}}(\bar{\nu}^q) \rangle, \tag{3.81}$$

where $\langle \bullet \rangle$ denotes the continuous averaging for an equal orientation distribution and is regarded as the homogenization on a micro-sphere with unit radius, which we defined in (3.71) for $p = 1$. Furthermore, the macroscopic Kirchhoff stresses for the unconstrained and constrained part is given by

$$\boldsymbol{\tau}_{\mathrm{f}} = n\psi_{\mathrm{f}}' \lambda^{1-p} \mathbf{h}, \tag{3.82}$$

with tensor $\mathbf{h} := \langle \bar{\lambda}^{p-2} \boldsymbol{\pi} \otimes \boldsymbol{\pi} \rangle$, and

$$\boldsymbol{\tau}_{\mathrm{c}} = -n\psi_{\mathrm{c}}' \mathbf{k}, \tag{3.83}$$

respectively, with $\mathbf{k} := \langle q\bar{\nu}^{q-2} \mathbf{a} \otimes \mathbf{a} \rangle$, where $\otimes$ denotes the dyadic product.

Finally, the integral over the continuous space orientations has to be solved numerically.

This can be done by discretizing the continuous orientation distribution of the unit sphere Ω. In this context, m discrete points are defined on the surface of the unit sphere with orientation vectors $\{\mathbf{\Pi}^i\}_{i=1,..,m}$ and with the associated weight factors $\{w^i\}_{i=1,..,m}$. The discrete micro-state variables $\{v^i\}_{i=1,..,m}$ are evaluated at the discrete points. Therefore, the numerical integration over the unit sphere of state variable v can be approximated by the discrete sum

$$\langle v \rangle := \frac{1}{|\Omega|} \int_{\Omega} v(A) \mathrm{d}A \approx \sum_{i=1}^{m} v^i w^i. \tag{3.84}$$

In the discrete setting, the numerical integration scheme has to satisfy some constraints. The average over all orientation vectors has to be

$$\langle \mathbf{\Pi} \rangle = \mathbf{0}. \tag{3.85}$$

In order to ensure a stress-free state of the reference configuration the dyadic product of the orientation vectors has to satisfy the following condition

$$\langle \mathbf{\Pi} \otimes \mathbf{\Pi} \rangle = \frac{1}{3} \mathbf{I}. \tag{3.86}$$

Bažant and Oh (1986) specified a 21-point integration scheme, which fulfill these conditions. These 21 points are defined on the hemisphere because of the symmetry of the unit sphere. The associated discrete points defined on the hemisphere for a Cartesian system and the associated weights are tabulated in Bažant and Oh (1986). Miehe et al. (2004) showed that this 21-point integration scheme provides the sufficient accuracy for all numerical considerations.

3.2.2 Unterberger model

A new multi-scale model to describe the mechanics of cross-linked actin networks was recently developed by Unterberger et al. (submitted). This work includes the basic idea of the network model by Miehe et al. (2004) and incorporates a generalized form of the Holzapfel-Ogden model for the contribution of the single filament. For convenience, the tube part of the micro-sphere model by Miehe et al. (2004) was neglected in this consideration. Further, an initial pre-stretch variable λ_0 was installed in the single filament model, such that

$$r = \lambda \lambda_0 r_0. \tag{3.87}$$

The extensible Holzapfel-Ogden model was generalized by substituting the square in equation (3.60) by an arbitrary exponent β, which is referred to as the effective extensional modulus, see Holzapfel and Ogden (submitted). This parameter describes the initial stiffnes of the single filament. By using the dimensionless force $f^\star$ and the dimensionless parameter α, which are defined in equation (3.61) and (3.62), respectively, and with equation (3.87),

the generalized extensible single filament model reads as

$$\frac{\lambda\lambda_0 r_0}{L} = 1 + \alpha f^\star - \frac{(1+2\alpha f^\star)(1+2\alpha f^\star)^\beta}{(1+f^\star+\alpha f^{\star 2})^\beta}\left(1-\frac{r_0}{L}\right), \tag{3.88}$$

see Unterberger et al. (submitted). To assemble the network model the derivative of the strain-energy function with respect to λ is required and can be calculated as follows

$$\psi_{\mathrm{f}}' = \frac{\partial\psi_{\mathrm{f}}}{\partial\lambda} = \frac{\partial\psi_{\mathrm{f}}}{\partial r}\frac{\partial r}{\partial\lambda} = f\lambda_0 r_0, \tag{3.89}$$

where the force f is the partial derivative of ψ_{f} with respect to r, i.e. $f = \partial\psi_{\mathrm{f}}/\partial r$ holds. The force is determined by the single filament model. Instead of (3.88) for the Holzapfel-Ogden model, we can use equation (3.11) and (3.12) for the freely-jointed chain model or equation (3.27) for the worm-like chain model.

Now, we are interested in the computation of the Cauchy stress tensor and doing this in the same way like Unterberger et al. (submitted), but we consider from the beginning an incompressible hyperelastic material, i.e. $J = 1$. The associated Cauchy stress tensor was derived in Section 2.3 and is recalled in the form

$$\boldsymbol{\sigma}_{\mathrm{f}} = 2\mathbf{F}\frac{\partial\Psi_{\mathrm{f}}(\mathbf{C})}{\partial\mathbf{C}}\mathbf{F}^\top - \zeta\mathbf{I}. \tag{3.90}$$

In this sense we have to analyze the derivation of the strain-energy function with respect to the right Cauchy-Green tensor. Considering that we neglect the tube part of the micro-sphere model, therefore the following deduction is based on the unconstrained chains. Using equation (3.80) and (3.89) we arrive at

$$\frac{\partial\Psi_{\mathrm{f}}}{\partial\mathbf{C}} = n\frac{\partial\psi_{\mathrm{f}}}{\partial\mathbf{C}} = n\frac{\partial\psi_{\mathrm{f}}}{\partial\lambda}\frac{\partial\lambda}{\partial\bar{\lambda}}\frac{\partial\bar{\lambda}}{\partial\mathbf{C}} = n\psi_{\mathrm{f}}'\frac{\partial\lambda}{\partial\bar{\lambda}}\frac{\partial\bar{\lambda}}{\partial\mathbf{C}}. \tag{3.91}$$

Consider first, the last partial derivative, which can be calculated with equation (3.69) and (3.67) as

$$\begin{aligned}\frac{\partial\bar{\lambda}}{\partial\mathbf{C}} &= \frac{\partial}{\partial\mathbf{C}}\sqrt{\boldsymbol{\Pi}\cdot\mathbf{C}\boldsymbol{\Pi}} = \frac{1}{2}\bar{\lambda}^{-1}\frac{\partial(\boldsymbol{\Pi}\cdot\mathbf{C}\boldsymbol{\Pi})}{\partial\mathbf{C}} \\ &= \frac{1}{2}\bar{\lambda}^{-1}(\boldsymbol{\Pi}\otimes\boldsymbol{\Pi}) \\ &= \frac{1}{2}\bar{\lambda}^{-1}\left(\mathbf{F}^{-1}\boldsymbol{\pi}\otimes\boldsymbol{\pi}\mathbf{F}^{-\top}\right)\end{aligned} \tag{3.92}$$

Using Leibniz's rule for differentiation under the integral sign and equation (3.71) we work out the following expression

$$\frac{\partial\lambda}{\partial\bar{\lambda}}\frac{\partial\bar{\lambda}}{\partial\mathbf{C}} = \lambda^{1-p}\left\langle\bar{\lambda}^{p-1}\frac{\partial\bar{\lambda}}{\partial\mathbf{C}}\right\rangle \tag{3.93}$$

Put the partial results together into (3.91) and rewrite equation (3.90)

$$\begin{aligned}\boldsymbol{\sigma}_{\mathrm{f}} &= 2\mathbf{F}\frac{\partial \Psi_{\mathrm{f}}(\mathbf{C})}{\partial \mathbf{C}}\mathbf{F}^{\top} - \zeta\mathbf{I} \\ &= 2n\psi_{\mathrm{f}}'\lambda^{1-p}\mathbf{F}\frac{1}{2}\left\langle \bar{\lambda}^{p-2}\mathbf{F}^{-1}\boldsymbol{\pi}\otimes\boldsymbol{\pi}\mathbf{F}^{-\top}\right\rangle \mathbf{F}^{\top} - \zeta\mathbf{I} \\ &= n\psi_{\mathrm{f}}'\lambda^{1-p}\left\langle \bar{\lambda}^{p-2}\boldsymbol{\pi}\otimes\boldsymbol{\pi}\right\rangle - \zeta\mathbf{I}.\end{aligned} \tag{3.94}$$

The final result of the Cauchy stress tensor for an incompressible material reads now

$$\boldsymbol{\sigma}_{\mathrm{f}} = n\psi_{\mathrm{f}}'\lambda^{1-p}\mathbf{h} - \zeta\mathbf{I} \quad \text{with} \quad \mathbf{h} = \langle \bar{\lambda}^{p-2}\boldsymbol{\pi}\otimes\boldsymbol{\pi}\rangle. \tag{3.95}$$

The latter result presents basically the same as (3.82) if $J = 1$. The stretch parameter λ is calculated by the micro-sphere model as well as the structure tensor $\mathbf{h}$, by using the homogenization procedure of (3.84). The result of λ is used in the single filament model. The solution of the generalized extensible single filament model (3.88) provides us the force f and henceforth we are able to calculate ψ_{f}'. Both the micro-sphere model and the single filament model are assembled and result in the Cauchy stress tensor $\boldsymbol{\sigma}_{\mathrm{f}}$.

4 Analysis of the tube part

In the previous section we introduced the concept of network models, in particular the micro-sphere model and the Unterberger model for an incompressible hyperelastic material, where the tube part of the micro-sphere model was neglected. Now we want to make up for this omission. For this purpose, we first have to incorporate the contribution of this tube constraint to the Cauchy stress tensor. Afterwards we will discuss the computation of the Cauchy stress tensor in particular about the structural tensors $\mathbf{h}$ and $\mathbf{k}$. The tube part supplies two additional parameters that need to be determined. By varying these two parameters, we show the effect of the tube part on the network model and discuss these results at the end of the section.

4.1 Incorporation of the tube part

To incorporate the tube part into the network model, we have to study the Cauchy stress tensor again, in particular the derivative of the strain-energy function with respect to $\mathbf{C}$. We defined the Cauchy stress tensor for an incompressible hyperelastic material in equation (2.61), which we recall again in the form

$$\boldsymbol{\sigma} = 2\mathbf{F}\frac{\partial \Psi(\mathbf{C})}{\partial \mathbf{C}}\mathbf{F}^{\top} - \zeta \mathbf{I}. \tag{4.1}$$

We know from (3.77) that the strain-energy function Ψ is additively decomposed into Ψ_{f} and Ψ_{c}. Hence, the Cauchy stress tensor is writable as

$$\boldsymbol{\sigma} = 2\mathbf{F}\left(\frac{\partial \Psi_{\mathrm{f}}}{\partial \mathbf{C}} + \frac{\partial \Psi_{\mathrm{c}}}{\partial \mathbf{C}}\right)\mathbf{F}^{\top} - \zeta \mathbf{I}. \tag{4.2}$$

The derivative of Ψ_{f} with respect to $\mathbf{C}$ is completely done in Section 3.2.2. In the same way we establish the derivative of Ψ_{c} with respect to $\mathbf{C}$. From equation (3.81) and (3.75), we get

$$\frac{\partial \Psi_{\mathrm{c}}}{\partial \mathbf{C}} = \frac{\partial}{\partial \mathbf{C}}\langle n\psi_{\mathrm{c}}(\bar{\nu}^{q})\rangle = \frac{\partial}{\partial \mathbf{C}}\langle n\psi_{\mathrm{c}}(\nu)\rangle. \tag{4.3}$$

Using the homogenization principle, which we defined in $(3.71)_2$, we continue to write

$$\frac{\partial \Psi_{\mathrm{c}}}{\partial \mathbf{C}} = \frac{\partial}{\partial \mathbf{C}}\left(\frac{1}{|\Omega|}\int_{\Omega} n\psi_{\mathrm{c}}(\nu)\mathrm{d}A\right) = \frac{1}{|\Omega|}\int_{\Omega} n\frac{\partial \psi_{\mathrm{c}}(\nu)}{\partial \mathbf{C}}\mathrm{d}A. \tag{4.4}$$

Now we have to evaluate

$$\frac{\partial \psi_{\mathrm{c}}(\nu)}{\partial \mathbf{C}} = \frac{\partial \psi_{\mathrm{c}}(\nu)}{\partial \nu}\frac{\partial \nu}{\partial \bar{\nu}}\frac{\partial \bar{\nu}}{\partial \mathbf{C}} = \psi_{\mathrm{c}}'\frac{\partial \nu}{\partial \bar{\nu}}\frac{\partial \bar{\nu}}{\partial \mathbf{C}}, \tag{4.5}$$

where the prime denotes the partial derivative with respect to ν. Since $\nu = \bar{\nu}^q$ it follows, therefore,

$$\frac{\partial \nu}{\partial \bar{\nu}} = q\bar{\nu}^{q-1}. \tag{4.6}$$

What remains is the analysis of $\partial\bar{\nu}/\partial\mathbf{C}$. The macro-area stretch is defined in equation (3.74) by

$$\bar{\nu} = \left(\mathbf{\Pi}\cdot\mathbf{C}^{-1}\mathbf{\Pi}\right)^{\frac{1}{2}}, \tag{4.7}$$

so that we obtain

$$\frac{\partial \bar{\nu}}{\partial \mathbf{C}} = \frac{1}{2}\frac{1}{(\mathbf{\Pi}\cdot\mathbf{C}^{-1}\mathbf{\Pi})^{\frac{1}{2}}}\frac{\partial(\mathbf{\Pi}\cdot\mathbf{C}^{-1}\mathbf{\Pi})}{\partial \mathbf{C}} = \frac{1}{2\bar{\nu}}\frac{\partial(\mathbf{\Pi}\cdot\mathbf{C}^{-1}\mathbf{\Pi})}{\partial \mathbf{C}}. \tag{4.8}$$

To perform this derivation, we require the following index notation, which is defined in Holzapfel (2000, p. 43),

$$\frac{\partial C_{ij}^{-1}}{\partial C_{k\ell}} = -\frac{1}{2}\left(C_{ik}^{-1}C_{\ell j}^{-1} + C_{i\ell}^{-1}C_{kj}^{-1}\right). \tag{4.9}$$

We execute the derivative in equation $(4.8)_2$ with respect to $\mathbf{C}$ in index notation in the following steps

$$\begin{aligned}
\frac{\partial}{\partial C_{k\ell}}(\Pi_i C_{ij}^{-1}\Pi_j) &= -\frac{1}{2}\left[\Pi_i\left(C_{ik}^{-1}C_{\ell j}^{-1} + C_{i\ell}^{-1}C_{kj}^{-1}\right)\Pi_j\right] \\
&= -\frac{1}{2}\left[\Pi_i C_{ik}^{-1}C_{\ell j}^{-1}\Pi_j + \Pi_i C_{i\ell}^{-1}C_{kj}^{-1}\Pi_j\right] \\
&= -\frac{1}{2}\left[\left(\mathbf{\Pi}\mathbf{C}^{-1}\right)_k\left(\mathbf{C}^{-1}\mathbf{\Pi}\right)_\ell + \left(\mathbf{\Pi}\mathbf{C}^{-1}\right)_\ell\left(\mathbf{C}^{-1}\mathbf{\Pi}\right)_k\right] \\
&= -\frac{1}{2}\left[\left(\mathbf{C}^{-\top}\mathbf{\Pi}\right)_k\left(\mathbf{\Pi}\mathbf{C}^{-\top}\right)_\ell + \left(\mathbf{C}^{-1}\mathbf{\Pi}\right)_k\left(\mathbf{\Pi}\mathbf{C}^{-1}\right)_\ell\right].
\end{aligned} \tag{4.10}$$

Since the right Cauchy Green tensor is symmetric, meaning

$$\mathbf{C}^{-1} = \mathbf{C}^{-\top}, \tag{4.11}$$

we obtain

$$\frac{\partial \mathbf{\Pi}\cdot\mathbf{C}^{-1}\mathbf{\Pi}}{\partial \mathbf{C}} = -\mathbf{C}^{-1}\mathbf{\Pi}\otimes\mathbf{\Pi}\mathbf{C}^{-\top} = -\mathbf{C}^{-1}\mathbf{\Pi}\otimes\mathbf{C}^{-1}\mathbf{\Pi}. \tag{4.12}$$

In equation (3.72), the area vector is defined by

$$\mathbf{a} = \mathbf{F}^{-\top}\mathbf{\Pi}. \tag{4.13}$$

We consider

$$\mathbf{F}^{-1}\mathbf{a} = \mathbf{F}^{-1}\mathbf{F}^{-\top}\mathbf{\Pi} = \mathbf{C}^{-1}\mathbf{\Pi} \tag{4.14}$$

and infer

$$\begin{aligned} \frac{\partial \bar{\nu}}{\partial \mathbf{C}} &= \frac{1}{2\bar{\nu}} \frac{\partial (\mathbf{\Pi} \cdot \mathbf{C}^{-1}\mathbf{\Pi})}{\partial \mathbf{C}} \\ &= -\frac{1}{2\bar{\nu}} \mathbf{F}^{-1}\mathbf{a} \otimes \mathbf{a}\mathbf{F}^{-\top}. \end{aligned} \tag{4.15}$$

Back again to equation (4.5), if we collect all partial results (4.6) and (4.15), we attain the following result

$$\frac{\partial \psi_{\mathrm{c}}(\nu)}{\partial \mathbf{C}} = -\psi_{\mathrm{c}}' q \bar{\nu}^{q-1} \frac{1}{2\bar{\nu}} \mathbf{F}^{-1}\mathbf{a} \otimes \mathbf{a}\mathbf{F}^{-\top}. \tag{4.16}$$

Insert latter equation in equation $(4.3)_2$, we achieve

$$\frac{\partial \Psi_{\mathrm{c}}}{\partial \mathbf{C}} = \left\langle n \frac{\partial \psi_{\mathrm{c}}}{\partial \mathbf{C}} \right\rangle = -\frac{1}{2} n \psi_{\mathrm{c}}' q \langle \bar{\nu}^{q-2} \mathbf{F}^{-1}\mathbf{a} \otimes \mathbf{a}\mathbf{F}^{-\top} \rangle. \tag{4.17}$$

Consider again the Cauchy stress tensor (4.2) in the form

$$\boldsymbol{\sigma} = 2\mathbf{F} \frac{\partial \Psi_{\mathrm{f}}}{\partial \mathbf{C}} \mathbf{F}^{\top} + 2\mathbf{F} \frac{\partial \Psi_{\mathrm{c}}}{\partial \mathbf{C}} \mathbf{F}^{\top} - \zeta \mathbf{I}. \tag{4.18}$$

Using the results, namely equation (3.95) for the unconstrained chain and equation (4.17) for the tube constraint, we obtain with

$$\mathbf{h} := \langle \bar{\lambda}^{p-2} \boldsymbol{\pi} \otimes \boldsymbol{\pi} \rangle \qquad \text{and} \qquad \mathbf{k} := \langle q \bar{\nu}^{q-2} \mathbf{a} \otimes \mathbf{a} \rangle \tag{4.19}$$

the following Cauchy stress tensor

$$\boldsymbol{\sigma} = n \psi_{\mathrm{f}}' \lambda^{1-p} \mathbf{h} - n \psi_{\mathrm{c}}' \mathbf{k} - \zeta \mathbf{I}. \tag{4.20}$$

To complete this section, we still need to assemble the derivative of the strain-energy function ψ_{c} with respect to ν. The derivation of the free energy function of the tube part ψ_{c} is carried out analogously to ψ_{FJC} in Section 3.1.1. The probability of the straight tube constraint, which is postulated in Miehe et al. (2004) and refers to Doi and Edwards (1986, p. 205), is with the normalization constant P_0 given by

$$P_{\mathrm{c}}(\nu) = P_0 \exp\left(-\alpha \left(\frac{r_0}{d_0} \right)^2 \nu \right). \tag{4.21}$$

The parameter α describes a numerical factor which depends on the shape of the cross section of the tube. All other parameters have already been introduced in Section 3.2.1. It is assumed that the undulations of the worm-like chain are constrained by the tube. For purely entropic response we get by means of equations (3.5) and (3.6) the following free

energy function

$$\begin{aligned}\psi_{\mathrm{c}} &= -k_{\mathrm{B}}T\ln p_{\mathrm{c}}(\nu) = -k_{\mathrm{B}}T\ln\left(p_0\exp\left(-\alpha\left(\frac{r_0}{d_0}\right)^2\nu\right)\right)\\ &= \underbrace{-k_{\mathrm{B}}T\ln p_0}_{=:\psi_0} + k_{\mathrm{B}}T\alpha\left(\frac{r_0}{d_0}\right)^2\nu.\end{aligned} \tag{4.22}$$

with constant ψ_0. In this way, the derivative of ψ_{c} with respect to ν yields

$$\frac{\partial\psi_{\mathrm{c}}}{\partial\nu} = \psi_{\mathrm{c}}' = \alpha k_{\mathrm{B}}T\left(\frac{r_0}{d_0}\right)^2 \tag{4.23}$$

For our purpose, we define

$$\widetilde{U} := \alpha\left(\frac{r_0}{d_0}\right)^2 \tag{4.24}$$

as a geometric parameter, so that ψ_{c}' reads as

$$\psi_{\mathrm{c}}' = k_{\mathrm{B}}T\widetilde{U}. \tag{4.25}$$

4.2 Implementation of Cauchy stress tensor

Now, we want to specify the Cauchy stress tensor (4.20) taking into account a simple shear deformation. This kind of deformation is described in detail in Section 2.1.4. Henceforth, the subscripts of matrix elements are labeled only with the second subscripts of the annotation of the axes. More precisely, the subscripts $1, 2$ and 3 refer to the x_1-, x_2- and x_3-axes, respectively. In Section 3.2.2 we already discussed about ψ_{f}'. This factor is contributed by the single filament model and is given in equation (3.89). The item ψ_{c}' was explained at the end of the previous section. The micro-stretch λ is calculated using equation (3.71) and by discretization of the continuous unit sphere into the 21 radius vectors $\mathbf{\Pi} \to \mathbf{\Pi}^i$. For this we have to determine the discrete items $\bar{\lambda}^i$ through

$$\bar{\lambda}^i = \|\mathbf{F}\mathbf{\Pi}^i\| \tag{4.26}$$

and thus we are able to compute λ by

$$\lambda = \left[\sum_{i=1}^{21}\left(\bar{\lambda}^i\right)^p w^i\right]^{1/p}. \tag{4.27}$$

As we already know, the material parameter n defines the filament density and p an additional network parameter, which we will address in depth in Chapter 5. Let us deal next with the implementation of the structural tensors $\mathbf{h}$ and $\mathbf{k}$. Using equation (3.67) we

execute the following steps

$$\begin{aligned}\mathbf{h} &= \langle \bar{\lambda}^{p-2}\boldsymbol{\pi}\otimes\boldsymbol{\pi}\rangle = \langle \bar{\lambda}^{p-2}\mathbf{F}\boldsymbol{\Pi}\otimes\boldsymbol{\Pi}\mathbf{F}^{\top}\rangle \\ &= \mathbf{F}\langle \bar{\lambda}^{p-2}\boldsymbol{\Pi}\otimes\boldsymbol{\Pi}\rangle\mathbf{F}^{\top}.\end{aligned} \tag{4.28}$$

By using the 21-point integration scheme we approach the averaging by

$$\widetilde{\mathbf{h}} := \langle \bar{\lambda}^{p-2}\boldsymbol{\Pi}\otimes\boldsymbol{\Pi}\rangle \approx \sum_{i=1}^{21} \left(\bar{\lambda}^{i}\right)^{p-2}\boldsymbol{\Pi}^{i}\otimes\boldsymbol{\Pi}^{i}w^{i}. \tag{4.29}$$

The additional non-affine tube parameter q is introduced in Section 3.2.1. In the following steps we analyze the area-stretch tensor $\mathbf{k}$ by using equation (3.72)

$$\begin{aligned}\mathbf{k} &= q\langle \bar{\nu}^{q-2}\mathbf{a}\otimes\mathbf{a}\rangle = q\langle \bar{\nu}^{q-2}\mathbf{F}^{-\top}\boldsymbol{\Pi}\otimes\boldsymbol{\Pi}\mathbf{F}^{-1}\rangle \\ &= q\mathbf{F}^{-\top}\langle \bar{\nu}^{q-2}\boldsymbol{\Pi}\otimes\boldsymbol{\Pi}\rangle\mathbf{F}^{-1}.\end{aligned} \tag{4.30}$$

We discretize $\bar{\nu}\to\bar{\nu}^{i}$ through

$$\bar{\nu}^{i} = \|\mathbf{F}^{-\top}\boldsymbol{\Pi}^{i}\| \tag{4.31}$$

and approximate the angle brackets in equation (4.30) by

$$\widetilde{\mathbf{k}} := \langle \bar{\nu}^{q-2}\boldsymbol{\Pi}\otimes\boldsymbol{\Pi}\rangle \approx \sum_{i=1}^{21} \left(\bar{\nu}^{i}\right)^{q-2}\boldsymbol{\Pi}^{i}\otimes\boldsymbol{\Pi}^{i}w^{i}. \tag{4.32}$$

Because of simple shear deformation in the x_1x_2-plane and the condition (3.85), which says that the average over all orientation vectors $\{\boldsymbol{\Pi}^{i}\}_{i=1,\dots,m}$ have to be $\mathbf{0}$, the structural and area-stretch tensors have the following forms in matrix notation

$$[\mathbf{h}] = \begin{bmatrix} h_{11} & h_{12} & 0 \\ h_{12} & h_{22} & 0 \\ 0 & 0 & h_{33}\end{bmatrix} \quad \text{and} \quad [\mathbf{k}] = \begin{bmatrix} k_{11} & k_{12} & 0 \\ k_{12} & k_{22} & 0 \\ 0 & 0 & k_{33}\end{bmatrix}, \tag{4.33}$$

respectively. After the computation of $\widetilde{\mathbf{h}}$ from $(4.28)_3$ and $\widetilde{\mathbf{k}}$ from $(4.30)_3$ we are able to work out the entries of $\mathbf{h}$ and $\mathbf{k}$ in the following way

$$\begin{aligned} h_{11} &= \widetilde{h}_{11} + 2\gamma\widetilde{h}_{12} + \gamma^{2}\widetilde{h}_{22}, & h_{12} &= \widetilde{h}_{12} + \gamma\widetilde{h}_{22}, \\ h_{22} &= \widetilde{h}_{22}, & h_{33} &= \widetilde{h}_{33}, \end{aligned} \tag{4.34}$$

and

$$\begin{aligned} k_{11} &= q\widetilde{k}_{11}, & k_{12} &= q\left(\widetilde{k}_{12} - \gamma\widetilde{k}_{11}\right), \\ k_{22} &= q\left(\widetilde{k}_{22} - 2\gamma\widetilde{k}_{12} + \gamma^{2}\widetilde{k}_{11}\right), & k_{33} &= q\widetilde{k}_{33}. \end{aligned} \tag{4.35}$$

	Cross-linker densities R	$1/40$	$1/20$	
T	Temperature	294	294	K
L_p	Persistence length	16	16	μm
L	Contour length	1.47	0.53	μm
r_0	End-to-end distance at zero force	1.33	0.48	μm
μ_0	Stretch modulus	38.6	38.6	nN
β	Effective extensional modulus	0.438	0.438	-
n	Filament density	10.2	28.5	$\mu\mathrm{m}^{-3}$
λ_0	Initial stretch	1.027	1.007	-
p	Averaging parameter	8	15	-

Table 4.1: Model parameters for cross-linked actin network, adopted from Unterberger et al. (submitted).

The remaining variable in equation (4.20), which we still have to determine is the Lagrange multiplier ζ. We consider only plane stresses in the x_1x_2-plane. This results in the following conditions

$$\sigma_{13} = \sigma_{23} = \sigma_{33} \equiv 0, \tag{4.36}$$

which we can enforce by

$$\zeta := n\psi_\mathrm{f}'\lambda^{1-p}h_{33} - n\psi_\mathrm{c}'k_{33}. \tag{4.37}$$

In this way, the normal Cauchy stress in x_1- and x_2-direction and the shear stress can be computed by

$$\begin{aligned}
\sigma_{11} &= n\psi_\mathrm{f}'\lambda^{1-p}h_{11} - n\psi_\mathrm{c}'k_{11} - \zeta \\
&= n\left(\psi_\mathrm{f}'\lambda^{1-p}h_{11} - \psi_\mathrm{c}'k_{11} - \psi_\mathrm{f}'\lambda^{1-p}h_{33} + \psi_\mathrm{c}'k_{33}\right) \\
&= n\left(\psi_\mathrm{f}'\lambda^{1-p}\left(h_{11} - h_{33}\right) + \psi_\mathrm{c}'\left(k_{33} - k_{11}\right)\right) \\
\sigma_{22} &= n\psi_\mathrm{f}'\lambda^{1-p}h_{22} - n\psi_\mathrm{c}'k_{22} - \zeta \\
&= n\left(\psi_\mathrm{f}'\lambda^{1-p}h_{22} - \psi_\mathrm{c}'k_{22} - \psi_\mathrm{f}'\lambda^{1-p}h_{33} + \psi_\mathrm{c}'k_{33}\right) \\
&= n\left(\psi_\mathrm{f}'\lambda^{1-p}\left(h_{22} - h_{33}\right) + \psi_\mathrm{c}'\left(k_{33} - k_{22}\right)\right) \\
\sigma_{12} &= n\left(\psi_\mathrm{f}'\lambda^{1-p}h_{12} - \psi_\mathrm{c}'k_{12}\right)
\end{aligned} \tag{4.38}$$

4.3 Effect of the tube part

In this section, we deal with the effects of the tube constraint on the network model. Under the consideration of simple shear deformation and by using the material parameters for a cross-linked actin network, which are published in Unterberger et al. (submitted) and reported in Table 4.1, we demonstrate the influence of the tube part on the Unterberger model. The tube part yields two additional parameters, the geometry parameter $\widetilde{U}$ and the averaging tube parameter q, which have to be determined. By varying these two parameters we illustrate the impact of the tube part on the model. We choose the values of the

parameter $\widetilde{U}$ in analogously to Miehe et al. (2004). They used, however, the freely-jointed chain model for the description of the single chain and obtained for the derivative of ψ_{c} with respect to ν the following expression

$$\psi_{\mathrm{c}}' = k_{\mathrm{B}} T N U, \tag{4.39}$$

where N is the number of segments of a chain. Comparing the latter equation with equation (4.25), we get the relation

$$\widetilde{U} = NU. \tag{4.40}$$

To show the effect of the additional contribution due to the tube constraint, Miehe et al. (2004) chose the fixed value of $N = 25$ and different values of $U = [0.5, 2.0, 5.0, 10.0]$. In order to maintain approximately the same magnitude for the geometrical parameter, we choose the following values of $\widetilde{U} = [0, 50, 100, 200]$. The parameter q varies with the values of $q = [0, 1, 2, 4, 7]$. If $\widetilde{U} = 0$ or $q = 0$, respectively, then this means that the tube constraint is neglected, i.e. $n\psi_{\mathrm{c}}'\mathbf{k} = \mathbf{0}$. A special case occurs when $q = 2$. Consider the area-stretch tensor $\mathbf{k}$ in equation (4.30), the macro-area stretch provides no contribution if $q = 2$ and $\mathbf{k}$ becomes with equation (3.86)

$$\mathbf{k} = 2\mathbf{F}^{-\top} \underbrace{\langle \mathbf{\Pi} \otimes \mathbf{\Pi} \rangle}_{=\frac{1}{3}\mathbf{I}} \mathbf{F}^{-1} = \frac{2}{3}\mathbf{F}^{-\top}\mathbf{F}^{-1} = \frac{2}{3}\mathbf{b}^{-1}. \tag{4.41}$$

The implementation of the Cauchy stress tensor (4.20) has been carried out in MATLAB by using the material parameters listed in Table 4.1. Here, the cross-linker density R is defined by the ratio of cross-linker to molar concentration. By doubling the cross-linker density from $R = 1/40$ to $1/20$, the network becomes denser, so that the contour length and the initial end-to-end distance decrease and the filament density increases.

In Figure 4.1 and 4.2 the normal Cauchy stresses σ_{11} and σ_{22} and the shear stress σ_{12} versus deformation γ are depicted. We consider only the experimental data up to a deformation of $30\,\%$, because the response above $30\,\%$ no longer reflects the actual properties of the network, for more details see Unterberger et al. (submitted). First, we keep q constant and vary the geometrical parameter $\widetilde{U}$, shown in Figure 4.1. Figures 4.1(a)-(c) represent the effect of $\widetilde{U}$ by setting $q = 3$ and by using the material parameters with a cross-linker density of $R = 1/40$. The same value of q is selected in Figures 4.1(d)-(f) but with different material parameters which were measured with a density of $R = 1/20$. By means of the material parameters for $R = 1/40$ and considering the special case, i.e. select $q = 2$, we depict the normal stresses σ_{11} and σ_{22} and the shear stress σ_{12} in Figures 4.1(g)-(i). Following this, we vary the averaging parameter q while we fix the geometrical parameter at $\widetilde{U} = 50$, illustrated in Figure 4.2. In Figures 4.2(a)-(c) the effect of the tube part is demonstrated with the use of the material parameters of $R = 1/40$ and in Figures 4.2(d)-(f) using the material parameters of the double cross-linker density, i.e. $R = 1/20$.

First, let us take a closer look at the curves in which the tube part has no influence on the model. This is represented in each picture in Figure 4.2 and 4.1 by the dark blue

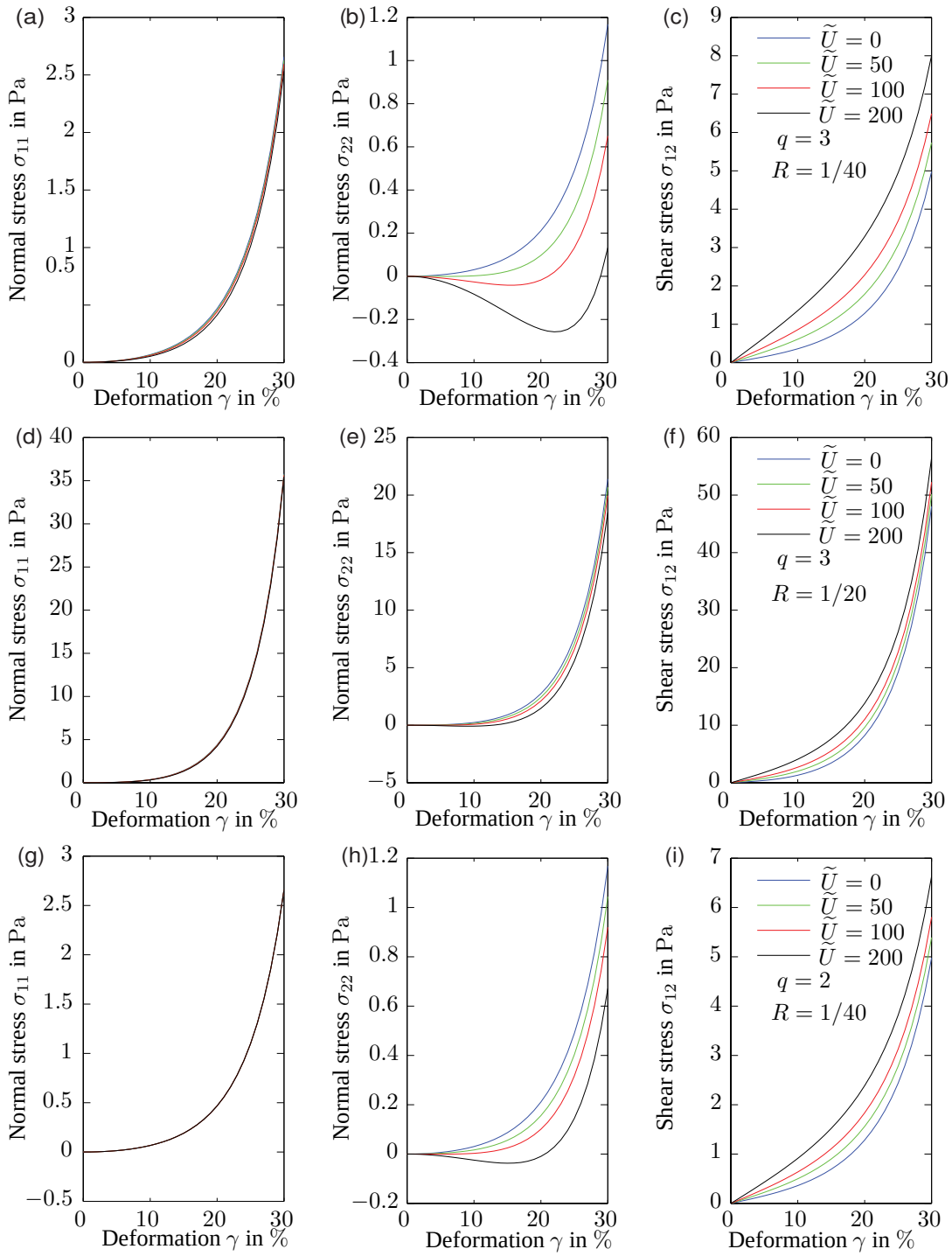

Figure 4.1: Illustration of the effect of the tube part by varying $\widetilde{U} = [0, 50, 100, 200]$ and fixed q. Normal stresses σ_{11} (a,d,g), σ_{22} (b,e,h) and shear stress σ_{12} (c,f,i) versus γ of actin networks with variable cross-linker density $R = 1/40$ in (a)-(c),(g)-(i) and $R = 1/20$ in (d)-(f). The averaging parameter is fixed at $q = 3$ in (a)-(f) and $q = 2$ in (g)-(i).

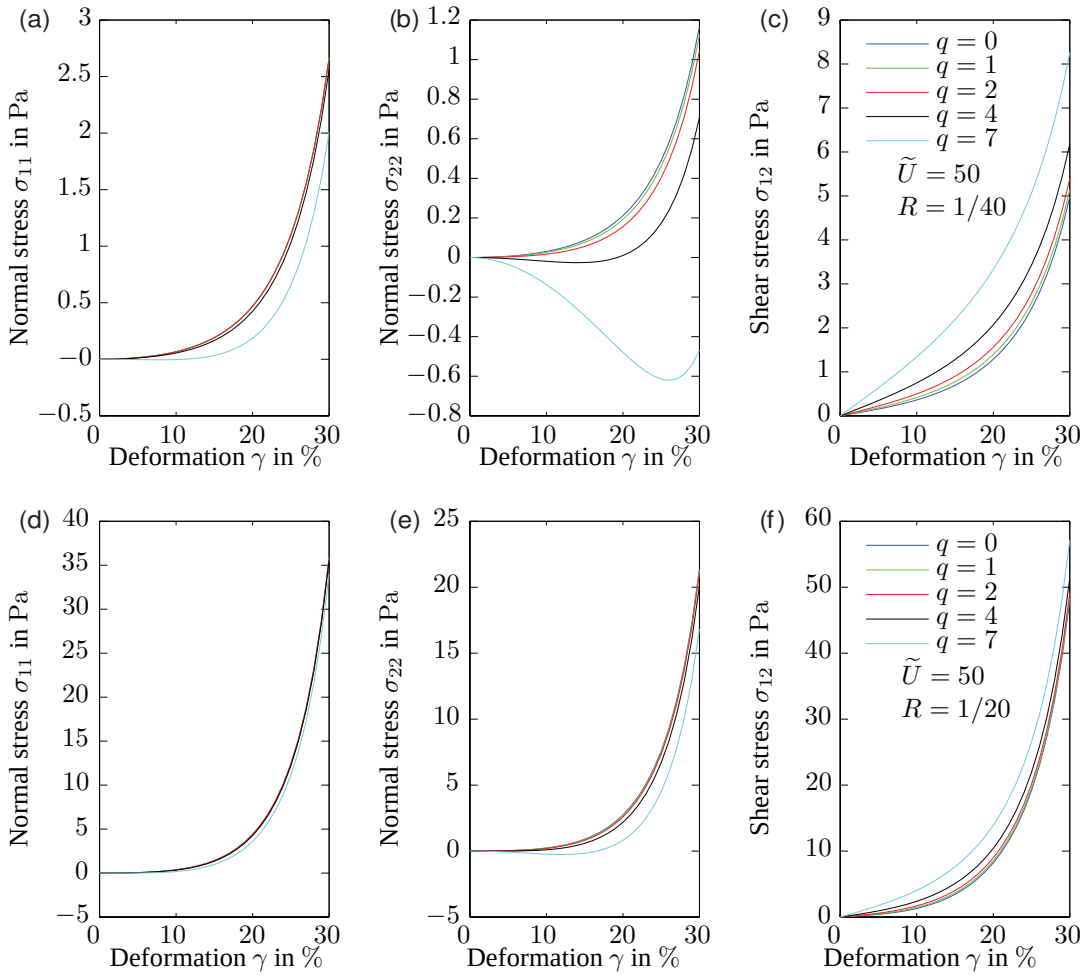

Figure 4.2: Representation of the effect of the tube part by varying the averaging parameter q with values of $q = [0, 50, 100, 200]$ and fixed $\widetilde{U}$. This is displayed by the normal Cauchy stresses σ_{11} (a),(d) σ_{22} (b),(e) and shear stress σ_{12} (c),(f) versus deformation γ. Using in (a)-(c) the material parameters of an actin network for $R = 1/40$ and in (d)-(f) for $R = 1/20$. The geometrical parameter is fixed at $\widetilde{U} = 50$ in (a)-(f).

curve, if either $\widetilde{U} = 0$ or $q = 0$. In this case, the stiffness for the normal stresses σ_{11} and σ_{22} is very low nearly zero at the deformation up to $10\,\%$. After that, the tangent of the curve begins to increase slightly and increases rapidly in the last third. Consequently, both normal stresses exhibit a small stiffness in the lower region and a high stiffness in the upper region of deformation. The response of the shear stress σ_{12} differs somewhat from the normal stress by increasing the deformation. It shows from the beginning a positive gradient and becomes slowly stiffer as the deformation increases. In all cases, the tangent is always positive by neglecting the tube part.

Before we continue to analyze the effect of the tube part in detail, we mention a few words, how these two parameters $\widetilde{U}$ and q affect the network in general. Equation (4.24) reveals that $\widetilde{U}$ is inversely proportional to the initial diameter of the cross section d_0 of the

tube. If we increase $\widetilde{U}$, that means that the diameter is decreased and it follows that the filaments between the cross-linkers have less freedom of movement. The network seems to be stiffer. The averaging parameter q affects the macro-area stretch exponentially. A general observation, which we see in Figure 4.1 and 4.2, is that the stiffness becomes lower for the normal stresses σ_{11} and σ_{22} if the parameters $\widetilde{U}$ or q increase. In contrast, shear stress σ_{12} shows a stiffer response by increasing the parameters.

Consider equations $(4.34)_{1,4}$, $(4.35)_{1,4}$ and $(4.38)_3$, we notice that by increasing the deformation, the impact on the structural tensor $\mathbf{h}$ in x_1-direction is more significant than on $\mathbf{k}$. Observe that $\widetilde{\mathbf{h}}$ and $\widetilde{\mathbf{k}}$ also depend on γ. This observation is confirmed by the Figures 4.1(a),(d),(e) and 4.2(a),(d), which indicate a minor effect of the tube part on normal stress σ_{11}. The only slight effect occurs at $q = 7$ according to Figure 4.2(a).

The normal stress in x_2-direction σ_{22} is much more affected by the tube part compared to the x_1-direction, that can be deduced from equations $(4.34)_{3,4}$, $(4.35)_{3,4}$ and $(4.38)_6$. This effect caused, that the characteristics of the curve changes from strictly monotonically increasing to a non-monotonic function. The tangent is negative in the lower region of the deformation and it changes the sign after the local minimum. By increasing the parameters $\widetilde{U}$ or q, the local minimum is getting smaller and is reached later at higher deformation. These statements are clearly seen in Figures 4.1(b),(h) and 4.2(b), but not so prominently in Figures 4.1(e) and 4.2(e). Note the different scales on the axis of ordinates in Figures 4.1(b),(e) and 4.2(b),(e), respectively. We used in Figures 4.1(d)-(f) and 4.2(d)-(f) the material parameters with a higher filament density $R = 1/20$, which results in higher values of stresses in the stretch part. The effect of the tube part on σ_{22} seems to be minimal by using the parameters for $R = 1/20$ (see Figures 4.1(e), 4.2(e)), but in the small scale, the negative response in x_2-direction can be observed just like in Figures 4.1(b) and 4.2(b).

Consider the equations associated with the shear stress σ_{12}, i.e. $(4.34)_2$, $(4.35)_2$ and $(4.38)_7$, the deformation has an equivalent effect on the structural tensor $\mathbf{h}$ and area-stretch tensor $\mathbf{k}$. By increasing $\widetilde{U}$ and q, respectively, the shear stress shows a significant response, depicted in Figures 4.1(c),(f),(i) and 4.2(c),(f).

If $q = 2$, then the entries of the area-stretch tensor $\mathbf{k}$ according to equation (4.41) are calculated as

$$\begin{aligned} k_{11} = k_{33} &= \frac{2}{3}, \\ k_{22} &= \frac{2}{3}(1+\gamma^2) \quad \text{and} \\ k_{12} &= -\frac{2}{3}\gamma. \end{aligned} \tag{4.42}$$

By equations $(4.38)_3$ and $(4.42)_1$, we note that the term of the tube constraint on the normal stress σ_{11} is zero and independent of $\widetilde{U}$. This is observed in Figure 4.1(g). The contribution of the tube part on the normal stress σ_{22} has the value of $-2\psi_c'\gamma^2/3$. This results in a smoother curve, compare Figure 4.1(b) with 4.1(h). The difference between the curves depicted in Figure 4.1(c) and 4.1(i), respectively, is slightly noticeable. The factor $\widetilde{k}_{12}$ is omitted in equation $(4.35)_4$ if $q = 2$.

We conclude this section by focusing again on the results of the normal stress in x_2-direction, which allows an obscure observation. It is not physically meaningful that stress changes the sign of the direction, during increasing deformation. In this way, there is not an acceptable explanation of the tube constraint. What we see clearly is that the tube part for normal stress in x_2-direction has a greater impact than in x_1-direction. Comparing Figures 4.1(a)-(c),(g)-(h) to 4.1(d)-(f) and Figures 4.2(a)-(c) to 4.2(d)-(f), respectively, we can infer that the cross-linker density has an impact on the effect of the tube part. The stiffer the network the greater the impact of the tube part. All in all we have to determine two additional parameters, which are not physically interpretable, and the effect of the tube constraint does not necessarily reflect a realistic sense. Therefore, we challenge the necessity of the tube part. As long as we cannot develop a better understanding of these two parameters, it makes no sense to incorporate the tube part into the model.

5 A closer look on the averaging parameter

In this chapter we focus our interest on the analysis of the parameter p of the model of Unterberger et al. (submitted), which is specified in equation (3.95). Most of the model parameters are physically interpretable and most of them are determined by the single filament model. The temperature T is determined by the experiments and it usually takes the value of room temperature $21\,^{\circ}\mathrm{C}$. The persistence length L_{p} is a material parameter which is postulated in the literature for many biopolymers with much controversy. For F-actin, however there is great consensus. Le Goff et al. (2002) published a value around $16\,\mu\mathrm{m}$. Based on the experimental data of a single actin filament by Liu and Pollack (2002), Unterberger et al. (submitted) used the nonlinear Least Squares tool (lsqnonlin) of MATLAB with fixed persistence length and temperature to determine the remaining parameters. The best fit was reached by the values $L = 11.264\,\mu\mathrm{m}, r_0 = 10.17\,\mu\mathrm{m}, \mu_0 = 38.6\,\mathrm{nN}$ and $\beta = 0.438$, see Unterberger et al. (submitted). The ratio $r_0/L = 0.91$ is very useful for finding the network parameters, because the contour length L refers to the length of the filament between the cross-linkers in the network. Therefore, this length varies with the density of the cross-linker. The number of filaments per unit volume n is determined by the ratio of the total length of the filaments to the reference volume. Unterberger et al. (submitted) calculate the relation between n and the contour length L through

$$n = \frac{15.0\,\mu\mathrm{m}^{-2}}{L}. \tag{5.1}$$

The parameters, the contour length L, the initial stretch λ_0 and the averaging parameter p, are the remaining parameters which are determined by fitting to rheological data using the nonlinear Least Squares tool of MATLAB. Values are published in Unterberger et al. (submitted) for a variety of examples with different cross-linker densities. The initial stretch and the contour length are just acting on the single filament model. The only parameter which has no physical interpretation is the averaging parameter p to which we turn now our attention.

5.1 Analysis of the structural tensor

The parameter p acts on the network scale and plays an important role in the structural tensor $\mathbf{h}$. To make the influence of this parameter visible, we visualize the structural tensor.

Therefore, we have to analyze the properties of $\mathbf{h}$. But before we start, we take a short excursion into the linear algebra.

Let $\mathbf{A}$ be a symmetric matrix with real entries, i.e. $\mathbf{A} = \mathbf{A}^\top$ and $\mathbf{A} \in \mathbb{R}^{n\times n}$, and let $\mathbf{v}$ be an eigenvector of $\mathbf{A}$ corresponding to the eigenvalues υ. Hereafter, we denote the complex conjugation of a complex number by the overline. Now we perform the following steps

$$\begin{aligned} \bar{\upsilon}\bar{\mathbf{v}}^\top\mathbf{v} &= \left(\overline{\upsilon\mathbf{v}}\right)^\top\mathbf{v} = \left(\overline{\mathbf{A}\mathbf{v}}\right)^\top\mathbf{v} \\ &= \bar{\mathbf{v}}^\top\bar{\mathbf{A}}^\top\mathbf{v} = \bar{\mathbf{v}}^\top\mathbf{A}\mathbf{v} \\ &= \bar{\mathbf{v}}^\top\left(\upsilon\mathbf{v}\right) = \upsilon\bar{\mathbf{v}}^\top\mathbf{v}. \end{aligned} \tag{5.2}$$

Since the product of a complex number with its complex conjugate number is real, the product of $\bar{\mathbf{v}}^\top\mathbf{v}$ is real and unequal zero, and it follows from (5.2), that $\bar{\upsilon} = \upsilon$, i.e $\upsilon \in \mathbb{R}$. All eigenvalues of a real, symmetric matrix are real. Let $\mathbf{v}_1, \mathbf{v}_2$ be eigenvectors of $\mathbf{A}$ corresponding to different eigenvalues υ_1, υ_2. Following these steps

$$\begin{aligned} \upsilon_1\mathbf{v}_1^\top\mathbf{v}_2 &= \left(\mathbf{A}\mathbf{v}_1\right)^\top\mathbf{v}_2 = \mathbf{v}_1^\top\mathbf{A}^\top\mathbf{v}_2 \\ &= \mathbf{v}_1^\top\left(\mathbf{A}\mathbf{v}_2\right) = \upsilon_2\mathbf{v}_1^\top\mathbf{v}_2 \\ \Rightarrow \quad 0 &= \underbrace{\left(\upsilon_1 - \upsilon_2\right)}_{\neq 0}\mathbf{v}_1^\top\mathbf{v}_2, \end{aligned} \tag{5.3}$$

we are able to conclude that the eigenvectors of $\mathbf{A}$ build an orthogonal system. The theorem about the principal component analysis (PCA) says that any real symmetric matrix is diagonalizable, meaning that it is similar to a diagonal matrix, see Fischer (2003, Sec. 5.7). This theorem reveals that there is an orthogonal matrix $\mathbf{E}^{-1} = \mathbf{E}^\top$ whose column vectors consists of the orthonormal eigenvectors of $\mathbf{A}$ and a diagonal matrix $\mathbf{D}$ consisting of the real eigenvalues of $\mathbf{A}$, such that

$$\mathbf{D} = \mathbf{E}^{-1}\mathbf{A}\mathbf{E} \tag{5.4}$$

holds.

Let us consider the following real quadratic form in $\mathbb{R}^3$

$$ax^2 + by^2 + cz^2 + 2dxy + 2exz + 2fyz = \begin{bmatrix} x & y & z \end{bmatrix}\begin{bmatrix} a & d & e \\ d & b & f \\ e & f & c \end{bmatrix}\begin{bmatrix} x \\ y \\ z \end{bmatrix} = \mathbf{x}^\top\mathbf{A}\mathbf{x}, \tag{5.5}$$

with the symmetric matrix $\mathbf{A}$. We know therefore, from the above considerations, that $\mathbf{A}$ has real eigenvalues and is diagonalizable by an orthogonal matrix $\mathbf{E}$ and is written in the form

$$\mathbf{A} = \mathbf{E}\mathbf{D}\mathbf{E}^\top. \tag{5.6}$$

Further, we are interested in classifying the hypersurface which is represented in (5.5). For

this purpose we want to transfer the equation (5.5) in the canonical form

$$\frac{x^2}{a^2} \pm \frac{y^2}{b^2} \pm \frac{z^2}{c^2} = \pm 1. \tag{5.7}$$

The first thing we have to do, is to eliminate the cross terms xy, xz, yz in equation (5.5), this means that we rotate the object in its ordinary coordinate system. With this in mind, we have to transform the matrix $\mathbf{A}$ into a diagonal matrix $\mathbf{D}$. Under the change of basis which we define through $\mathbf{x} := \mathbf{E}\mathbf{y}$ or $\mathbf{y} = \mathbf{E}^\top \mathbf{x}$, respectively and with (5.6) we obtain

$$\mathbf{x}^\top \mathbf{A}\mathbf{x} = \mathbf{x}^\top \mathbf{E}\mathbf{D}\mathbf{E}^\top \mathbf{x} = \left(\mathbf{E}^\top \mathbf{x}\right)^\top \mathbf{D} \left(\mathbf{E}^\top \mathbf{x}\right) = \mathbf{y}^\top \mathbf{D}\mathbf{y}. \tag{5.8}$$

In this way, the eigenvectors of $\mathbf{A}$ represent the directions of the principal axes and the eigenvalues of $\mathbf{A}$ determine the type of the hypersurface. If all eigenvalues are positive we obtain the equation of an ellipsoid which is given in the canonical form with real and positive semiaxes $a, b, c \in \mathbb{R}_+$

$$\frac{x^2}{a^2} + \frac{y^2}{b^2} + \frac{z^2}{c^2} = 1. \tag{5.9}$$

For the sake of completeness, the volume of an ellipsoid is given by

$$V = \frac{4}{3}\pi abc. \tag{5.10}$$

In the reference configuration, which means that no deformation is applied to the object $\mathbf{F} = \mathbf{I}$, the structural tensor $\mathbf{h}$ is represented by sphere with radius $1/3$. That is because, the discrete macro stretch $\bar{\lambda}^i = 1$ for all i and therefore $\mathbf{h} = \langle \mathbf{\Pi} \otimes \mathbf{\Pi} \rangle = 1/3\, \mathbf{I}$ holds by condition (3.85). As a result, the volume in the reference configuration is determined by

$$V_{\text{ref}} = \frac{4\pi}{81}. \tag{5.11}$$

If $p = 2$, the structural tensor results in $\mathbf{h} = 1/3\, \mathbf{b}$, which we see later in eqaution (5.26). Since we have assumed that the material is incompressible ($\det \mathbf{F} = 1$), it follows that $\det \mathbf{b} = 1$, independent of the deformation mode. This again means that the volume of structural tensor is equal to the reference volume if $p = 2$

$$V(\mathbf{h}, p = 2) = V_{\text{ref}}. \tag{5.12}$$

But this does not mean, that the eigenvalues of $\mathbf{b}$ are always the same in consideration of different deformation modes, see Section 5.2. If we change the value of p, the volume of $\mathbf{h}$ changes of course. In this way we interpret the ratio of the current volume to reference volume as a measure for the non-affinity.

Let us now return to the analysis of the structural tensor. We consider an incompressible material, i.e. $\det \mathbf{F} = 1$, in view of a simple shear and an equibiaxial deformation. Both types of deformations have already been introduced in Section 2.1.4. Consider again the

structural tensor $\mathbf{h}$, which we have obtained in equation (4.28) and (4.29) in Section 4.2,

$$\mathbf{h} = \mathbf{F}\langle\bar{\lambda}^{p-2}\mathbf{\Pi}\otimes\mathbf{\Pi}\rangle\mathbf{F}^{\top}, \tag{5.13}$$

with

$$\widetilde{\mathbf{h}} = \langle\bar{\lambda}^{p-2}\mathbf{\Pi}\otimes\mathbf{\Pi}\rangle \approx \sum_{i=1}^{21}\left(\bar{\lambda}^{i}\right)^{p-2}\mathbf{\Pi}^{i}\otimes\mathbf{\Pi}^{i}w^{i}. \tag{5.14}$$

Again, the discrete macro stretch is defined by

$$\bar{\lambda}^{i} = \|\mathbf{F}\mathbf{\Pi}^{i}\|, \tag{5.15}$$

which is always positive and real if $\mathbf{\Pi}^{i} \neq \mathbf{0}$. The weights w^{i}, which are given in Bažant and Oh (1986), are also positive and real. Since the dyadic product of $\mathbf{\Pi}\otimes\mathbf{\Pi}$ is obviously commutative, it is implied that the result of it is a symmetric tensor and that means that $\widetilde{\mathbf{h}} = \widetilde{\mathbf{h}}^{\top}$ is symmetric. This yields with equation (5.13) that $\mathbf{h}$ is symmetric

$$\mathbf{h}^{\top} = \left(\mathbf{F}\widetilde{\mathbf{h}}\mathbf{F}^{\top}\right)^{\top} = \mathbf{F}\widetilde{\mathbf{h}}\mathbf{F}^{\top} = \mathbf{h} \tag{5.16}$$

and its entries are real $\mathbf{h} \in \mathbb{R}^{3\times 3}$.

Next, we want to show that all eigenvalues of $\mathbf{h}$ are positive. Considering a simple shear deformation we got in Section 4.2 the following matrix notation for the structural tensor

$$[\mathbf{h}] = \begin{bmatrix} \widetilde{h}_{11} + 2\gamma\widetilde{h}_{12} + \gamma^{2}\widetilde{h}_{22} & \widetilde{h}_{12} + \gamma\widetilde{h}_{22} & 0 \\ \widetilde{h}_{12} + \gamma\widetilde{h}_{22} & \widetilde{h}_{22} & 0 \\ 0 & 0 & \widetilde{h}_{33} \end{bmatrix}. \tag{5.17}$$

The criterion of Sylvester (Fischer 2003, p. 327) states that a real symmetric matrix is positive definite if and only if all leading principal minors are positive. In other words, if all the following matrices, the upper left 1-by-1 corner of $\mathbf{h}$, the upper left 2-by-2 corner of $\mathbf{h}$ and $\mathbf{h}$ itself, have a positive determinant. This criterion is satisfied if

$$h_{11}h_{22} - h_{12}^{2} > 0 \tag{5.18}$$

holds. Continue with the calculation of latter equation by using the corresponding entries of $\mathbf{h}$, which are given in equation 5.17, thus follows

$$\widetilde{h}_{11}\widetilde{h}_{22} - \widetilde{h}_{12}^{2} > 0. \tag{5.19}$$

In order to prove this inequality, we need the Cauchy-Schwarz inequality, which is given in Heuser (2006, Sec. 12) and which we formulate in the following way

Theorem 5.1.1. (Chauchy-Schwarz inequality)

$$\left|\sum_{i=1}^{n} x_i y_i\right|^2 \leq \left(\sum_{j=1}^{n} x_j^2\right)\left(\sum_{k=1}^{n} y_k^2\right) \tag{5.20}$$

Equality holds if and only if x and y are linearly dependent.

Proof. see Heuser (2006, p. 97) □

The entries of $\widetilde{\mathbf{h}}$ are computed by the 21-point integration formula, as we have done in equation (4.29). In this way we are able to compute each matrix entry by

$$\widetilde{h}_{j\ell} = \sum_{i=1}^{21} \left(\bar{\lambda}^i\right)^{p-2} \left(\Pi_j^i\right)\left(\Pi_\ell^i\right) w^i. \tag{5.21}$$

The subscript j of Π_j denotes the vector entries corresponding to the j-th axis direction. By using the computational formulation of $\widetilde{h}_{j\ell}$ in equation (5.19) we obtain

$$\left(\sum_{i=1}^{21} \left(\bar{\lambda}^i\right)^{p-2} \left(\Pi_1^i\right)^2 w^i\right)\left(\sum_{i=1}^{21} \left(\bar{\lambda}^i\right)^{p-2} \left(\Pi_2^i\right)^2 w^i\right) - \left(\sum_{i=1}^{21} \left(\bar{\lambda}^i\right)^{p-2} \left(\Pi_1^i\right)\left(\Pi_2^i\right) w^i\right)^2 > 0. \tag{5.22}$$

With the theorem of Chauchy-Schwarz inequality, we can estimate the second term of latter equation

$$\left(\sum_{i=1}^{21} \left(\bar{\lambda}^i\right)^{p-2} \left(\Pi_1^i\right)\left(\Pi_2^i\right) w^i\right)^2 \geq \left(\sum_{i=1}^{21} \left(\bar{\lambda}^i\right)^{p-2} \left(\Pi_1^i\right)^2 w^i\right)\left(\sum_{i=1}^{21} \left(\bar{\lambda}^i\right)^{p-2} \left(\Pi_2^i\right)^2 w^i\right). \tag{5.23}$$

We denote through $\mathbf{\Pi}_\ell$ the vector which contains all entries of the 21 orientation vectors $\mathbf{\Pi}_\ell$ in ℓ-direction. Since $\mathbf{\Pi}_1$ is linearly independent to $\mathbf{\Pi}_2$ we get a strictly-less sign at the inequality of Chauchy-Schwarz. Hence, we satisfy the inequality (5.18) and thus the structural tensor is positive definite and it holds

$$\mathbf{x}^\top \mathbf{h} \mathbf{x} > 0 \qquad \text{for all } \mathbf{x} \in \mathbb{R}^3. \tag{5.24}$$

In the case of equibiaxial deformation, we obtain a structural tensor with the following diagonal matrix

$$[\mathbf{h}] = \begin{bmatrix} \lambda^2 \widetilde{h}_{11} & 0 & 0 \\ 0 & \lambda^2 \widetilde{h}_{22} & 0 \\ 0 & 0 & \lambda^{-4} \widetilde{h}_{33} \end{bmatrix}. \tag{5.25}$$

Since each diagonal element is positive, we also obtain a positive definite structural tensor $\mathbf{h}$.

Finally, we are able to illustrate the structural tensor as an ellipsoid in the three-dimensional space. The eigenvectors of $\mathbf{h}$ represent the principal directions of the ellipsoid and the associated eigenvalues represent the length of the semiaxes.

5.2 Geometrical interpretation of the structural tensor

The parameter p has an influence on micro- and macro-stretches and these depend on the deformation gradient. We are unable to interpret the parameter p physically, but we are able to interpret it in the geometrical sense, what we are doing now. First, we consider what it means when we increase the parameter p, if we perform an equibiaxial deformation. After that we consider the effect of p when applying simple shear deformation. In both considerations, we choose two different values of p and compare them. The first value is fixed at $p = 2$ since this is a special case of the structural tensor. This results in $\bar{\lambda}^{2-2} = 1$ and consequently we get by definition of $\mathbf{h}$ and equation (3.86) and (2.25)

$$\mathbf{h} = \mathbf{F} \underbrace{\langle \mathbf{\Pi} \otimes \mathbf{\Pi} \rangle}_{=\frac{1}{3}\mathbf{I}} \mathbf{F}^{\top} = \frac{1}{3}\mathbf{b}. \tag{5.26}$$

The second selected value of p is consistent with the averaging parameter that was determined in the experiment for the sample $R = 1/40$ of Unterberger et al. (submitted), which is $p = 8$. From the previous section, we know that the structural tensors are real, symmetric and positive definite, for both equibiaxial deformation and simple shear deformation. Thus we may represent the structural tensor as an ellipsoid. We label the direction of the principal axes by 1-, 2- and 3-direction. The axes of the coordinate system are denoted by x_1, x_2 and x_3, respectively.

Let us now discuss the effect of p at equibiaxial deformation. We perform an uniform stretch in the direction of x_1- and x_2-axes of $5\,\%$, thus the deformation gradient in matrix form reads as

$$[\mathbf{F}] = \begin{bmatrix} 1.05 & 0 & 0 \\ 0 & 1.05 & 0 \\ 0 & 0 & \frac{1}{1.05^2} \end{bmatrix}. \tag{5.27}$$

The resulting ellipsoids with the two different values of p are depicted in Figure 5.1. The left one shows the normal projection on the x_1x_2-plane and the right one the projection on the x_1x_3-plane. If $p = 2$ the resulting structural tensor in matrix form looks like

$$[\mathbf{h}] = \frac{1}{3} \begin{bmatrix} 1.05^2 & 0 & 0 \\ 0 & 1.05^2 & 0 \\ 0 & 0 & \frac{1}{1.05^4} \end{bmatrix}. \tag{5.28}$$

The associated eigenvalues and eigenvectors can be easily determined, which are $\upsilon_{1,2} = 0.367$ and $\upsilon_3 = 0.274$ with the standard basis for the three-dimensional space $\mathbf{e}_1, \mathbf{e}_2$ and $\mathbf{e}_3$, respectively. The subscripts denote the principal axes directions. In contrast, the eigen-

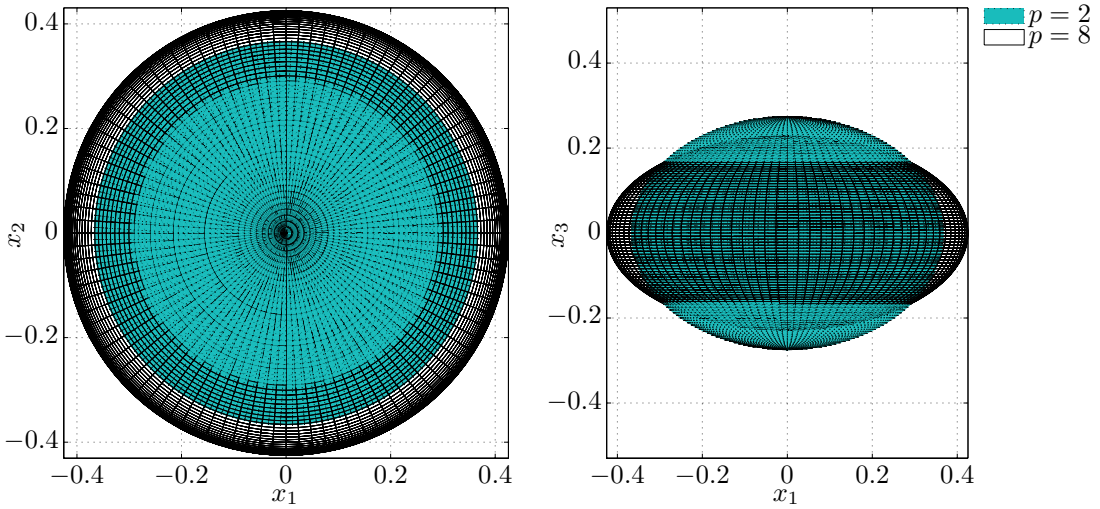

Figure 5.1: Visualization of $\mathbf{h}$ for $p = 2$ and $p = 8$ at equibiaxial deformation with uniform stretch in x_1- and x_2-direction of $5\,\%$. The ellipsoids are shown here in top view (left) and front view (right).

values of $\mathbf{h}$ at $p = 8$ are $\upsilon_{1,2} = 0.425$ and $\upsilon_3 = 0.228$ with unchanged eigenvectors. These values can be read in the images of Figure 5.1. To sum up, we observe a uniform stretch in 1- and 2-direction and a contraction in 3-direction by increasing p. The volume of the ellipsoid is also increasing if p increases, although only very slightly. The stretch in 1- or 2-direction is greater than the contraction in 3-direction.

Consider next the geometrical representation of the structural tensor with the use of simple shear deformation. We select the amount of deformation at $\gamma = 20\,\%$. In matrix notation the deformation gradient has the following form

$$[\mathbf{F}] = \begin{bmatrix} 1 & 0.2 & 0 \\ 0 & 1 & 0 \\ 0 & 0 & 1 \end{bmatrix} . \tag{5.29}$$

The associated visualized structural tensors for $p = 2$ and $p = 8$ are depicted in Figure 5.2. On the left side of Figure 5.2 we view the x_1x_2-plane and on the right side the x_1x_3-plane. We are able to easily compute $\mathbf{h}$ if $p = 2$. Using equation (5.26), the structural tensor is written in matrix notation as follows

$$[\mathbf{h}] = \frac{1}{3} \begin{bmatrix} 1.04 & 0.2 & 0 \\ 0.2 & 1 & 0 \\ 0 & 0 & 1 \end{bmatrix} . \tag{5.30}$$

The associated eigenvalues of $\mathbf{h}$ are $\upsilon_1 = 0.407$, $\upsilon_2 = 0.273$ and $\upsilon_3 = 0.333$, respectively, with the corresponding eigenvectors $\mathbf{v}_1 = [0.741\ 0.671\ 0]^\top$, $\mathbf{v}_2 = [0.671\ 0.741\ 0]^\top$ and $\mathbf{v}_3 = [0\ 0\ 1]^\top$, respectively. This eigenvectors form an orthonormal basis of $\mathbb{R}^3$. By changing $p = 8$ the eigenvectors remain the same with associated eigenvalues of

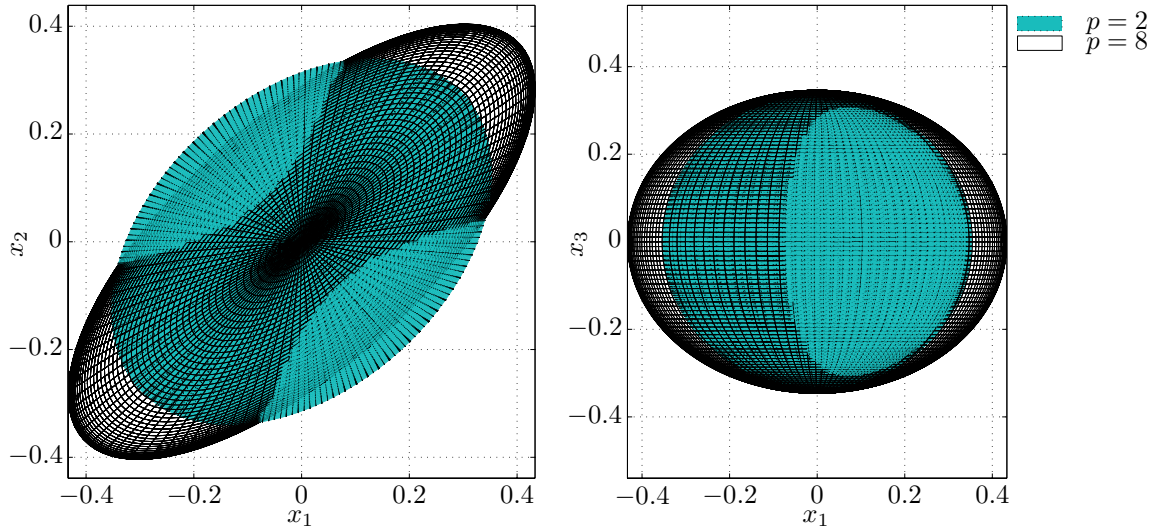

Figure 5.2: Visualisation of **h** for $p = 2$ and $p = 8$ at simple shear deformation with an deformation of $20\,\%$. The ellipsoids are shown here in top view (left) and front view (right).

$\upsilon_1 = 0.546, \upsilon_2 = 0.229$ and $\upsilon_3 = 0.346$.

First of all we can say that a stretch in 1-direction, a smaller stretch in 3-direction and a contraction in 2-direction occurs by increasing p. The quantity of the stretch in 1-direction is greater than the quantity of the contraction in the 2-direction. This observations are illustrated in Figure 5.2. As in the case of equibiaxial deformation, the volume increases as well. At this point, we demonstrate in Figure 5.3 the change in volume as a function of p normalized by reference volume. There is an affine deformation for $p = 2$ which yields

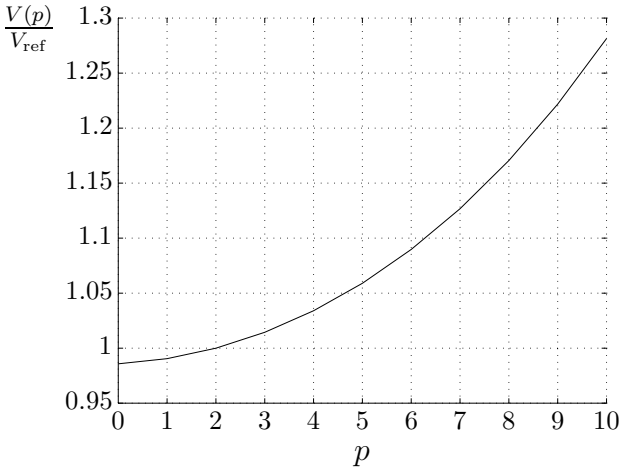

Figure 5.3: Demonstration of the change in volume by increasing p. The current volume $V(p)$ is normalized by the reference volume V_{ref}.

that $V(p)/V_{\text{ref}} = 1$. The measure of non-affinity increases non-linearly by increasing p.

The second thing is that we perceive a rotation of the principal axes with respect to the x_1- and x_2-axes. In general, the angle between two nonzero vectors $\mathbf{x}, \mathbf{y}$ can be calculated by the dot product, through

$$\theta = \arccos\left(\frac{\mathbf{x}\cdot\mathbf{y}}{\|\mathbf{x}\|\|\mathbf{y}\|}\right). \tag{5.31}$$

The principal axes in the undeformed configuration are described by the standard basis of the Euclidean space. By using the eigenvectors associated with the 1-direction $\mathbf{e}_1$ and $\mathbf{v}_1$, or the eigenvectors associated with the 2-direction $\mathbf{e}_2$ and $\mathbf{v}_2$, we calculate the rotation angle with equation (5.31). The resulting angle is about $\theta = 42.1°$. In Figure 5.4 we demonstrate this rotation of the principal axes. The parallelogram represents the deformation of a

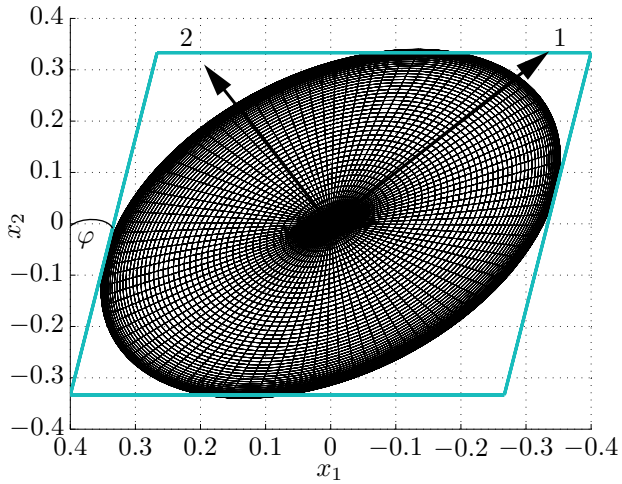

Figure 5.4: Representation of the rotation of the ellipsoid at $p = 2$ of the 1- and 2-principal axes directions. Symbolical description of simple shear deformation with $\varphi = \arctan\gamma$ by the parallelogram.

rectangle under simple shear and the ellipse corresponds to the ellipsoid in the x_1x_2-plane if $p = 2$. The arrows in Figure 5.4 show the principial axes in 1- and 2-direction of the ellipsoid.

An interesting observation is that this value of θ coincides with the formulation of the relation between the angle for the principal axes of the left Cauchy-Green tensor $\mathbf{b} = \mathbf{F}\mathbf{F}^\top$ and the amount of deformation γ, which is given by Ogden (1997, p. 103) in the following way

$$\tan 2\theta = \frac{2}{\gamma}. \tag{5.32}$$

Consider equation (5.26), which states that $\mathbf{h} = 1/3\,\mathbf{b}$ if $p = 2$, it is easy to see the above agreement. By increasing p, the eigenvectors do not change, thus the above formulation holds for arbitrary values of p. In this sense, we are able to infer, that the principal axes in 1-, 2-direction of $\mathbf{h}$ rotate by the same angle as the Eulerian principal axes of $\mathbf{b}$ by considering simple shear deformation. Now we can easily compute the rotation angle θ

by equation (5.32). The rotation of the ellipsoid in x_1x_2-plane is independent of p. To substantiate this statement we compare the gained equation $(2.27)_1$ from Section 2.1.3

$$\mathbf{b} = \mathbf{R}\mathbf{U}^2\mathbf{R}^\top \tag{5.33}$$

with

$$\begin{aligned} \mathbf{h} &= \mathbf{F}\langle\bar{\lambda}^{p-2}\mathbf{\Pi}\otimes\mathbf{\Pi}\rangle\mathbf{F}^\top \\ &= \mathbf{R}\mathbf{U}\langle\bar{\lambda}^{p-2}\mathbf{\Pi}\otimes\mathbf{\Pi}\rangle\mathbf{U}^\top\mathbf{R}^\top. \end{aligned} \tag{5.34}$$

Since $\langle\bar{\lambda}^{p-2}\mathbf{\Pi}\otimes\mathbf{\Pi}\rangle$ is symmetric and positive definite and acts in the reference configuration, i.e. it has the same properties as $\mathbf{U}$, we define the tensor $\widetilde{\mathbf{U}}^2 = \mathbf{U}\langle\bar{\lambda}^{p-2}\mathbf{\Pi}\otimes\mathbf{\Pi}\rangle\mathbf{U}^\top$, where the properties of a stretch tensor are maintained and thus it follows

$$\mathbf{h} = \mathbf{R}\widetilde{\mathbf{U}}^2\mathbf{R}^\top. \tag{5.35}$$

Latter equation differs from equation (5.33) only by the stretch tensor, but both formulations are subject to the same rotation tensor.

6 Material parameters for fibrin

In the previous sections we discussed models for single filaments and biological networks. A closer examination was carried out on the Unterberger model, see Section 3.2.2, which includes the Holzapfel-Ogden model, see Section 3.1.3. Both models have been developed only recently. The Holzapfel-Ogden model fits very well the experimental data to dsDNA from Bustamante et al. (2000) and F-actin from Liu and Pollack (2002), see Holzapfel and Ogden (submitted). Experimental data of actin networks was obtained via rheological experiments by Unterberger et al. (submitted), which are very well described by the Unterberger model. The resulting material parameters are summarized in Table 4.1. Based on the Holzapfel-Ogden model and the Unterberger model, we want to examine the characteristics of another biopolymer. We look for suitable material parameters for fibrin. Based on the experimental data of a single fibrin fiber of Hudson et al. (2010), we first analyze the properties of the single filament by fitting the Holzapfel-Ogden model. Afterwards we continue the study of the properties of its network based on the experimental data of Kang et al. (2009) by fitting the Unterberger model. But before we begin, we give a review of the properties of fibrin which have been discussed previously in the literature.

6.1 Properties of fibrin

In the last few years several research groups investigated the mechanical properties of fibrin fibers and attempted to justify these properties. The molecular origins of the extensibility of fibrin are still not fully understood. These groups of researchers issued different values of material parameters especially for the persistence length. This disagreement made it difficult to obtain meaningful values for the Holzapfel-Ogden model. Storm et al. (2005) determined a persistence length of fibrin which is $L_{\mathrm{p}} = 0.5\,\mu\mathrm{m}$. By contrast Houser et al. (2010) reached an average persistence length of $0.1 - 0.6\,\mathrm{nm}$ and Brown et al. (2007) published a persistence length of $L_{\mathrm{p}} = 0.8\,\mathrm{nm}$. To be careful these persistence lengths were obtained by execution of different experiments. Hudson et al. (2010), Houser et al. (2010), and Brown et al. (2007) used atomic force microscopy to determine mechanical properties of single fibrin fibers. Whereas the determination of mechanical properties of fibrin by Storm et al. (2005) are based on fibrin protofibril networks.

Further experiments on fibrin networks were done by Kang et al. (2009) and Brown et al. (2009). Kang et al. (2009) conducted experiments with different cross-linker densities. One experiment describes rather a network consisting of semiflexible filaments, called fine clot, and the other more like a network of rigid filaments, referred to as coarse clot. Semiflexible polymers are usually described by an entropic model. Stiff polymers are bet-

ter modeled by enthalpic models that are based on the orientation and stretching of fibers, see Kang et al. (2009). At this point it should be noted that the Holzapfel-Ogden model is a mixture of entropic and enthalpic models. From the experiments on fine clots, Kang et al. (2009) determined a persistence length of $L_\mathrm{p} = 0.5\,\mu\mathrm{m}$, which coincides with Storm et al. (2005), and for coarse clots, which is more physiological, a $L_\mathrm{p} > 1\,\mathrm{mm}$. It seems as if the determination of the persistence length of fibrin is still ambiguous. The values span a range of seven orders of magnitude. According to the opinion of Hudson et al. (2010) and Houser et al. (2010) fibrin fibers behave as elastomeric elements, they do not fit into the conventional categories of flexible, semiflexible or stiff biopolymers.

Fibrin exhibits viscoelastic properties which are analyzed in detail in Weisel (2004). Unligated fibers could be stretched 2.2 times their length and ligated fibers 2.8 times their length without permanent damage and they still return to their initial length, see Liu et al. (2006). These authors conclude, that the effect of ligation of fibrin is extraordinary, because this would usually make the fibers stiffer and less extensible, but this holds not for fibrin. The reason could be that the ligation occurs directly along the fiber axis, this has been suggested in Liu et al. (2006). The individual fibrin fibers have a larger extensibility than the fibrin networks, see Liu et al. (2006). Thus it can be assumed, that the clot rupture does not stem from the rupture of the individual fibers but rather from the branch points. Recent publications argue that this extraordinary extensibility originates from the stretching of an unstructured $\alpha\mathrm{C}$ region, for example see Houser et al. (2010). In contrast Brown et al. (2009) proposed that this behavior comes from the unfolding of a coiled coil domain between the D and E region, see Figure 1.3. The properties of fibrin are still not totally explored, but we are trying now to determine suitable material parameters for fibrin.

6.1.1 Characterization of a single fibrin fiber

Before we proceed to the network model we first have to determine the material parameters of the single fibrin fiber. We use the experimental data of Hudson et al. (2010) and fit the parameters of the extensible Holzapfel-Ogden model to these data. The single fibrin fiber was stretched by the tip of an atomic foce microscope (AFM) and this stretching process was imaged by a fluorescence microscope. Houser et al. (2010) described these experiments in more detail. The resulting data yield a force versus strain curve, which is very useful for determining the six material parameters of the extensible Holzapfel-Ogden model (3.60), which are $L, r_0, T, L_\mathrm{p}, \mu_0, \beta$. We chose T corresponding to the room temperature, meaning $T = 21^\circ\mathrm{C}$. On the molecular structure of fibrin, which has a length of $45\,\mathrm{nm}$ and which we refer to as r_0, Houser et al. (2010) determined a persistence length in the range of $0.1-0.6\,\mathrm{nm}$ and a relation between the contour length and the relaxed origin length r_0, which is about $L = (2.4 \pm 0.4)r_0$. In agreement with this we fixed the contour length at $L = 135\,\mathrm{nm}$. By using the MATLAB's nonlinear Least Squares tool we fitted the model (3.60) with fixed $T, L,$ and r_0. The circles in Figure 6.1 represent the experimental data of Houser et al. (2010) and the curve the fit of equation (3.60). In the lower region it indicates a lower stiffness and a much higer stiffnes in the upper region when r reaches

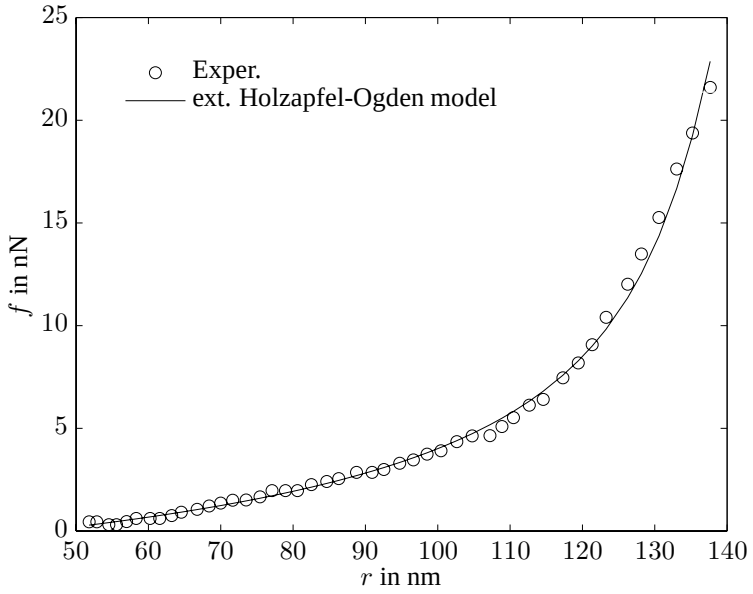

Figure 6.1: Single fibrin fiber force versus end-to-end distance curve. Experimental data were obtained by Hudson et al. (2010) (circles). The curve through the data depicts the extensible Holzapfel-Ogden model (3.60) with $T = 294\,\mathrm{K}, L_\mathrm{p} = 3.99\,\mathrm{mm}, L = 135\,\mathrm{nm}, r_0 = 45\,\mathrm{nm}, \mu_0 = 455.4\,\mathrm{nN}$, and $\beta = 2.5$.

L. The resulting free parameters are $L_\mathrm{p} = 3.99\,\mathrm{mm}, \mu_0 = 455.4\,\mathrm{nN}, \beta = 2.5$. A unique solution could not be found, but this was the one with the best fit. The received value for the persistence length is questionable. The persistence length is much greater than the contour length, which would imply that fibrin belongs in the category of rigid biopolymers. In contrast, the end-to-end distance at zero force is much less than the contour length, which suggests that it is a semiflexible biopolymer. Although the value of L_p is doubtful, however the fit is very good in Figure 6.1.

6.1.2 Characterization of a fibrin network

Biological materials consisting of cross-linked biopolymers exhibit a nonlinear elastic response by applying simple shear deformation. The experimental data which we use to analyze the network model (3.95), relate to Kang et al. (2009). In a different way, Brown et al. (2009) carried out an experiment on fibrin networks by use of uniaxial tensile tests. They observed a significant change in volume during the deformation. To account for these effects in the model they modified the eight chain model by Arruda and Boyce (1993). In the model of Brown et al. (2009), they defined a two-state formulation of a single fiber. The fiber can either be in the folded or in the unfolded state. For small forces, where the fiber is in the folded state, they argued that the force-extension relation is linear. In the unfolded state at large force, they assumed that the fibrin fiber behaves like a worm-like

chain polymer. This individual fiber model was then used in the eight chain model. Brown et al. (2009) used for the model fit a persistence length of L_p and assumed a fiber density of $0.5\,\mu\mathrm{m}^{-3}$. The network is incompressible in the fully folded and unfolded state, but it shows a negative compressibility during the transition process from folded to unfolded state. This statement is explained in detail by Purohit et al. (2011), a follow-up edition of Brown et al. (2009).

Unterberger et al. (submitted) fitted their proposed model to experimental data from rheological experiments of cross-linked actin networks. Therefore, we want to fit the Unterberger model (3.95) to experimental data from rheological experiments of fibrin networks. Such experiments were executed by Kang et al. (2009). In their experiments they used a strain controlled rheometer (RFS-III, Rheometrics) with 25 mm parallel plate geometry and increased constantly the deformation with strain rate of $0.01\,\mathrm{s}^{-1}$. Further, they executed experiments with different conditions of fibrin networks. One condition is referred to as coarse clot. It reflects more the physiological conditions and is displayed as a network of stiff filaments. The other labeled as fine clot visualized a network of semiflexible filaments. The results of the single filament of fibrin, which we obtained in Section 6.1.1, suggest that we deal with a rigid biopolymer rather than semiflexible. Therefore we focus on the experimental data of the coarse clot by Kang et al. (2009) and attempt to fit the model (3.95). In Figure 6.2 we represent the data of Kang et al. (2009) by the circles, which were obtained by averaging three samples with same condition. The green circles refer to shear stress versus strain and the red circles refer to normal stress versus strain. Since Unterberger et al. (submitted) measured the normal stresses with positive sign, we take the experimental data of the normal stresses of Kang et al. (2009) with opposite sign, see Figure 6.2.

These experimental data reflect a network with rigid fibers for wich Kang et al. (2009) postulated a persistence length which is greater than $1\,\mathrm{mm}$. The obtained persistence length of the Holzapfel-Ogden model is in agreement with this. We fit the Unterberger model (3.95) by using the single filament parameters, which we achieved in Section 6.1.1, the stretching modulus $\mu_0 = 455.44\,\mathrm{nN}$, the temperatur $T = 294\,\mathrm{K}$, the effective extensional modulus $\beta = 2.5$, and the persistence length $L_\mathrm{p} = 3.99\,\mathrm{mm}$. The remaining fitting parameters are the filament density n, the end-to-end distance at zero force r_0, the initial stretch λ_0, the contour length L, and the averaging network parameter p. One of the best fits by using the nonlinear least square tools of MATLAB yields the following values for the parameters, $n = 64\,\mu\mathrm{m}^{-3}, r_0 = 48.43\,\mathrm{nm}, \lambda_0 = 1.044, L = 116\,\mathrm{nm}$, and $p = 25$.

The fit is acceptable for the shear stresses and slightly worse for the normal stesses. It is of course more difficult to fit two sets of experimental data simultaneously. The data of normal stress show an inflection point, the origin of which is unknown, see Figure 6.2. We only used the experimental data up to a deformation of about $43\,\%$ and the values of the ordinates are very large-scale in the result of Kang et al. (2009). Thus there may be a considerable error stem from measuring the data in the original diagram. Further, it is difficult to give a reasonable interpretation of these obtained parameters. We are not able to compare this result with others. Brown et al. (2009) accomplished the experiments in a

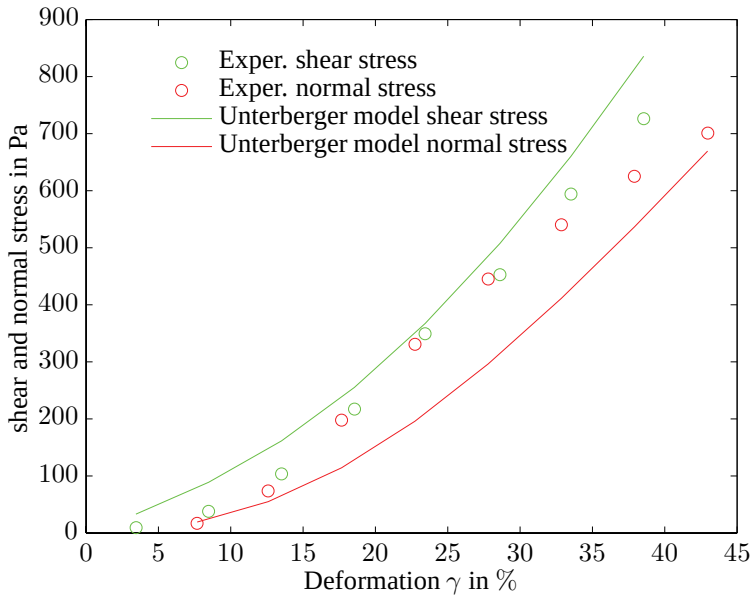

Figure 6.2: Network of fibrin fiber shear stress and normal stress versus strain curve. Experimental data were obtained by Kang et al. (2009). Green circles depict shear stress vs. strain and red circles normal stress vs. strain. The curve through the data depicts the Unterberger model (3.95) with $T = 294\,\mathrm{K}, L_\mathrm{p} = 3.99\,\mathrm{nm}, L = 116\,\mathrm{nm}, r_0 = 48.43\,\mathrm{nm}, \mu_0 = 455.44\,\mathrm{nN}, n = 64\,\mu\mathrm{m}^{-3}, \lambda_0 = 1.044, \beta = 2.5, p = 25$.

completely different way and their results are far-off from ours.

The research on fibrin properties came up very recently. But it is a very important biopolymer for haemostasis and wound healing. It also plays a role in forming of thrombosis. The mechanical properties are still not fully established yet. The reason for its extraordinary elasticity not fathomed. Therefore many question are still open and contradictory statements are not uncommon.

7 Concluding remarks

In the present work we dealt with a theoretical approach to modeling biological materials. Thereby we focused on models which determine the mechanical properties of biopolymers and networks of biopolymers. The thesis was motivated by the exploration to get a better understanding of mechanisms behind disease progression (e.g. cardiovascular diseases and cancer). The framework of these models which we highlighted in this work was provided by the classical continuum mechanics. On the level for an individual biopolymer we were familiar with two different approaches of polymer models, the freely-jointed chain and the worm-like chain model. Recently a new mathematical description of the WLC model was published, referred to as Holzapfel-Ogden model. It was based on pure mechanical formulation and the extensible case of a polymer was incorporated from the beginning.

On the level of networks of biopolymers we discussed the Unterberger model and its underlying idea which originated from the micro-sphere model. We showed that the omission of the tube part from the micro-sphere model was justified in our considerations. Most of the material parameters of the Unterberger model were determined by the single filament model. The number of filaments per unit volume, the distance between branch points, the initial stretch and the averaging parameter were material parameters which belonged to the network model. All of these parameters except the averaging parameter were physically interpretable. Therefore we took a closer look at this averaging parameter by visualizing the structural tensor for different deformation modes and various averaging parameters. It was interpreted as a measure for the non-affinity of the deformation.

The presented models fitted excellently the experimental data of a single filamentous actin and cross-linked actin networks, respectively. Furthermore, these two models should be applicable to other biopolymers, but this was of course a major undertaking in consideration of the complexity of the human body. Fibrin is such a complex protein which structure and properties are still obscure. Fibrin is a very important protein for hemostasis and blood clotting. We fitted the models to experimental data of fibrin fibers and fibrin networks. A very good fit for the single fiber was obtained but the values of the parameters remained questionable. More difficult was to fit the network model. We dealt purely theoretical with modeling on biological materials and exactly at this point lacked the important experimental part. To use experimental data from the literature complicated the determination of some parameters. We were not able to fix many parameters, because they were unknown or the range of their magnitude was extremely variable. This resulted in a set of non-unique solutions of the fits and made it more difficult to submit meaningful interpretations. To support the applicability of these two recently developed models to other biopolymers, further experiments are required.

Bibliography

ALBERTS, B., JOHNSON, A., LEWIS, J., RAFF, M., ROBERTS, K., AND WALTER, P. *Molecular Biology of the Cell*. Garland Science, New York, 5th edn., 2008.

AN, S.S., FABRY, B., TREPAT, X., WANG, N., AND FREDBERG, J.J. Do biophysical properties of the airway smooth muscle in culture predict airway hyperresponsiveness. *Am. J. Respir. Cell Mol. Biol.*, 35:55–64, 2006.

ANTMAN, S.S. *Nonlinear Problems of Elasticity*. Springer, New York, 2nd edn., 2005.

ARRUDA, E.M. AND BOYCE, M.C. A three-dimensional constitutive model for the large stretch behavior of rubber elastic materials. *J. Mech. Phys. Solids*, 41:389–412, 1993.

BAŽANT, Z.P. AND OH, B.H. Efficient numerical integration on the surface of a sphere. *Z. Angew. Math. Mech.*, 66:37–49, 1986.

BROWN, A.E., LITVINOV, R.I., DISCHER, D.E., AND WEISEL, J.W. Forced unfolding of coiled-coils in fibrinogen by single-molecule AFM. *Biophys. J.*, 92:L39–L41, 2007.

BROWN, A.E., LITVINOV, R.I., DISCHER, D.E., PUROHIT, P.K., AND WEISEL, J.W. Multiscale mechanics of fibrin polymer: Gel stretching with protein unfolding and loss of water. *Science*, 325:741–744, 2009.

BUSTAMANTE, C., MARKO, J.F., SIGGIA, E.D., AND SMITH, S. Entropic elasticity of λ-phage DNA. *Science*, 265:1599–1600, 1994.

BUSTAMANTE, C., SMITH, S.B., LIPHARDT, J., AND SMITH, D. Single-molecule studies of DNA mechanics. *Curr. Opin. Struct. Biol.*, 10:279–285, 2000.

COHEN, A. A Padé approximant to the inverse Langevin function. *Rheol. Acta*, 30:270–273, 1991.

DOI, M. AND EDWARDS, S.F. *The theory of polymer dynamics*. Clarendon Press, Oxford, 1986.

FERNÁNDEZ, P., PULLARKAT, P.A., AND OTT, A. A master relation defines the nonlinear viscoelasticity of single fibroblasts. *Biophys. J.*, 90:3796–3805, 2006.

FISCHER, G.. *Lineare Algebra. Eine Einführung für Studienanfänger*. Vieweg, Wiesbaden, 14., durchges. Aufl., 2003.

FIXMAN, M. AND KOVAC, J. Polymer conformational statistics. III. Modified Gaussian models of stiff chains. *J. Chem. Phys.*, 58:1564–1568, 1973.

HEUSER, H. *Lehrbuch der Analysis, Teil 1*. Mathematische Leitfäden. Teubner, Wiesbaden, 16., durchg. Aufl., 2006.

HOLZAPFEL, G.A. *Nonlinear Solid Mechanics: A Continuum Approach for Engineering*. Wiley, Chichester, 2000.

HOLZAPFEL, G.A. AND OGDEN, R.W. On the bending and stretching elasticity of biopolymer filaments. *J. Elasticity*, 104:319–342, 2011.

HOLZAPFEL, G.A. AND OGDEN, R.W. Elasticity of biopolymer filaments. submitted.

HOUSER, J.R., HUDSON, N.E., PING, L., O'BRIEN III, E.T., SUPERFINE, R., LORD, S.T., AND FALVO, M.R. Evidence that αC region is origin of low modulus, high extensibility, and strain stiffening in fibrin fibers. *Biophys. J.*, 99:3038–3047, 2010.

HUDSON, N.E., HOUSER, J.R., O'BRIEN III, E.T., TAYLOR II, R.M., SUPERFINE, R., LORD, S.T., AND FALVO, M.R. Stiffening of individual fibrin fibers equitably distributes strain and strengthens networks. *Biophys. J.*, 98:1632–1640, 2010.

KAMM, R.D. AND MOFRAD, M.R.K. Introduction, with the biological basis for cell mechanics. In KAMM, R.D. AND MOFRAD, M.R.K., editors, *Cytoskeletal mechanics: models and measurements*. Cambridge University Press, Cambridge, 2006.

KANG, H., WEN, Q., JANMEY, P.A., TANG, J.X., CONTI, E., AND MACKINTOSH, F.C. Nonlinear elasticity of stiff filament networks: Strain stiffening, negative normal stress, and filament alignment in fibrin gels. *J. Phys. Chem. B*, 113:3799–3805, 2009.

KOVAC, J. AND CRABB, C.C. Modified Gaussian model for rubber elasticity. 2. The wormlike chain. *Macromolecules*, 15:537–541, 1982.

KRATKY, O. AND POROD, G. Röntgenuntersuchung gelöster Fadenmoleküle. *Recl. Trav. Chim. Pays-Bas.*, 68:1106–1123, 1949.

KUHN, W. Über die Gestalt fadenförmiger Moleküle in Lösungen. *Kolloid-Zeitschrift*, 68: 2–15, 1934.

KUHN, W. Beziehungen zwischen Molekülgröße, statistischer Molekülgestalt und elastischen Eigenschaften hochpolymerer Stoffe. *Kolloid-Zeitschrift*, 76:258–271, 1936.

KUHN, W. AND GRÜN, F. Beziehungen zwischen elastischen Konstanten und Dehnungsdoppelbrechung hochealstischer Stoffe. *Kolloid-Zeitschrift*, 101:248–271, 1942.

LEE, G.Y. AND LIM, C.T. Biomechanics approaches to studying human diseases. *Trends Biotechnol.*, 25:111–118, 2007.

LIU, W., JAWERTH, L.M., SPARKS, E.A., FALVO, M.R., HANTGAN, R.R., SUPERFINE, R., LORD, S.T., AND GUTHOLD, M. Fibrin fibers have extraordinary extensibility and elasticity. *Sience*, 313:634, 2006.

LIU, X. AND POLLACK, G.H. Mechanics of F-actin characterized with microfabricated cantilevers. *Biophys. J.*, 83:2705–2715, 2002.

MACKINTOSH, F.C., KÄS, J., AND JANMEY, P.A. Elasticity of semiflexible biopolymer networks. *Phys. Rev. Lett.*, 75:4425–4428, 1995.

MARKO, J.F. AND SIGGIA, E.D. Stretching DNA. *Macromolecules*, 28:8759–8770, 1995.

LE GOFF, L., HALLATSCHEK, O., FREY, E., AND AMBLARD, F. Tracer studies on F-actin fluctuations. *Phys. Rev. Lett.*, 89:258101, 2002.

VAN DER MAAREL, J.R. *Introduction to biopolymer physics*. World Scientific, Singapore, 2008.

MIEHE, C., GÖKTEPE, S., AND LULEI, F. A micro-macro approach to rubber-like materials—Part I: The non-affine micro-sphere model of rubber elasticity. *J. Mech. Phys. Solids*, 52:2617–2660, 2004.

MOSESSON, M.W. Fibrinogen and fibrin structure and functions. *J. Thromb. Haemost.*, 3: 1894–1904, 2005.

NASH, G.B., O'BRIEN, E., GORDON-SMITH, E.C., AND DORMANDY, J.A. Abnormalities in the mechanical properties of red blood cells caused by plasmodium falciparum. *Blood*, 74:855–861, 1989.

OGDEN, R.W. *Non-linear Elastic Deformations*. Dover, New York, 1997.

OHASHI, T. AND SATO, M. Remodeling of vascular endothelial cells exposed to fluid shear stress: experimental and numerical approach. *Fluid Dyn. Res.*, 37:40–59, 2005.

OTT, A., MAGNASCO, M., SIMON, A., AND LIBCHABER, A. Measurement of the persistence length of polymerized actin using fluorescence microscopy. *Phys. Rev. E*, 48: R1642–R1645, 1993.

PUROHIT, P.K, LITVINOV, R.I., BROWN, A.E., DISCHER, D.E., AND WEISEL, J.W. Protein unfolding accounts for the unusual mechanical behavior of fibrin networks. *Acta Biomater.*, 7:2374–2383, 2011.

RUBINSTEIN, M. AND COLBY, R.H. *Polymers Physics*. Oxford University Press, New York, 2003.

SMITH, S.B., CUI, Y., AND BUSTAMANTE, C. Overstretching B-DNA: The elastic response of individual double-stranded and single-stranded DNA molecules. *Science*, 271: 795–799, 1996.

STORM, C., PASTORE, J.J., MACKINTOSH, F.C., LUBENSKY, T.C., AND JANMEY, P.A. Nonlinear elasticity in biological gels. *Nature*, 435:191–194, 2005.

SURESH, S. Biomechanics and biophysics of cancer cells. *Acta Biomater.*, 3:413–438, 2007.

TRELOAR, L.R. The photoelastic properties of short-chain molecular networks. *Trans. Faraday Soc.*, 50:881–896, 1954.

TRELOAR, L.R. *The Physics of Rubber Elasticity*. Oxford University Press, Oxford, 3rd edn., 1975.

TRICKEY, W.R., LEE, G.M., AND GUILAK, F. Viscoelastic properties of chondrocytes from normal and osteoarthritic human cartilage. *J. Orthop. Res.*, 18:891–898, 2000.

UNTERBERGER, M.J., SCHMOLLER, K.M., BAUSCH, A.R., AND HOLZAPFEL, G.A. A new approach to model cross-linked actin networks: Multiscale continuum formulation and computation analysis. submitted.

VOET, D., VOET, J.G., PRATT, C.W., BECK-SICKINGER, A.G., AND HAHN, U. *Lehrbuch der Biochemie*. Wiley-VCH, Weinheim, 2., aktualisierte u. erw. Aufl., 2010.

WANG, M.C. AND GUTH, E. Statistical theory of networks of non-Gaussian flexible chains. *J. Chem. Phys.*, 20:1144–1157, 1952.

WEISEL, J.W. The mechanical properties of fibrin for basic scientists and clinicians. *Biophys. Chem.*, 112:267–276, 2004.

ZENG, D., JUZKIW, T., READ, A.T., CHAN, D.W.-H., GLUCKSBERG, M.R., ETHIER, C.R., AND JOHNSON, M. Young's modulus of elasticity of schlemm's canal endothelial cells. *Biomech. Model. Mechanobiol.*, 9:19–33, 2010.